
Exact Pareto Optimal Search for Multi-Task Learning and Multi-Criteria Decision-Making

Debabrata Mahapatra
Department of Computer Science
School of Computing
National University of Singapore
debabrata@u.nus.edu

Vaibhav Rajan
Department of Information Systems and Analytics
School of Computing
National University of Singapore
vaibhav.rajan@nus.edu.sg

Abstract

Given multiple non-convex objective functions and objective-specific weights, Chebyshev scalarization (CS) is a well-known approach to obtain an Exact Pareto Optimal (EPO), i.e., a solution on the Pareto front (PF) that intersects the ray defined by the inverse of the weights. First-order optimizers that use the CS formulation to find EPO solutions encounter practical problems of oscillations and stagnation that affect convergence. Moreover, when initialized with a PO solution, they do not guarantee a controlled trajectory that lies completely on the PF. These shortcomings lead to modeling limitations and computational inefficiency in multi-task learning (MTL) and multi-criteria decision-making (MCDM) methods that utilize CS for their underlying non-convex multi-objective optimization (MOO). To address these shortcomings, we design a new MOO method, EPO Search. We prove that EPO Search converges to an EPO solution and empirically illustrate its computational efficiency and robustness to initialization. When initialized on the PF, EPO Search can trace the PF and converge to the required EPO solution at a linear rate of convergence. Using EPO Search we develop new algorithms – PESA-EPO, that approximates the PF for a posteriori MCDM, and GP-EPO for preference elicitation in interactive MCDM; experiments on benchmark datasets confirm their advantages over competing alternatives. EPO Search scales linearly with the number of decision variables which enables its use for training deep networks. Empirical results on real data from personalized medicine, e-commerce and hydrometeorology demonstrate the efficacy of EPO Search for deep MTL.

1 Introduction

Multi-objective optimization (MOO) has numerous real-world applications ranging from engineering design to public sector planning (Stewart et al. 2008). A MOO problem can have multiple, possibly infinite, Pareto optimal (PO) solutions, represented by the Pareto front (PF). A MOO problem is often solved by scalarization that transforms it to a single objective optimization (SOO) problem. A widely used technique, in optimization, decision analysis and more recently, in artificial intelligence (see, e.g., Miettinen (1998), Reeves and MacLeod (1999), Ozbey and Karwan (2014), Daulton et al. (2022)), is the weighted Chebyshev (or Tchebycheff) scalarization (CS). Given m objective functions $f_j(\mathbf{x})$, for $j \in [m]$, on a decision or (feasible) solution space \mathbb{X} and an input *weight* vector $\mathbf{r} \in \mathbb{R}_+^m$, CS minimizes the objective with maximum relative weighted value:

$$\mathbf{x}_r^* = \arg \min_{\mathbf{x} \in \mathbb{X}} \|\mathbf{r} \odot \mathbf{f}(\mathbf{x})\|_\infty = \arg \min_{\mathbf{x} \in \mathbb{X}} \max_{j \in [m]} r_j f_j(\mathbf{x}), \quad (1)$$

where \odot is the element-wise product operator. A key advantage of CS, over alternative scalarizations, is that it satisfies the necessary and sufficient conditions for modeling *all* PO solutions of a

non-convex MOO problem – the complete PF can be obtained by varying the weight values \mathbf{r} (Steuer et al. 1993, Kaliszewski 1995). The solution to (1), in general (weak PO solutions are an exception, see §2.1), lies at the intersection of the PF and the ray $\mathbf{r}^{-1} = (1/r_1, \dots, 1/r_m)$ as shown in Figure 1b. We call this an **Exact Pareto Optimal (EPO)** solution.

In this paper, our focus is on first order methods, which can scale to high-dimensional solution spaces, to find EPO solutions for differentiable f_j 's. To the best of our knowledge, extant literature does not provide a robust first-order iteration strategy with convergence guarantees to find EPO solutions. A first order method like gradient descent to solve (1) has the following practical and theoretical limitations. First, it uses gradients of only one of the objectives in each iteration, which changes frequently around the \mathbf{r}^{-1} ray. As a result, there are oscillations in the trajectory, which slows convergence during descent. Second, if the gradient magnitude vanishes for the objective with highest weighted value, descent stagnates. In such cases, movement in each iteration is negligibly small. Third, when initialized with a PO solution, it does not guarantee that the trajectory to the required EPO solution remains on the PF. Further, the non-differentiable max function in the ℓ_∞ norm of (1) makes convergence rate analysis for gradient-based methods non-trivial. These shortcomings lead to computational inefficiency and modeling limitations in methods, such as those outlined below, that utilize CS in solving their underlying non-convex MOO problems.

Consider neural multi-task learning (MTL) where each objective is a loss function (usually non-convex) for a task and a MOO solution corresponds to trained neural network parameters. Linear scalarization (that solves $\arg \min_{\mathbf{x} \in \mathcal{X}} \mathbf{r}^T \mathbf{f}(\mathbf{x})$) is commonly used to train MTL models, where the weights specify relative priorities among tasks. CS is theoretically advantageous for non-convex functions and is also more interpretable (see §2.1.2, 2.3). However, first order solvers that optimize the min-max formulation in (1) face challenges during training of deep networks due to the aforementioned problems of oscillations and stagnation. Since the gradient of only one of the objectives is used in each iteration, optimization effectively leads to just single-task learning which ultimately deteriorates the model's predictive accuracy. The same problem occurs when a relatively high priority is given to a task – the other tasks are completely ignored during training. This may be alleviated through second order methods but they are not scalable to high-dimensional parameter spaces in deep networks.

As another example, consider multi-criteria decision-making (MCDM), where the decision maker (DM) has to choose the most suitable PO solution of the underlying (non-convex) MOO problem. We study two approaches – (i) a posteriori methods, where multiple PO solutions are computed that collectively provide an approximate view of the PF and enables the DM to select one desired solution and (ii) interactive methods, where the DM progressively articulates preferences among solutions and proceeds towards a satisfactory solution while interacting with the MOO solver. The DM's preferences are assumed to follow an (unknown) utility function that can score and order PO solutions, and is monotonic, i.e., a solution that Pareto dominates another has higher utility. In both these cases, there are multiple calls to the MOO solver, each time after a PO solution is obtained. If the min-max formulation (1) is used, and the trajectory between consecutive solutions is not on the PF, the MCDM approach has high computational burden. Moreover, such solvers also need to be re-initialized and re-started at PF discontinuities where they may halt prematurely.

We design a new approach, called EPO Search, to efficiently find EPO solutions for non-convex MOO, which addresses these limitations. Using EPO Search we develop techniques that advance the state-of-the-art in first order methods for (a) PF approximation for a posteriori MCDM, (b) preference elicitation in interactive MCDM and (c) training deep multi-task neural networks. The four main contributions of this paper are as follows.

1. We design and analyze search direction strategies that *balance* the dual goals of moving towards the PF as well as towards the \mathbf{r}^{-1} ray, which equip us to combine gradient descent with carefully controlled ascent in objectives with less relative weights to avoid their local minima. By using a linear combination of all objective gradients, while moving in a balancing search direction, EPO Search avoids the problems of oscillations and stagnation. We prove, under mild assumptions and without assuming convexity, that, from a random initialization, EPO Search converges to the EPO solution, or, if an exact solution does not exist, to a PO solution closest to the \mathbf{r}^{-1} ray. When initialized at an arbitrary PO solution, we prove that EPO Search converges to the desired EPO solution with a trajectory close to the PF and under mild regularity conditions, we prove that the convergence rate, even for non-convex objectives, is linear. EPO Search scales linearly with the gradient dimension

per iteration and thus, can efficiently find (local) EPO solutions in high-dimensional solution spaces. We extend EPO Search for solving constrained MOO problems without compromising on its computational efficiency. Our empirical results on benchmark MOO problems support the theoretical claims of scalability and accuracy of EPO Search.

2. Using PESA (Stanojević and Glover 2020) to generate a diverse set of weight vectors, we develop the algorithm PESA-EPO to approximate the PF. Leveraging the PF tracing ability of EPO Search, PESA-EPO efficiently finds multiple PO solutions without multiple optimizer calls, and without premature halts at PF discontinuities. On several benchmark convex and non-convex MOO problems, both with and without constraints, PESA-EPO leads to better or comparable PF approximation in lower execution time, compared to competing gradient-based as well as evolutionary MOO algorithms.

3. In probabilistic preference elicitation, a Gaussian Process (GP), which can model any (including non-linear and non-convex) function, is used to learn the DM’s unknown utility. Pairwise comparisons from the DM are used to interactively learn the GP parameters in a Bayesian active learning framework, where, in each interaction, the DM specifies her preference between the two presented PO solutions. To reduce their computational burden, previous approaches, e.g., Chin et al. (2018), Zintgraf et al. (2018), sample these PO solutions from a discrete subset of the solution space (see §2.2.2), which affects their accuracy of preference learning. Further, since sampling from the GP does not guarantee a PO solution, previous methods impose monotonicity constraints during or employ postprocessing heuristics after sampling from the GP; these steps either deteriorate performance or increase computational time. We address these limitations by developing GP-EPO where we explore the PF at high resolution, by sampling \mathbf{r}^{-1} rays (in a lower m -dimensional space, instead of the entire solution space) and then efficiently find PO solutions through EPO Search to present to the DM. Our approach obviates the need to explicitly model monotonicity constraints. Further, over the interactions, GP-EPO moves from one EPO solution to another with linear convergence rate. Evaluation on benchmark problems show that GP-EPO learns the utility with substantially better accuracy, compared to extant GP-based methods, in just a few interactions.

4. In MOO-based neural MTL, which models tradeoffs among objectives, previous methods either do not use task-specific priorities or yield multiple PO solutions for an input set of diverse relative priorities. An EPO solution models task priorities specified by the \mathbf{r}^{-1} ray, thus prioritizing tasks that are challenging to learn; without losing the benefits of MTL that allows shared learning from other datasets and tasks. Compared to gradient descent to solve (1) for network training, EPO Search offers a more robust iterative procedure that overcomes the problems of oscillation and stagnation; further, its ability to use the gradients of all objectives and escape minima of lower priority objectives leads to improved MTL. The per-iteration complexity of EPO Search remains linear in the gradient dimensions (similar to the best previous methods that neither use input priorities nor allow regularization constraints) enabling its use for deep MTL networks. We evaluate the efficacy of EPO Search for MTL on three real datasets from different domains: personalized medicine, e-commerce and hydrometeorology. In all cases, the use of EPO Search leads to higher predictive accuracy compared to single-task learning, the direct use of linear and Chebyshev scalarization during training and competing MTL models.

The rest of the paper is organized as follows. Background and related work are presented in §2. We then describe our theory and algorithms for EPO Search in §3. Algorithms PESA-EPO, GP-EPO and EPO Search for MTL are described in §4. Experimental results are in §5, followed by our concluding discussion in §6.

2 Background and Related Work

We describe relevant concepts and related work from three streams of literature – multi-objective optimization (MOO), multi-criteria decision making (MCDM) and multi-task learning (MTL).

2.1 Multi-Objective Optimization

We consider a multi-objective optimization (MOO) problem with m non-negative differentiable objective functions, $f_j : \mathcal{X} \rightarrow \mathbb{R}_+$ for $j \in [m]$, where $\mathcal{X} \subset \mathbb{R}^n$. This formulation is fairly general, since problems with different specifications can be converted to this form. For instance, if an objective f_j

is negative at its minimizer, i.e., $\min_{\mathbf{x} \in \mathcal{X}} f_j(\mathbf{x}) = f_j^* \leq 0$, then, to make it non-negative, one can reformulate as $f_j(\mathbf{x}) := f_j(\mathbf{x}) - f_j^{**}$, where f_j^{**} is a lower bound on the minimum: $f_j^{**} \leq f_j^*$. The vector \mathbf{f}^{**} consisting of the lower bounds of all objectives is called as a ‘‘utopia’’ point, which makes $\mathbf{f} - \mathbf{f}^{**}$ a non-negative vector valued function. We develop MOO algorithms for unconstrained problems in the main paper, and extend them to solve constrained MOO problems in §B.

We use \mathbf{f} to denote both a vector valued function and a point in the *Objective Space* \mathbb{R}^m , which should be unambiguous from the context. The range of \mathbf{f} , denoted by \mathcal{O} , is a subset of the positive cone $\mathbb{R}_+^m := \{\mathbf{f} \in \mathbb{R}^m \mid f_j \geq 0 \forall j \in [m]\}$. The partial ordering for any two points $\mathbf{f}^1, \mathbf{f}^2 \in \mathbb{R}^m$, denoted by $\mathbf{f}^1 \geq \mathbf{f}^2$ is defined by $\mathbf{f}^1 - \mathbf{f}^2 \in \mathbb{R}_+^m$, which implies $f_j^1 \geq f_j^2$ for every $j \in [m]$ and strict inequality $\mathbf{f}^1 > \mathbf{f}^2$ occurs when there is at least one j for which $f_j^1 > f_j^2$. Geometrically, $\mathbf{f}^1 > \mathbf{f}^2$ means that \mathbf{f}^1 lies in the positive cone pivoted at \mathbf{f}^2 , i.e., $\mathbf{f}^1 \in \{\mathbf{f}^2\} + \mathbb{R}_+^m := \{\mathbf{f}^2 + \mathbf{f} \mid \mathbf{f} \in \mathbb{R}_+^m\}$, and $\mathbf{f}^1 \neq \mathbf{f}^2$.

For a minimization problem, a solution $\mathbf{x}^1 \in \mathcal{X}$ is (weakly) *dominated* by another solution $\mathbf{x}^2 \in \mathcal{X}$ if $(\mathbf{f}(\mathbf{x}^1) \geq \mathbf{f}(\mathbf{x}^2)) \wedge \mathbf{f}(\mathbf{x}^1) > \mathbf{f}(\mathbf{x}^2)$. Note that $\mathbf{f}(\mathbf{x}^1) \not\geq \mathbf{f}(\mathbf{x}^2)$ if \mathbf{x}^1 is not dominated by \mathbf{x}^2 , i.e. $\mathbf{f}(\mathbf{x}^1) \notin \{\mathbf{f}(\mathbf{x}^2)\} + \mathbb{R}_+^m$. A solution \mathbf{x}^* is **Pareto optimal (PO)** if it is not dominated by any other solution. Weak PO solutions are weakly dominated by other PO solutions. The set of all global PO solutions is $\mathcal{P}_{glo} := \{\mathbf{x}^* \in \mathcal{X} \mid \forall \mathbf{x} \in \mathcal{X} \setminus \{\mathbf{x}^*\}, \mathbf{f}(\mathbf{x}^*) \not\geq \mathbf{f}(\mathbf{x})\}$, and the set of local PO solutions is:

$$\mathcal{P} := \{\mathbf{x}^* \in \mathcal{X} \mid \exists \mathcal{N}_\epsilon(\mathbf{x}^*) \subset \mathcal{X} \text{ for an } \epsilon > 0, \text{ s.t. } \forall \mathbf{x} \in \mathcal{N}_\epsilon(\mathbf{x}^*) \setminus \{\mathbf{x}^*\}, \mathbf{f}(\mathbf{x}^*) \not\geq \mathbf{f}(\mathbf{x})\}, \quad (2)$$

where $\mathcal{N}_\epsilon(\mathbf{x}^*) = \{\mathbf{x} \in \mathcal{X} \mid \|\mathbf{x} - \mathbf{x}^*\| < \epsilon\}$ is an open neighbourhood of \mathbf{x}^* in \mathcal{X} . Note that $\mathcal{P}_{glo} \subset \mathcal{P}$. The set of multi-objective values of the PO solutions, $\mathbf{f}(\mathcal{P}) \subset \mathcal{O}$, is called the **Pareto front (PF)**. Excellent surveys on MOO can be found in, e.g., Gandibleux (2002), Wiecek et al. (2016).

2.1.1 Descent Methods for Converging to the Pareto Front.

Gradient-based MOO solvers, such as in Fliege and Svaiter (2000), Vieira et al. (2012), find a PO solution by starting from an arbitrary initialization $\mathbf{x}^0 \in \mathbb{R}^n$ and iteratively obtaining the next solution \mathbf{x}^{t+1} that dominates the previous one \mathbf{x}^t (i.e., $\mathbf{f}^{t+1} \leq \mathbf{f}^t$, where $\mathbf{f}^t := \mathbf{f}(\mathbf{x}^t)$), by moving *against* a direction $\mathbf{d} \in \mathbb{R}^n$ with a step size $\eta > 0$ as $\mathbf{x}^{t+1} = \mathbf{x}^t - \eta \mathbf{d}$, such that there is descent in every objective, $f_j^{t+1} \leq f_j^t \forall j \in [m]$. This can happen only if \mathbf{d} has positive angles with the gradients of every objective function at \mathbf{x}^t :

$$\mathbf{d}^T \nabla_{\mathbf{x}} f_j^t \geq 0, \quad \text{for all } j \in [m]; \quad (3)$$

we call such a \mathbf{d} a *descent direction*. Note, by convention, the move is against \mathbf{d} , i.e., along $-\mathbf{d}$.

Désidéri (2012) showed that descent directions can be found in the *Convex Hull* of the gradients,

$$\mathcal{CH}_{\mathbf{x}} := \left\{ \sum_{j=1}^m \nabla_{\mathbf{x}} f_j \beta_j \mid \beta \in \mathcal{S}^m \right\} \quad (4)$$

where $\mathcal{S}^m := \left\{ \beta \in \mathbb{R}_+^m \mid \sum_{j=1}^m \beta_j = 1, \text{ and } \beta_j \geq 0 \forall j \in [m] \right\}$ is the $m - 1$ dimensional simplex. Their multiple gradient descent algorithm (MGDA) converges to a local PO by iteratively using the descent direction: $\mathbf{d}^* = \arg \min_{\mathbf{d} \in \mathcal{CH}_{\mathbf{x}}} \|\mathbf{d}\|_2^2$. Although descent-based methods provide convergence guarantees (Tanabe et al. 2022), they cannot find EPO solutions.

2.1.2 Scalarization.

The popular approach of linear scalarization (LS) of a MOO problem with an input weight vector $\mathbf{r} \in \mathbb{R}_+^m$ finds

$$\mathbf{x}^*(\mathbf{r}) = \arg \min_{\mathbf{x} \in \mathcal{X}} \langle \mathbf{r}, \mathbf{f}(\mathbf{x}) \rangle = \arg \min_{\mathbf{x} \in \mathcal{X}} \mathbf{r}^T \mathbf{f}(\mathbf{x}). \quad (5)$$

If the range of \mathbf{f} , i.e. \mathcal{O} , is convex then for every $\bar{\mathbf{x}}^* \in \mathcal{P}$, there exists an \mathbf{r} such that $\bar{\mathbf{x}}^* = \mathbf{x}^*(\mathbf{r})$. The weight vector \mathbf{r} is an element in the dual of the objective space (Luenberger 1997), and represents a hyperplane in the objective space. The hyperplane of \mathbf{r} at $\mathbf{f}_{\mathbf{r}}^* = \mathbf{f}(\mathbf{x}^*(\mathbf{r}))$ has to be both a tangent and a support to the PF, i.e., $\mathbf{r}^T \mathbf{f} \geq \mathbf{r}^T \mathbf{f}_{\mathbf{r}}^*$ for all $\mathbf{f} \in \mathcal{O}$. If any of the objectives is non-convex, i.e., the range \mathcal{O} is a non-convex set, LS cannot guarantee to reach every optimal point in the PF by

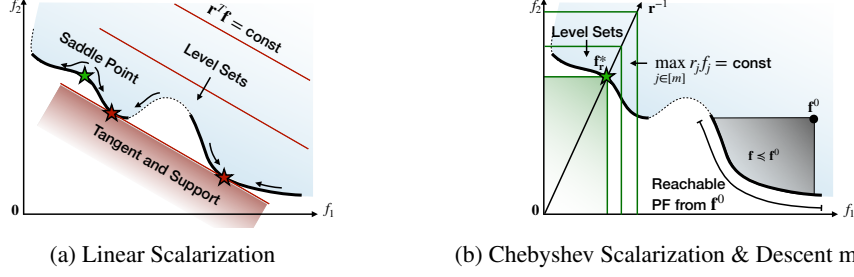


Figure 1: (Color Online) Figure 1a shows how linear scalarization can have non-unique Pareto optimal points (red) for the same weight \mathbf{r} ; among the 3 optima, the green one, a saddle point for LS (5), cannot be attained. Figure 1b shows Chebyshev scalarization (1) can attain the green optimum; it also illustrates how a *descent-only* search cannot find the preferred optimal \mathbf{f}_r^* starting from a random initialization \mathbf{x}^0 , where $\mathbf{f}^0 = \mathbf{f}(\mathbf{x}^0)$. Any descent direction \mathbf{d} will keep the objective vector \mathbf{f}^{t+1} of next iterate $\mathbf{x}^{t+1} = \mathbf{x}^t - \eta \mathbf{d}$ in the black shaded region.

varying the weights (Boyd and Vandenberghe (2004)[Ch 4.7]), because the tangent hyperplane at a point on the PF is not necessarily a support if \mathcal{O} is non-convex. Moreover, even a single vector \mathbf{r} can have non-unique PO solutions; see Figure 1a.

Definition 1. Given a weight vector $\mathbf{r} \in \mathbb{R}_+^m$, an *Exact Pareto Optimal (EPO) solution* belongs to the set:

$$\mathcal{P}_{\mathbf{r}} = \{\mathbf{x}^* \in \mathcal{P} \mid r_1 f_1^* = \dots = r_j f_j^* = \dots = r_m f_m^*\}, \quad \text{where } f_j^* = f_j(\mathbf{x}^*). \quad (6)$$

For any EPO solution \mathbf{x}_r^* , $\mathbf{f}_r^* = \mathbf{f}(\mathbf{x}_r^*)$ is a point on the PF intersecting the ray towards $\mathbf{r}^{-1} := (1/r_1, \dots, 1/r_m)$ (see Figure 1b), i.e., \mathbf{f}_r^* is perfectly *proportional* to the \mathbf{r}^{-1} ray. CS, i.e., a solution to (1), is an EPO solution, as illustrated in Figure 1b, because, its c -level set $\mathcal{L}_c = \{\mathbf{f} \in \mathbb{R}^m \mid \max_{j \in [m]} r_j f_j \leq c\}$ can also be written as $\{c\mathbf{r}^{-1}\} - \mathbb{R}_+^m$, the negative orthant pivoted at $c\mathbf{r}^{-1}$. Therefore, if $\mathcal{L}_c \cap \mathcal{O}$ is a singleton set then the corresponding solution is an EPO point w.r.t. \mathbf{r} .

Although for convex MOO problems LS and CS may be considered equivalent (Luque et al. 2007), they differ for non-convex MOO. Unlike LS, CS provides both necessary and sufficient condition for weak Pareto optimality of non-convex MOO problems. CS has extensions such as augmented CS (Steuer 1989, Miettinen 1998) that eliminates the corner case of weak PO solutions. However, such extensions lose the exactness property of CS for its strong PO solutions, and we leverage the exactness property for our algorithms. These scalarization methods, their variants and generalizations (Gembicki and Haimes 1975, Pascoletti and Serafini 1984, Wierzbicki 1986, Marler and Arora 2004) specify a desired PO solution through their parameters. However, to our knowledge, there is no robust first-order iterative strategy that guarantees convergence to a desired EPO solution starting from a random initialization.

2.2 Multi-Criteria Decision-Making (MCDM)

MCDM aims to solve decision-making problems involving multiple conflicting objectives (Wallenius et al. 2008, Köksalan and Wallenius 2012). We focus on continuous MCDM problems, with differentiable objectives, where the solution alternatives are (or can relaxed to be) in a continuous space. Based on how a DM participates in the solution process MCDM approaches can be categorized into (Hwang et al. 1979, Miettinen 1998): (i) a priori methods where preferences are specified before the MOO problem is solved (ii) a posteriori methods where multiple PO solutions are computed from which the DM selects one and (iii) interactive methods where the DM progressively articulates preferences and, along with the MOO solver, iteratively proceeds towards a satisfactory solution.

In each of these categories, there are various ways to articulate preferences (Miettinen 1998). Preferences may be articulated by comparison of PO solutions, e.g., through pairwise comparisons (e.g., Korhonen et al. (1984), Köksalan and Sagala (1995)) or selection from a set of solutions (e.g., Greco et al. (2010)). A utility function $u : \mathbb{R}^m \rightarrow \mathbb{R}$ that assigns a scalar value to every objective vector

(Keeney et al. 1993), may be used to model the DM’s preferences and create a total ordering among the PO solutions. The utility is commonly assumed (Fishburn 1968) to satisfy the monotonicity property: for any two alternatives \mathbf{x}^1 and \mathbf{x}^2 , if \mathbf{x}^1 dominates \mathbf{x}^2 (i.e. $\mathbf{f}^1 \preceq \mathbf{f}^2$), then $u(\mathbf{f}^1) \geq u(\mathbf{f}^2)$, where $\mathbf{f}^i = \mathbf{f}(\mathbf{x}^i)$. The oracle solution maximizes the DM’s (unknown) utility:

$$\mathbf{x}_{orc} = \arg \max_{\mathbf{x} \in \mathcal{X}} u(\mathbf{f}(\mathbf{x})). \quad (7)$$

The DM’s utility may be learnt in both a posteriori and interactive MCDM, e.g., in Jing et al. (2019), a utility function is constructed using the PF approximation from an a posteriori method; preference elicitation (PE) methods may be used in interactive MCDM (see §2.2.2).

2.2.1 A Posteriori Methods and Pareto Front Approximation.

In a posteriori methods, the ability of an algorithm to quickly and evenly approximate the PF is crucial Das and Dennis (1997, 1998). Many Multi-Objective Evolutionary Algorithms (MOEA) have been developed to approximate the PF, e.g., (Zhang and Li 2007, Li and Zhang 2009, Qi et al. 2014, Zhang et al. 2015, Deb et al. 2002, Deb and Jain 2014, Zhang et al. 2018, Li et al. 2019). They are effective in practice and scale well to many objectives (Emmerich and Deutz 2018). However, they do not scale well to high-dimensional solution spaces.

In gradient-based MOO, a scalarization method is run several times with a diverse set of parameters to generate well spread out PF approximations. The simple LS method fails to generate evenly spread solutions from a set of evenly spread weights (Das and Dennis 1997). To address this problem, Das and Dennis (1998) developed a direction-based scalarization method called Normalized Boundary Intersection (NBI) that finds PO solutions along many directions normal to the Convex Hull of the Individual Minima (CHIM) of the objective functions. Several improvements of NBI have been proposed (Ismail-Yahaya and Messac 2002, Shukla 2007, Siddiqui et al. 2012) but they remain computationally inefficient as they require re-initializations at PF discontinuities and do not scale well to many objectives. Stanojević and Glover (2020) proposed a recursive sampling strategy Pattern Efficient Set Algorithm (PESA) that samples weights/directions from the simplex spread uniformly, and scales well with number of objectives. They used an NBI type scalarization called Targeted Direction Model (TDM) to find direction specific solutions. However, similar to NBI, their method also has to solve many SOO problems, one for each direction ray.

2.2.2 Preference Elicitation for Interactive MCDM.

Preference Elicitation (PE) aims to infer the DM’s unknown utility function using the DM’s responses to queries in interactive MCDM. We assume the queries to the DM are in the form of pairwise comparison of alternatives, which is cognitively less demanding compared to other query types (such as value assignment) (Tesauro 1988, Forgas 1995). Methods such as Conjoint Analysis (Rao 2010, Angur et al. 1996) and Best-Worst Method (Oztas and Erdem 2021) are well-known for discrete MCDM problems. In continuous MCDM, the utility is a fixed parametric function of the objective values, e.g., Chebyshev utility that uses CS (Steuer 1989, Steuer et al. 1993, Dell and Karwan 1990, Ozbey and Karwan 2014, Reeves and MacLeod 1999); and in Preference Robust Optimization (PRO), where Vayanos et al. (2020) model the utility as a linear function and Haskell et al. (2018) model it as a quasi-concave function. These methods cannot model non-convex PE problems, where either the MOO problem or the utility function could be non-convex. See Appendix G for an extended discussion.

In contrast to these methods, the Bayesian active learning framework for PE (Eric et al. 2007, Zintgraf et al. 2018, Roijers et al. 2021) uses Gaussian Process (GP) to model the utility that can model *any* class of functions. Further, this can model uncertainty in the DM’s stated preferences and works well with less data – requiring just a few interactions with the DM to learn preferences (Deisenroth et al. 2013). Appendix H has an overview of Bayesian optimization with GP.

The prior for the unknown utility function, $P(u)$, is modelled as $\text{GP}(\mu, \kappa)$, where $\mu : \mathbb{R}^m \rightarrow \mathbb{R}$ and $\kappa : \mathbb{R}^m \times \mathbb{R}^m \rightarrow \mathbb{R}_+$ are the mean and covariance functions respectively. Learning proceeds by alternating between querying the DM based on the current GP and updating the GP posterior after obtaining the resulting comparison from the query. Thus, the observational data from which the GP is learnt is $\mathcal{D}_t = \{c_1, \dots, c_{t'}\}$, where t is the number of pairwise queries to the DM, and an ordered pair $c = (\mathbf{x}^i, \mathbf{x}^j)$ represents the DM’s *comparison* of two alternatives as “ \mathbf{x}^i is preferred to \mathbf{x}^j ”, suggesting $u(\mathbf{f}^i) \geq u(\mathbf{f}^j)$. If the DM values both alternatives equally, then the dataset can include

both $(\mathbf{x}^i, \mathbf{x}^j)$ and $(\mathbf{x}^j, \mathbf{x}^i)$, making $|\mathcal{D}_t| = t' \geq t$. Inconsistencies in DM’s response are modelled as additive noise: $u(\mathbf{f}^i) + \epsilon_i \geq u(\mathbf{f}^j) + \epsilon_j$, where $\epsilon_i, \epsilon_j \sim \mathcal{N}(0, \sigma)$. For such noisy pairwise comparison data, Chu and Ghahramani (2005) developed a probit likelihood model for $P(\mathcal{D}_t|u)$, wherein the posterior, $P(u|\mathcal{D}_{t+1}) \propto P(u)P(\mathcal{D}_t|u)$, is analytically non-tractable, but can be approximated to a GP using Laplace approximation. In the beginning, when there is no comparison data, $\mathcal{D}_0 = \phi$, the GP prior is usually initialized with a zero mean function.

Let $\check{\mathcal{X}}_{\mathcal{D}_t}$ be the discrete set of alternatives presented to the DM, and $\mathbf{x}_{inc}^t \in \check{\mathcal{X}}_{\mathcal{D}_t}$ be the incumbent solution, where \mathbf{x}_{inc}^t is preferred to all other solutions in $\check{\mathcal{X}}_{\mathcal{D}_t}$. In each iteration, selection of a new alternative to create the next query is done using an *acquisition function* $\alpha^t : \mathbb{R}^m \rightarrow \mathbb{R}$. A commonly used acquisition function in previous works on interactive PE, e.g., Eric et al. (2007), is the *Expected Improvement* (Moćkus (1975)) function which is optimized to *suggest* a new alternative:

$$\mathbf{x}_{sug}^t = \arg \max_{\mathbf{x} \in \check{\mathcal{X}}} \alpha^t(\mathbf{f}(\mathbf{x})), \quad (8)$$

where $\check{\mathcal{X}}$ is a discrete subset of \mathcal{X} . The DM is then asked to compare between \mathbf{x}_{inc}^t and \mathbf{x}_{sug}^t . The new comparison datapoint $(\mathbf{x}_{inc}^t, \mathbf{x}_{sug}^t)$ is included in the dataset, and the posterior is updated to $GP(\mu^{t+1}, \kappa^{t+1})$ to approximate $P(u|\mathcal{D}_{t+1})$. This iterative procedure is continued until, either $\|\mathbf{f}_{sug}^t - \mathbf{f}_{inc}^t\| \leq \epsilon$ for a small $\epsilon > 0$ or the DM is satisfied with \mathbf{x}_{sug}^t .

Previous GP-based approaches have two important limitations. First, they optimize over a discrete subset, $\check{\mathcal{X}}$, of the entire search space, because μ^t and κ^t can be highly non-linear, which renders the global optimization of a^t (8) computationally expensive, especially if \mathcal{X} is high dimensional. Decreasing the size of the discrete subset improves computational efficiency but reduces accuracy of preference learning. Second, additional monotonicity constraints need to be enforced because sampling from a GP does not guarantee a PO solution. Several heuristics to address this problem have been proposed (Chin et al. 2018, Zintgraf et al. 2018, Roijers et al. 2021) that either deteriorate performance or increase the computational burden.

2.3 Multi-Task Learning

Multi-Task Learning (MTL) has been studied extensively in machine learning (see, e.g., Zhang and Yang (2021)). Learning multiple tasks together leads to inductive bias towards hypotheses that can explain more than one task and has been found to improve model generalization in machine learning (Caruana 1997).

A multi-task neural network is trained for multiple tasks simultaneously and inductive transfer is enabled through shared parameters, most commonly through fixed layers common to all tasks (Ruder 2017) (Appendix I has an overview of neural networks). Figure 2 (left) shows a schematic of a MTL network for two tasks T1, T2 with objective (loss) functions f_1, f_2 respectively. The network has one or more shared layers with parameters θ_s and task-specific layers with parameters θ_1, θ_2 that are learnt during training. For conflicting tasks, we cannot assume that parameters learned through SOO are effective across all tasks as trade-offs among the tasks are not explicitly modeled. In such cases, PO solutions from MOO yield better models, as shown by Sener and Koltun (2018). They extended MGDA to handle high-dimensional gradients, thereby making it usable for deep MTL models. However, their method finds a single arbitrary PO solution and cannot be used by MTL designers to explore solutions with different trade-offs. This is illustrated in Figure 1b.

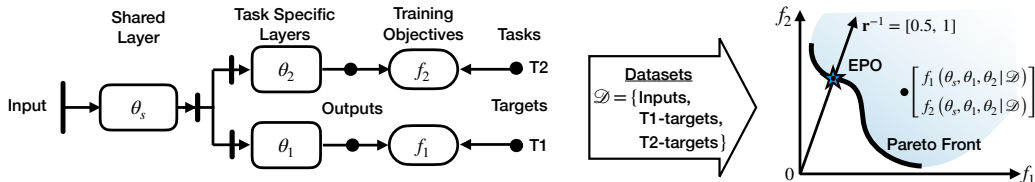


Figure 2: Left: Schematic of a MTL DNN for 2 tasks; Right: MOO-based network training yields multiple PO solutions for f_1, f_2 forming a PF, EPO solution (trained network parameters) for priorities $r_1 = 2, r_2 = 1$.

Current MTL approaches which use MOO for training, do not explicitly model task-specific priorities. While LS has been used in SOO settings, to our knowledge, CS, has not been used in MTL.

Task-specific priorities through CS can be effected through EPO Search for model training. The related, Pareto MTL (PMTL) algorithm by Lin et al. (2019), finds multiple solutions on the PF through a decomposition strategy and may be modified to find EPO solutions. They use several reference vectors $\mathbf{u}^k, k = 1, \dots, K$, each of unit magnitude, to partition the solution space into K sub-regions $\Omega_k := \left\{ \mathbf{x} \in \mathbb{R}^n \mid \langle \mathbf{u}^k, \mathbf{f}(\mathbf{x}) \rangle \geq \langle \mathbf{u}^{k'}, \mathbf{f}(\mathbf{x}) \rangle, \forall k' \neq k \right\}$. With this decomposition, if $\mathbf{u}^k = \mathbf{r}^{-1}$, then the EPO solution $\mathbf{x}_r^* \in \Omega_k$. There are two phases in their algorithm. In phase one, starting from a random initialization, they find a point $\mathbf{x}_r^0 \in \Omega_k$, such that the corresponding $\mathbf{u}^k = \mathbf{r}^{-1}$. In phase two, they iterate using descent-only directions to reach a PO $x^* \in \mathcal{P}$. However, their method does not guarantee that the outcome of second phase x^* also lies in Ω_k . Moreover, to reach a desired EPO solution, they have to increase the number of reference vectors \mathbf{u}^k exponentially with increase in number of objectives m . Their method, by design, does not reach an EPO solution but only in the sub-regions of the PF between the references (see §5.1 and Appendix D.3).

3 Exact Pareto Optimal Search Algorithms

Our key idea is to gain control over the trajectory of objective vectors in the objective space \mathbb{R}^m so that an iterative algorithm can efficiently reach the desired solution. To *anchor* the iterations, we design suitable vector fields on \mathbb{R}^m by defining their direction:

Definition 2 (Anchoring Direction). *We call an element of the tangent space \mathcal{T} of the objective space \mathbb{R}^m an Anchoring direction, denoted by $\mathbf{a}(\mathbf{f}) \in \mathcal{T}_{\mathbb{R}^m}(\mathbf{f})$, where $\mathbf{f} \in \mathbb{R}^m$ is the footpoint.*

To find the EPO solution by an iterative procedure, it is not sufficient to advance only along the descent directions (3) because it leads to an arbitrary solution in the PF. Moreover, even if $\mathbf{f}^{t+1} < \mathbf{f}^t$ for every t , the solution may not lie on the \mathbf{r}^{-1} ray (figure 1b), and hence will not satisfy the condition in (6). Therefore, apart from a descent direction that moves the objective vector \mathbf{f}^t closer to the PF, we also need to consider a search direction $\mathbf{d} \in \mathbb{R}^n$ (tangent space of \mathbb{X}) that moves the objective vector \mathbf{f}^t “closer” to the \mathbf{r}^{-1} ray. To find such a direction, in §3.1, first we define a general *Proportionality Gauge* (PG) to measure the closeness between \mathbf{f}^t and \mathbf{r}^{-1} and analyze its properties. Then we present three specific examples of PGs whose (scaled) gradient fields, called as *balancing anchor directions*, can advance the iterates $\{\mathbf{f}^t\}_{t=1,2,\dots}$ closer towards the \mathbf{r}^{-1} ray, while maintaining $\mathbf{f}^{t+1} \not\prec \mathbf{f}^t$. In §3.2, we present *descending anchor direction* to advance closer to the PF with $\mathbf{f}^{t+1} < \mathbf{f}^t$. We then develop two MOO algorithms in §3.4 and §3.5 to reach an EPO solution, starting from a random initialization in \mathbb{X} and \mathcal{P} respectively, by using both balancing and descending anchor directions.

3.1 Proportionality of Vectors and Balancing Direction

Definition 3 (Proportionality Gauge). *A function $\omega : \mathbb{R}_+^m \times \mathbb{R}_{++}^m \rightarrow \mathbb{R}_+$ is called a Proportionality Gauge, if, for any given inputs $\mathbf{f} \in \mathbb{R}_+^m$ and $\mathbf{r} \in \mathbb{R}_{++}^m$, we have:*

1. $\omega(\mathbf{f}, \mathbf{r}^{-1}) = 0$ only when \mathbf{f} is a positive scalar multiple of \mathbf{r}^{-1} , and
2. $\omega_r(\cdot) = \omega(\cdot, \mathbf{r}^{-1})$ is differentiable w.r.t \mathbf{f} and increases monotonically along $(1 - \lambda)\mathbf{r}^{-1} + \lambda\mathbf{f}$, for $\lambda \geq 0$, with increment in λ .

For a given weight vector \mathbf{r} and a point \mathbf{f} , we define an anchor direction as $\mathbf{a}(\mathbf{f}) := s\nabla_{\mathbf{f}}\omega_{\mathbf{r}}$ for some $s > 0$. We use it to characterize a search direction $\mathbf{d} \in \mathbb{R}^n$ to move the objective vector $\mathbf{f}(\mathbf{x})$ closer to \mathbf{r}^{-1} ray.

Lemma 1. *If all the objective functions are differentiable, then for any direction $\mathbf{d} \in \mathbb{R}^n$ satisfying $\mathbf{a}^T \mathbf{F} \mathbf{d} \geq 0$, where \mathbf{F} is the Jacobian of \mathbf{f} at \mathbf{x} , and $\max_j \{\mathbf{d}^T \nabla_{\mathbf{x}} f_j\} > 0$, there exists a step size $\eta_0 > 0$ such that for all $\eta \in [0, \eta_0]$*

$$\omega(\mathbf{f}(\mathbf{x} - \eta\mathbf{d}), \mathbf{r}^{-1}) \leq \omega(\mathbf{f}(\mathbf{x}), \mathbf{r}^{-1}), \quad \text{and} \quad (9a)$$

$$\mathbf{f}(\mathbf{x} - \eta\mathbf{d}) \not\prec \mathbf{f}(\mathbf{x}). \quad (9b)$$

A move against the search direction \mathbf{d} of Lemma 1 reduces the variations in relative objective values $f_j r_j$ to make them equal: brings *balance* among the values of $\mathbf{f} \odot \mathbf{r} = [f_1 r_1, \dots, f_m r_m]$. Therefore, we call this \mathbf{d} a *Balancing Search Direction*, and a *Balancing Anchor Direction*. We call a

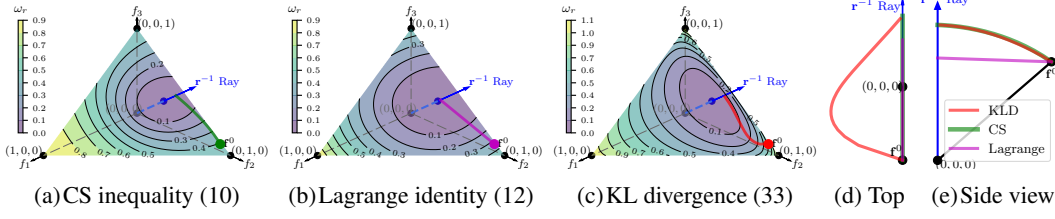


Figure 3: (Color Online) Contour plots in 3c, 3a and 3b show the variation of $\omega_{\mathbf{r}}$ in proportionality measuring functions (33), (10) and (12) respectively on the 2-d simplex \mathcal{S}^3 . These sub-figures use the same weight vector, $\mathbf{r} = [0.6, 0.2, 0.2]$, and the same view, perspective projection on \mathcal{S}^3 from $(1, 1, 1)$ direction towards origin. The trajectories from \mathbf{f}^0 to \mathbf{r}^{-1} ray are obtained by solving $\frac{d\mathbf{f}(t)}{dt} = -\mathbf{a}$ with same initial condition $\mathbf{f}(0) = \mathbf{f}^0 = [0.01, 0.9, 0.09]$ and time interval $t \in [0, 1.5]$ (integrated numerically in 150 steps), where \mathbf{a} is the corresponding anchor direction in (34), (11) and (13) respectively. Figures 3e and 3d show the orthogonal projections of these trajectories on the planes spanned by $\{\mathbf{r}^{-1}, \mathbf{f}^0\}$ and $\{\mathbf{r}^{-1} - \mathbf{f}^0, (\mathbf{r}^{-1} - \mathbf{f}^0) \times (\mathbf{r}^{-1} + \mathbf{f}^0)\}$ respectively, where \times is the vector cross product operator.

balancing anchor direction \mathbf{a} *Scale Invariant* to \mathbf{r} if $\nabla_{\mathbf{f}} \omega_{s\mathbf{r}} = \nabla_{\mathbf{f}} \omega_{\mathbf{r}}$ for all $s > 0$. Using the scale invariant property, we further narrow down the characteristics of a balancing search direction.

Theorem 1. *If a balancing anchor direction \mathbf{a} is scale invariant to \mathbf{r} and all the objective functions are differentiable at \mathbf{x}^t , then moving against a direction $\mathbf{d} \in \mathbb{R}^n$ with $F\mathbf{d} = s\mathbf{a}$, for some $s > 0$, yields a non-dominated solution \mathbf{x}^{t+1} such that $\mathbf{f}(\mathbf{x}^{t+1})$ is closer to the \mathbf{r}^{-1} ray than $\mathbf{f}(\mathbf{x}^t)$.*

Note that for a small step size η , the difference between the consecutive objective vectors can be approximated as $\Delta\mathbf{f} = \mathbf{f}^{t+1} - \mathbf{f}^t \approx -\eta F\mathbf{d}$ from the first order Taylor series expansion. So, the search direction in Theorem 1 moves the objective vector *against* the balancing anchor direction \mathbf{a} (i.e., along $-\mathbf{a}$) in the objective space. In the following, we propose three different functions – using Cauchy–Schwarz inequality, Lagrange’s identity and KL divergence – for gauging the proportionality between two vectors and analyze them based on their respective balancing anchor directions.

3.1.1 Proportionality Gauge from Cauchy–Schwarz (CSZ) Inequality:

The CSZ inequality of our non-zero vectors $\mathbf{f}, \mathbf{r}^{-1} \in \mathbb{R}_+^m$, $\langle \mathbf{f}, \mathbf{r}^{-1} \rangle^2 \leq \|\mathbf{f}\|^2 \|\mathbf{r}^{-1}\|^2$, is tight (equal) when both the vectors are proportional to each other. Rearranging the terms to one side, we get the following

$$\omega(\mathbf{f}, \mathbf{r}^{-1}) = \frac{1}{2} \left(1 - \frac{\langle \mathbf{f}, \mathbf{r}^{-1} \rangle^2}{\|\mathbf{f}\|^2 \|\mathbf{r}^{-1}\|^2} \right), \quad (10)$$

which satisfies properties 1 and 2 of a proportionality gauge. Figure 3a shows the corresponding $\omega_{\mathbf{r}}$ in case of 3 objectives and a particular weight vector. We formulate its anchoring direction as

$$\mathbf{a}(\mathbf{f}) = \langle \vec{\mathbf{f}}, \vec{\mathbf{r}^{-1}} \rangle^2 \vec{\mathbf{f}} - \langle \vec{\mathbf{f}}, \vec{\mathbf{r}^{-1}} \rangle \vec{\mathbf{r}^{-1}}, \quad (11)$$

where $\vec{\mathbf{v}}$ is the ℓ_2 normalization of a vector \mathbf{f} . This \mathbf{a} is scale invariant to \mathbf{r}^{-1} and has the same direction as the gradient $\mathbf{a} = \|\mathbf{f}\| \nabla_{\mathbf{f}} \omega_{\mathbf{r}}$. Its main benefit is drawn from the following.

Claim 1. *The anchor direction \mathbf{a} in (11) is always orthogonal to the objective vector \mathbf{f} : $\mathbf{a}^T \mathbf{f} = 0$.*

The change in consecutive objective vectors $\Delta\mathbf{f} = \mathbf{f}^{t+1} - \mathbf{f}^t$ is approximately aligned to $-\mathbf{a}^t$. Therefore, Claim 1 suggests that $\Delta\mathbf{f}^T \mathbf{f}^t \approx 0$. In other words, since \mathbf{f} is an all positive vector, changes in some objectives Δf_j are positive and others are negative. The advantage of an orthogonal anchoring direction lies in its ability to simultaneously ascend and descend which helps in escaping a PO solution that is not an EPO solution (formalized in Theorem 3).

Since \mathbf{a} is a linear combination of \mathbf{f} and \mathbf{r}^{-1} , the trajectory of the objective vectors lies in the span of $\{\mathbf{r}^{-1}, \mathbf{f}^0\}$. However, it does not result in the shortest trajectory to reach \mathbf{r}^{-1} ray (see Figure 3e). The shortest path between a point \mathbf{f}^0 and the \mathbf{r}^{-1} ray is the line segment from \mathbf{f}^0 orthogonal to the \mathbf{r}^{-1} ray, wherein every $\Delta\mathbf{f}$, and hence $\mathbf{a}(\mathbf{f})$, should be orthogonal to the \mathbf{r}^{-1} ray at all $\mathbf{f} \in \mathbb{R}^m$.

3.1.2 Proportionality Gauge from Lagrange's Identity:

The difference between both sides of CSZ inequality, known as Lagrange's Identity, can be a proportionality gauge:

$$\omega(\mathbf{f}, \mathbf{r}^{-1}) = \frac{1}{2\|\mathbf{r}^{-1}\|^2} (\|\mathbf{f}\|^2 \|\mathbf{r}^{-1}\|^2 - \langle \mathbf{f}, \mathbf{r}^{-1} \rangle^2) = \frac{1}{\|\mathbf{r}^{-1}\|^2} \frac{1}{4} \sum_{j=1}^m \sum_{k=1}^m (f_j r_k^{-1} - f_k r_j^{-1})^2. \quad (12)$$

It satisfies both conditions 1 and 2 of a proportionality measuring function. The factor $1/\|\mathbf{r}^{-1}\|^2$ in (12) makes its anchoring direction scale invariant to \mathbf{r} and we equate to the gradient $\nabla_{\mathbf{f}} \omega_{\mathbf{r}}$:

$$\mathbf{a}(\mathbf{f}) = \mathbf{f} - \frac{\langle \mathbf{f}, \mathbf{r}^{-1} \rangle}{\|\mathbf{r}^{-1}\|^2} \mathbf{r}^{-1}. \quad (13)$$

This anchor direction can yield the trajectory of shortest path, as shown in figure 3e.

Claim 2. *The anchor direction \mathbf{a} in (13) is always orthogonal to the \mathbf{r}^{-1} ray: $\mathbf{a}^T \mathbf{r}^{-1} = 0$.*

Note, when \mathbf{f} and \mathbf{r}^{-1} are not proportional, \mathbf{a} and \mathbf{f} are not orthogonal as $\mathbf{a}^T \mathbf{f} > 0$. As a result, this anchor direction may not escape a PO solution that is not EPO, because orthogonality of \mathbf{a} and \mathbf{f} is a necessary condition for non-convergence at a non-EPO solution in Theorem 3. In its proof, we discuss a corner case where the \mathbf{a} in (13) cannot escape a non-EPO solution.

3.1.3 Proportionality Gauge from KL Divergence:

In §A.1, we present this proportionality gauge, which measures the KL divergence between $\frac{\mathbf{f} \odot \mathbf{r}}{\|\mathbf{f} \odot \mathbf{r}\|_1}$ and the uniform vector $\mathbf{1}/m$. Figure 3c shows the corresponding $\omega_{\mathbf{r}}$ in case of 3 objectives. However, we do not use it since its anchoring direction neither produces the shortest path nor belongs to $\text{span}(\{\mathbf{r}^{-1}, \mathbf{f}^0\})$, as shown in Figures 3c and 3d.

We compare the proportionality gauges and their anchor directions in §A.2.

3.2 Descending Direction

When the iterate \mathbf{f}^t is on or close to the \mathbf{r}^{-1} ray, i.e. $\omega(\mathbf{f}^t, \mathbf{r}^{-1}) < \epsilon$ for small $\epsilon > 0$, to reach the EPO solution, we require descent for every objective. To guarantee descent for all, we choose

$$\mathbf{a}(\mathbf{f}) = \mathbf{f}. \quad (14)$$

Because if the search direction satisfies $\mathbf{F}\mathbf{d} = \mathbf{f}$, then $\mathbf{d}^T \nabla_{\mathbf{x}} f_j = f_j \geq 0$ for all $j \in [m]$ as $\mathbf{f} \in \mathbb{R}_+^m$, hence \mathbf{d} would be a descent direction. When $\mathbf{a} = \mathbf{f}$, we call it a *Descending Anchor* direction. It can be considered as the gradient field of $\frac{1}{2} \|\mathbf{f}\|^2$.

3.3 Quadratic Program for Modelling the Search Direction

We now develop iterative methods to find the EPO solution w.r.t a weight vector \mathbf{r} . In each iteration, we solve a *Quadratic Programming* (QP) problem to obtain a search direction $\mathbf{d} \in \mathcal{T}_{\mathcal{X}}(\mathbf{x}^t)$, the tangent plane (or cone, if \mathcal{X} is constrained, see §B) at $\mathbf{x}^t \in \mathcal{X}$, such that it corresponds to an anchor direction $\mathbf{a} \in \mathcal{T}_{\mathcal{O}}(\mathbf{f}^t)$, the tangent plane at $\mathbf{f}(\mathbf{x}^t) \in \mathcal{O} \subset \mathbb{R}^m$.

We model the search direction as a linear combination of the objective gradients, i.e., $\mathbf{d} = \sum_{j=1}^m \beta_j \nabla_{\mathbf{x}} f_j = \mathbf{F}^T \boldsymbol{\beta}$ and compute the optimal coefficients $\boldsymbol{\beta}^* \in \mathbb{R}^m$ by solving

$$\boldsymbol{\beta}^* = \arg \min_{\|\boldsymbol{\beta}\|_1 \leq 1} \|\mathbf{F}\mathbf{F}^T \boldsymbol{\beta} - \mathbf{a}\|^2, \quad (15)$$

so that $\mathbf{F}\mathbf{d}$ is aligned to the anchor direction as much as possible. Note that, unlike Désidéri (2012), we do not restrict \mathbf{d} to the convex hull of the positive gradients $\mathcal{CH}_{\mathbf{x}}$ (4) to model only descent directions. With coefficients $\boldsymbol{\beta}$ in the ℓ_1 ball, we facilitate gradient ascent for some of the objectives whenever necessary by allowing \mathbf{d} to be in the convex hull of both positive and negative gradients:

$$\mathcal{CH}_{\mathbf{x}}^{\pm} := \left\{ \sum_{j=1}^m \nabla_{\mathbf{x}} f_j \beta_j^+ + \sum_{j=1}^m -\nabla_{\mathbf{x}} f_j \beta_j^- \mid [\boldsymbol{\beta}^+, \boldsymbol{\beta}^-]^T \in \mathcal{S}^{2m} \right\}. \quad (16)$$

Depending on the choice of anchor direction in (15), there could be two **modes of operation**:

Algorithm 1 EPO Search for Random initialization

```

1: Input:  $\mathbf{x}^0 \in \mathbb{X}$ ,  $\mathbf{r} \in \mathbb{R}^m$ ,  $\eta$ ,  $\epsilon_1$ ,  $\epsilon_2$   $\triangleright \mathbf{x}^0 \notin \mathcal{P}$ 
2: while maximum iterations not reached do
3:   if  $\omega_{\mathbf{r}}(\mathbf{f}(\mathbf{x}^t)) \leq \epsilon_1$  then  $\mathbf{a} =$  Lagrange anchor from (13)  $\triangleright$  Balance mode
4:   else  $\mathbf{a} =$  Descending anchor from (14)  $\triangleright$  Descent mode
5:    $\mathbf{d}_{nd} = \mathbf{F}^T \boldsymbol{\beta}^*$ ,  $\boldsymbol{\beta}^*$  obtained by solving the QP (17)  $\triangleright$  (39) for constrained MOO
6:   if  $\|\mathbf{d}_{nd}\| \leq \epsilon_2$  then break  $\triangleright$  Check for convergence
7:    $\mathbf{x}^{t+1} = \mathbf{x}^t - \eta \mathbf{d}_{nd}$ 
8: Output:  $(\mathbf{x}^t, \mathbf{f}^t)$ 

```

1. **Balance mode**, where a balancing anchor directions, based on either CSZ inequality (11) or Lagrange's identity (13), is used to improve the proportionality between \mathbf{f} and \mathbf{r}^{-1} .
2. **Descent mode**, where a descending anchor direction (14) is used to decrease $f_j \forall j \in [m]$.

3.4 EPO Search from Random Initialization

When the goal is to find the EPO solution for a given \mathbf{r} starting from a random initialization $\mathbf{x}^0 \in \mathbb{X}$, we use the balance mode with the anchor direction from Lagrange's identity (13) for every iteration until \mathbf{f}^t is (nearly) proportional to \mathbf{r}^{-1} , $\omega(\mathbf{f}^t, \mathbf{r}^{-1}) < \epsilon_1$ for a small $\epsilon_1 > 0$. After that, we use the descent mode until convergence, $\|d\| \leq \epsilon_2$ for a small $\epsilon_2 > 0$. We extend the QP in (15) (see §B.1 for its extension to constrained MOO problem) to solve

$$\boldsymbol{\beta}^* = \arg \min_{\|\boldsymbol{\beta}\|_1 \leq 1} \|\mathbf{F}\mathbf{F}^T \boldsymbol{\beta} - \mathbf{a}\|^2 \quad (17a)$$

$$\text{s.t. } \boldsymbol{\beta}^T \mathbf{F} \nabla f_j \geq 0 \quad \forall j \in \mathbf{J} = \begin{cases} \mathbf{J}^* & \text{in balance mode} \\ [m] & \text{in descent mode} \end{cases}, \quad (17b)$$

$$\text{where } \mathbf{J}^* = \left\{ j \in [m] \mid j = \arg \max_{j' \in [m]} f_{j'} r_{j'} \right\} \quad (17c)$$

is the index set of maximum relative objective values. We call the resulting $\mathbf{d}_{nd} = \mathbf{F}^T \boldsymbol{\beta}^*$ a *Non-Dominating Search Direction*, because it can yield a solution \mathbf{x}^{t+1} that is not dominated by \mathbf{x}^t , i.e. $\mathbf{f}^{t+1} \not\prec \mathbf{f}^t$. We state this formally for the balance mode in Lemma 2 and descent mode in Lemma 3 with a regularity assumption. In the terminology of differentiable maps, \mathbf{x}^t is a *Regular Point* of the vector valued function \mathbf{f} , if its Jacobian $\mathbf{F}(\mathbf{x}^t)$ is full rank.

Lemma 2. *If \mathbf{x}^t is a regular point of the differentiable vector function \mathbf{f} in a balance mode, i.e. $\omega(\mathbf{f}^t, \mathbf{r}^{-1}) > \epsilon_1$, then the non-dominating direction obtained from QP (17) makes*

1. *non-negative angles with the gradients of maximum relative objectives: $\mathbf{d}_{nd}^T \nabla_{\mathbf{x}^t} f_j \geq 0 \forall j \in \mathbf{J}^*$ (17c),*

2. *a positive angle with the balancing anchor direction (13) in the objective space: $\mathbf{a}^T \mathbf{F} \mathbf{d}_{nd} > 0$.*

Lemma 3. *If \mathbf{x}^t is a regular point of the differentiable vector function \mathbf{f} in a descent mode, i.e. $\omega(\mathbf{f}^t, \mathbf{r}^{-1}) \leq \epsilon_1$, then the non-dominating direction obtained from QP (17) makes a non-negative angle with every gradient, $\mathbf{d}_{nd}^T \nabla_{\mathbf{x}^t} f_j^t \geq 0 \forall j \in [m]$, and a positive angle with at least one gradient.*

A positive angle with the gradient means moving against \mathbf{d}_{nd} will reduce the corresponding objective value. Lemmas 2 and 3 are true even without the constraint (17b) ((39d) for constrained MOO) if $\mathbf{a} \in \{\mathbf{F}\mathbf{d} \mid \mathbf{d} \in \mathcal{CH}_{\mathbf{x}}^{\pm}\}$, where $\mathcal{CH}_{\mathbf{x}}^{\pm}$ is defined in (16). Also, the Lemmas are true at certain *irregular* points $\mathbf{x} \in \mathbb{X}$ whose Jacobian matrices are not full rank (discussed in the proof).

We summarize our EPO Search procedure for random initialization in Algorithm 1. A practically useful variation to improve the descent mode is discussed in Appendix D.2.

3.4.1 Convergence.

We prove the convergence of Algorithm 1 in two steps. First we define an admissible set $\mathcal{A}_{\mathbf{f}^t}^{\mathbf{r}} \subset \mathbb{R}^m$ that contains potential objective vectors $\mathbf{f}^{t+1} = \mathbf{f}(\mathbf{x}^{t+1})$ to which the EPO Search in Algorithm 1

can reach. Then we prove that the sequence of sets $\{\mathcal{A}_{\mathbf{f}^t}^r\}_t$ converges to \mathcal{P}_r , the set containing the EPO solutions. The results hold true for both constrained and unconstrained MOO problems, as detailed in the proofs.

To characterize the properties of \mathbf{x}^{t+1} obtained by moving against \mathbf{d}_{nd} , we define some sets in \mathbb{R}^m that are illustrated in Figure 4. The set of all attainable objective vectors that dominate the \mathbf{f}^t is denoted as $\mathcal{V}_{\leq \mathbf{f}^t}$ (18). The set of all attainable objective vectors that have better proportionality than \mathbf{f}^t is denoted as $\mathcal{M}_{\mathbf{f}^t}^r$ (19). During a descent mode $\mathbf{f}^{t+1} \in \mathcal{V}_{\leq \mathbf{f}^t}$, and in a balance mode $\mathbf{f}^{t+1} \in \mathcal{M}_{\mathbf{f}^t}^r$. For the t^{th} iteration, we define a point $\check{\mathbf{f}}^t \in \mathbb{R}^m$ as in (20), where λ^t is the maximum relative objective value. Finally, using $\check{\mathbf{f}}^t$, we define the admissible set¹ of an iteration in EPO Search Algorithm 1 as $\mathcal{A}_{\mathbf{f}^t}^r$ (22a) for any mode, balance or descent.

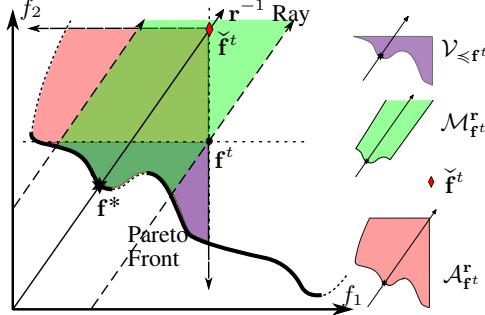


Figure 4: (Color Online). Illustration of the sets associated with the admissible set $\mathcal{A}_{\mathbf{f}^t}^r$ in the objective space \mathbb{R}^2 , at iteration t . This admissible set contains the objective vector \mathbf{f}^{t+1} of next iteration.

$$\mathcal{V}_{\leq \mathbf{f}^t} = \{\mathbf{f} \in \mathcal{O} \mid \mathbf{f} \leq \mathbf{f}^t\} \quad (18)$$

$$\mathcal{M}_{\mathbf{f}^t}^r = \{\mathbf{f} \in \mathcal{O} \mid \omega_r(\mathbf{f}) \leq \omega_r(\mathbf{f}^t)\} \quad (19)$$

$$\check{\mathbf{f}}^t = \lambda^t (1/r_1, \dots, 1/r_m), \quad (20)$$

$$\text{where } \lambda^t = \max \{f_j^t r_j \mid j \in [m]\}$$

$$\begin{aligned} \mathcal{A}_{\mathbf{f}^t}^r &= \{\mathbf{f} \in \mathcal{O} \mid \mathbf{f} \leq \check{\mathbf{f}}^t\} \quad (21) \\ &\supset \underbrace{(\mathcal{A}_{\mathbf{f}^t}^r \cap \mathcal{M}_{\mathbf{f}^t}^r)}_{\text{balance mode}} \cup \underbrace{\mathcal{V}_{\leq \mathbf{f}^t}}_{\text{descent mode}} \end{aligned}$$

Clearly, the admissible set contains all the points in \mathcal{O} that dominate the \mathbf{f}^t , $\mathcal{V}_{\leq \mathbf{f}^t} \subset \mathcal{A}_{\mathbf{f}^t}^r$. Moreover, when $\omega_r(\mathbf{f}^t) > 0$, it also has points with better proportionality than \mathbf{f}^t , $\mathcal{A}_{\mathbf{f}^t}^r \cap \mathcal{M}_{\mathbf{f}^t}^r \neq \emptyset$. Therefore, using Lemmas 2 and 3, we can state the following.

Lemma 4. *If \mathbf{x}^t is a regular point of \mathbf{f} , there exists a step size $\eta_0 > 0$, such that for every $\eta \in [0, \eta_0]$, the objective vector of $\mathbf{x}^{t+1} = \mathbf{x}^t - \eta \mathbf{d}_{nd}$ lies in the t^{th} admissible set: $\mathbf{f}(\mathbf{x}^{t+1}) \in \mathcal{A}_{\mathbf{f}^t}^r$.*

We extend the regularity assumption of \mathbf{f} to all points in $\mathcal{X} \setminus \mathcal{P}$ to state the convergence result.

Theorem 2. *If \mathbf{f} is a differentiable regular vector valued objective, then the sequence of admissible sets $\{\mathcal{A}_{\mathbf{f}^t}^r\}$, which correspond to the solutions $\{\mathbf{x}^t\}$ produced according to Lemma 4 starting from a non-Pareto Optimal point $\mathbf{x}^0 \notin \mathcal{P}$, converges by decreasing monotonically $\mathcal{A}_{\mathbf{f}^{t+1}}^r \subset \mathcal{A}_{\mathbf{f}^t}^r$.*

When \mathcal{P}_r is a singleton set then $\{\mathcal{A}_{\mathbf{f}^t}^r\}$ converges to \mathcal{P}_r . Note, if an EPO solution does not exist for the given preference $\mathcal{P}_r = \emptyset$, i.e. \mathbf{r}^{-1} ray does not intersect the PF \mathcal{P} , then EPO search finds the intersection point between \mathbf{r}^{-1} ray and $\partial\mathcal{O}$, the boundary of the attainable objective vectors. If the \mathbf{r}^{-1} ray does not intersect $\partial\mathcal{O}$, then EPO search finds the point in $\partial\mathcal{O}$ that is maximally proportional to the \mathbf{r}^{-1} ray.

3.5 EPO Search for Tracing the Pareto Front from $\mathbf{x}^0 \in \mathcal{P}$

If the initialization \mathbf{x}^0 itself is a PO solution, then we can modify the EPO search of Algorithm 1 to trace the PF from \mathbf{x}^0 to \mathbf{x}_r^* , an EPO solution w.r.t. weight vector \mathbf{r} , and obtain new PO solutions along the trajectory. In the modified algorithm we use CSZ inequality-based anchor direction (11) in the balance mode because it is orthogonal to the objective vector (see Claim 1), and guarantees to escape the local PO at \mathbf{x}^t to a new point (justified in the proof of Theorem 3). However, if we use only the balance mode until $\omega(\mathbf{f}^t, \mathbf{r}^{-1}) \geq \epsilon_1$ for a small $\epsilon_1 > 0$, the trajectory may drift away from the PF, especially for convex objective functions (see §D.1.1). Therefore, to ensure that the objective

¹The admissible set of an iteration in the CS (1) is $\{\mathbf{f} \in \mathcal{O} \mid f_{j^*} \leq f_{j^*}^t\}$, where $j^* = \arg \max_{j \in [m]} f_j^t r_j$.

Algorithm 2 EPO Search for Pareto Optimal Initialization

```

1: Input:  $\mathbf{x}^0 \in \mathbb{X}$ ,  $\mathbf{r} \in \mathbb{R}^m$ ,  $\eta$ ,  $\epsilon_1, \epsilon_2$  ▷  $\mathbf{x}^0 \in \mathcal{P}$ 
2:  $mode = 0$  ▷ 0 for balance mode, 1 for descent mode
3: while  $\omega_{\mathbf{r}}(\mathbf{f}(\mathbf{x}^t)) > \epsilon_1$  or  $t < \text{maximum iterations}$  do ▷ CSZ inequality-based  $\omega$  (10)
4:   if  $mode = 0$  then  $\mathbf{a} = \text{CSZ inequality-based anchor}$  (11) ▷ Balance mode
5:   else  $\mathbf{a} = \text{descent anchor from}$  (14) ▷ Descent mode
6:    $\mathbf{d}_{nd} = \mathbf{F}^T \boldsymbol{\beta}^*$ ,  $\boldsymbol{\beta}^*$  obtained by solving the QP (22) ▷ (40) for constrained MOO
7:   if  $mode = 0$  and  $\|\mathbf{d}_{nd}\| \leq \epsilon_2$  then break ▷ Check for convergence only in balance mode
8:    $\mathbf{x}^{t+1} = \mathbf{x}^t - \eta \mathbf{d}_{nd}$ ,  $mode = 1 - mode$  ▷ Alternates mode while tracing the PF
9: Output:  $\{\mathbf{x}^i\}_{i=0}^t$  ▷ Trace of EPO Search on  $\mathcal{P}$ 

```

vectors \mathbf{f}^t in EPO search trajectory stay close to the PF, we alternate between the balance mode and descent mode in every iteration. To ensure the proportionality gauge (10) does not increase in the descent mode, we extend the QP (15) (see §B.2 for its extension to constrained MOO) as follows

$$\boldsymbol{\beta}^* = \arg \min_{\|\boldsymbol{\beta}\|_1 \leq 1} \|\mathbf{F}\mathbf{F}^T \boldsymbol{\beta} - \mathbf{a}\|^2 \quad (22a)$$

$$\text{s.t. } \mathbb{1}_{des} \boldsymbol{\beta}^T \mathbf{F}\mathbf{F}^T \mathbf{a}^{bal} \geq 0, \quad (22b)$$

$$\text{and } \mathbb{1}_{des} \boldsymbol{\beta}^T \mathbf{F} \nabla f_j \geq 0 \quad \forall j \in [m], \quad (22c)$$

where \mathbf{a}^{bal} is the balancing anchor direction (11), and $\mathbb{1}_{des}$ is an indicator variable for descent mode, which applies the constraint (22b) only in the descent mode. But the stopping criteria is checked only in the balance mode: the goal is to keep *balancing* the relative objective vector $\mathbf{r} \odot \mathbf{f}$ until it is proportional to uniformity $\mathbf{1}$. Note, this balance mode ignores the constraints in (17b) for objectives of J^* (17c) because, if \mathbf{f}^t is on (close to) the PF, then an $f_{j^*}^t$ for $j^* \in J^*$ may need to increment to move towards the EPO solution. Algorithm 2 summarizes the entire method.

3.5.1 Convergence.

We prove the contra-positive: convergence is not achieved until the iterate \mathbf{x}^t is close to $\mathbf{x}_{\mathbf{r}}^* \in \mathcal{P}_{\mathbf{r}}$, and $\omega_{\mathbf{r}}(\mathbf{f}(\mathbf{x}^t))$ keeps decreasing. At an \mathbf{x}^t , the set of descent directions is given by $\mathcal{D}_{\mathbb{X}}^{\mathbf{f}}(\mathbf{x}^t) = \{\mathbf{d} \in \mathcal{T}_{\mathbb{X}}(\mathbf{x}^t) \mid \mathbf{d}^T \nabla_{\mathbf{x}^t} f_j \geq 0, \forall j \in [m]\}$. A necessary condition to check if \mathbf{x}^t is a PO solution, i.e., $\mathcal{D}_{\mathbb{X}}^{\mathbf{f}}(\mathbf{x}^t) = \{\mathbf{0}\}$, is given by Pareto Criticality:

$$\text{there exists a } \boldsymbol{\beta} \in \mathcal{S}^m, \text{ s.t. } \mathbf{F}^T \boldsymbol{\beta} = \mathbf{0}. \quad (23)$$

The Jacobian at an $\mathbf{x}^* \in \mathcal{P}$ is not full rank. However, \mathbf{x}^* is called a *Regular Pareto Optimal* solution if its Jacobian $\mathbf{F}(\mathbf{x}^*)$ has rank $m - 1$ (Zhang et al. 2008). Previous gradient-based methods (Fliege and Svaiter 2000, Désidéri 2012) use the Pareto criticality condition as a stopping criterion, since they use descent directions in every iteration. Therefore, they stop at any local PO solution. In contrast, our method is not designed to find $\boldsymbol{\beta}$ for a descent direction, hence does not stop prematurely at any local PO solution; it traces the Pareto front until an EPO solution is found.

Theorem 3. *If $\mathbf{x}^* \in \mathcal{P}$ is a regular Pareto Optimal solution, and its non-dominating direction $\mathbf{d}_{nd} = \mathbf{F}^T \boldsymbol{\beta}^*$ is obtained by the QP (22) with Cauchy-Schwarz inequality-based balancing anchor (11), then $\mathbf{d}_{nd} = \mathbf{0}$ if and only if $\mathbf{x}^* \in \mathcal{P}_{\mathbf{r}}$.*

Theorem 3 holds for certain cases when the regularity assumptions are not satisfied (discussed in the proof). In our extension to solving constrained MOO problems, we make an additional assumption (see §B.2) and restate the above result in Theorem 5.

3.6 Convergence Rate and Iteration Complexity

The convergence rate of a gradient-based SOO method to reach a stationary point is well known to be sub-linear for non-convex problems and linear for convex problems (Nesterov 2004). Tanabe et al. (2022) extended this result for descent-based MOO methods to reach a Pareto stationary point: sub-linear for non-convex and linear for convex MOO problems.

EPO Search has two modes of operation. In Algorithm 1, when the random initialization is not a PO solution, first the balance mode iterations decrease the value of ω down towards a small value ϵ to align the objective vector to the \mathbf{r}^{-1} ray. Then, the descent mode iterations decrease each objective to reach an EPO solution that also satisfies the Pareto critical condition (23). The descent mode is similar to solving a non-convex SOO problem of the objective $\frac{1}{2}\|\mathbf{f}(\mathbf{x})\|^2$, with sub-linear convergence rate. Here, we show that the balance mode has linear convergence rate. This result is significant because it shows that the EPO Search Algorithm 2, where the initialization is a PO solution, can converge at linear rate to the desired PO solution, even for a non-convex MOO problem. Note, Algorithm 2 traces the PF by alternating between balance and descent modes, where the descent mode does not increase ω but balance mode decreases ω .

We analyze the composite objective function $\omega_{\mathbf{r}} \circ \mathbf{f}$ to prove linear convergence of the balance mode when optimizing non-convex objectives \mathbf{f} . The following Polyak-Łojasiewicz (PŁ) type inequality (Polyak 1963, Hardt 1975, Karimi et al. 2016) is instrumental in our analysis.

Lemma 5. *There exists a $\tau > 0$ such that the proportionality gauges $\omega_{\mathbf{r}}$ (10),(12) and their respective anchor directions \mathbf{a} in (11), (13) satisfy*

$$\frac{1}{2}\|\mathbf{a}(\mathbf{f})\|^2 \geq \tau\omega_{\mathbf{r}}(\mathbf{f}) \quad \forall \tau \leq \begin{cases} \langle \vec{\mathbf{f}}_0, \mathbf{r}^{-1} \rangle^2 \\ 1 \end{cases} \quad \text{and} \quad \forall \mathbf{f} \in \begin{cases} \mathcal{M}_{\mathbf{f}^0}^{\mathbf{r}} & \text{if Cauchy-Schwarz inequality} \\ \mathcal{O} & \text{if Lagrange's identity,} \end{cases} \quad (24)$$

where $\mathbf{f}^0 = \mathbf{f}(\mathbf{x}^0)$ is the initialization, $\vec{\mathbf{v}}$ is the ℓ_2 normalization of vector \mathbf{v} , and $\mathcal{M}_{\mathbf{f}^0}^{\mathbf{r}}$ is as in (19).

The inequality (24) suggests that the magnitude of anchor direction grows quadratically w.r.t. the value of the proportionality gauge. Our additional assumptions are as follows.

Assumption 1 (Compactness). *The image \mathcal{O} of the objectives is a compact set in \mathbb{R}^m , upper bounded by a nadir point \mathbf{f}^{ndr} and lower bounded by a minimum magnitude $M > 0$: $M \leq \|\mathbf{f}\| \leq \|\mathbf{f}^{ndr}\| \forall \mathbf{f} \in \mathcal{O}$. The anchor directions (11) and (13) are bounded by W : $\|\mathbf{a}(\mathbf{f})\| \leq W \forall \mathbf{f} \in \mathcal{O}$.*

Assumption 2 (Smoothness). *The gradients of each objective function is Lipschitz smooth: $\|\nabla f_j(\mathbf{x}^1) - \nabla f_j(\mathbf{x}^2)\| \leq L_j\|\mathbf{x}^1 - \mathbf{x}^2\|$ where $L_j > 0$ for all $j \in [m]$; and $L_{\mathbf{f}} = \max_{j \in [m]} L_j$. The gradient of ω is also assumed to be Lipschitz smooth: $\|\nabla\omega_{\mathbf{r}}(\mathbf{f}^1) - \nabla\omega_{\mathbf{r}}(\mathbf{f}^2)\| \leq L_{\omega}\|\mathbf{f}^1 - \mathbf{f}^2\|$.*

Since the Jacobian is $\mathbf{F} : \mathcal{X} \rightarrow \mathbb{R}^{m \times n}$ is a smooth function, the singular values of \mathbf{F} , $\sigma_j : \mathcal{X} \rightarrow \mathbb{R}_+$ for $j \in [m]$, where $\sigma_1 \leq \sigma_2 \leq \dots \leq \sigma_m$, are also smooth functions. Note, $\sigma_1(\mathbf{x}^*) = 0$ for all $\mathbf{x}^* \in \mathcal{P}$ due to the Pareto criticality condition (23). So far, we assumed Jacobian $\mathbf{F}(\mathbf{x})$ is full rank if $\mathbf{x} \notin \mathcal{P}$ and rank $m - 1$ if $\mathbf{x} \in \mathcal{P}$, as the regularity condition. We make this assumption more specific by considering a δ -neighbourhood around the PF as

$$\mathcal{P}^{\delta} := \{\mathbf{x} \in \mathcal{X} \mid \exists \mathbf{x}^* \in \mathcal{P} \text{ s.t. } \sigma_1(\nu\mathbf{x}^* + (1-\nu)\mathbf{x}) < \delta \forall \nu \in [0, 1]\}. \quad (25)$$

$\mathcal{X} \setminus \mathcal{P}^{\delta}$ can be considered as the operating region for the balance mode of EPO Search Algorithm 1, and \mathcal{P}^{δ} as the operating region of EPO Search Algorithm 2 that traces the PF.

Assumption 3 (Regularity). *There exists a $\delta > 0$ such that the smallest singular value $\sigma_1(\mathbf{x}) \geq \delta$ for all $\mathbf{x} \in \mathcal{X} \setminus \mathcal{P}^{\delta}$ and the second smallest singular value $\sigma_2(\mathbf{x}) \geq \delta$ for all $\mathbf{x} \in \mathcal{P}^{\delta}$.*

With the above three assumptions, we state the linear convergence rate result.

Theorem 4 (Convergence Rate, Iteration Complexity). *If the stepsize is any $\eta \in (0, \eta_0)$, where $\eta_0 = \frac{c_0}{c_0 + \max\{2c_1, 3c_2, 4c_3\}}$, $c_0 = \frac{\delta^2}{s_0\sqrt{m}W^2}$, $c_1 = \frac{1}{2}(L_{\omega} + \frac{L_{\mathbf{f}}m}{s_1})$, $c_2 = \frac{1}{2}L_{\omega}L_{\mathbf{f}}m^2$, $c_3 = \frac{1}{8}L_{\omega}L_{\mathbf{f}}^2m^2$, $s_0 = s_1 = 1$ when $\omega_{\mathbf{r}} = (10)$, and $s_0 = \|\mathbf{f}^{ndr}\|$ and $s_1 = M$ when $\omega_{\mathbf{r}} = (12)$, then the balance mode iterations, using either (11) or (13) as anchor direction, decrease $\omega_{\mathbf{r}}$ linearly:*

$$\omega_{\mathbf{r}}(\mathbf{f}^{t+1}) \leq (1 - 2\tau\eta p(\eta))\omega_{\mathbf{r}}(\mathbf{f}^t) \leq \dots \leq (1 - 2\tau\eta p(\eta))^{t+1}\omega_{\mathbf{r}}(\mathbf{f}^0), \quad (26)$$

where the polynomial $p(\eta) = c_0 - c_1\eta - c_2\eta^2 - c_3\eta^3$ is positive for all $\eta \in (0, \eta_0)$. Consequently, the maximum number of iterations (iteration complexity) required to decrease $\omega_{\mathbf{r}}$ down to ϵ is $O(\log(\frac{1}{\epsilon}))$.

3.6.1 Time Complexity per Iteration:

Both the m dimensional QP problems (17) and (22) are convex, having linear constraints and are independent of the dimension n of the solution space. The former has at most $s = 3m$ inequality constraints, and the latter has at most $s = 3m + 1$ inequality constraints; both have $2m$ inequality constraints for ℓ_1 ball. The QPs can be solved efficiently, e.g., using interior point methods (Cai et al. 2013, Zhang et al. 2021) in $O(m^2s) = O(m^3)$ time. The complexity of the Jacobian matrix multiplication $\mathbf{F}\mathbf{F}^T$ is $O(nm^2)$. Thus, the per-iteration time complexity of both Algorithms 1 and 2 is $O(nm^2 + m^3)$.

4 EPO Search for MCDM and MTL

4.1 Pareto Front Approximation for A posteriori MCDM

With the tracing capability of our algorithm we can move from one PO solution to another, and discover new ones in the path. We use this feature to generate a diverse set of optimal solutions by tracing towards the EPO solutions for different weight vectors. We adopt the *Pattern Efficient Set* Algorithm (PESA) by Stanojević and Glover (2020) for generating a diverse set of weight vectors in the $m - 1$ dimensional Simplex \mathcal{S}^m . PESA is a recursive sampling procedure to approximate the simplex \mathcal{S}^m . Instead of sampling \mathbf{r} , we directly sample the rays \mathbf{r}^{-1} since it is directly (not inversely) associated with the anchor directions. The sampling process in PESA is as follows: given a set of m rays $\mathbf{R}^0 = \{\mathbf{r}_k^{-1} \in \mathcal{S}^m \mid k \in [m]\}$, the next new ray \mathbf{r}_{new}^{-1} is sampled as a convex combination of rays in \mathbf{R}^0 , i.e. $\mathbf{r}_{new}^{-1} = \frac{1}{m} \sum_{k=1}^m \mathbf{r}_k^{-1}$. This new ray creates m more sets, $\mathbf{R}^{0j} = \mathbf{R}^0 \setminus \{\mathbf{r}_j^{-1}\} \cup \{\mathbf{r}_{k+1}^{-1}\}$ for all $j \in [m]$, and one can recursively sample rays from these m sets. Thus, the convex hull of the original set \mathbf{R}^0 is “filled”. If \mathbf{R}^0 consists of the axes of positive orthant in \mathbb{R}^m , then this recursive sampling process approximates the entire simplex.

We integrate this sampling rule with EPO Search algorithm and develop the PESA-EPO Search Algorithm 3 for approximating the PF. Instead of a set of \mathbf{r}^{-1} rays, we maintain a set of PO solutions $\mathbf{R} = \{\mathbf{x}_k^*\}_{k=1}^m$, and sample the next ray as

$$\mathbf{r}_{new}^{-1} = \frac{1}{|\mathbf{R}|} \sum_{\mathbf{x} \in \mathbf{R}} \frac{\mathbf{f}(\mathbf{x})}{\|\mathbf{f}(\mathbf{x})\|_1}. \quad (27)$$

We then run EPO search (Algorithm 2) to trace the PF from $\mathbf{f}(\mathbf{x}_k^*)$ to \mathbf{r}_{new}^{-1} ray for each $\mathbf{x}_k^* \in \mathbf{R}$. This generates m trajectories on the PF. Let ${}^k\mathbf{x}_{\mathbf{r}_{new}^{-1}}^*$ be the end point of the trajectory starting at \mathbf{x}_k^* . This creates m new sets, $\mathbf{R} \setminus \{\mathbf{x}_k^*\} \cup \{{}^k\mathbf{x}_{\mathbf{r}_{new}^{-1}}^*\}$ for all $k \in [m]$, and the same procedure is repeated recursively. The procedure starts with an initial set \mathbf{R} consisting of the optimal solutions of individual objectives, and the recursion stops at a given input depth. In the collection of points obtained from the trajectories, there could be solutions that are dominated by others. In a post-processing step, the dominated solutions are removed.

Note that, the PF $\mathbf{f}(\mathcal{P}) \subset \partial\mathcal{O}$ may be disconnected. But the trajectories of EPO Search can move between different portions of \mathcal{P} if \mathcal{O} is one connected component, which for unconstrained MOO is trivially true, and for constrained MOO is true when the domain \mathcal{X} is a connected component. In case of a bi-objective optimization with a connected PF, a recursion depth of just 1 can approximate the PF. Because for $m = 2$, the PF will be at most a 1-dimensional manifold, and the trajectories of traced EPO Search are also 1-dimensional. This is further clarified in our empirical results (§5.3).

4.2 Preference Elicitation in Interactive MCDM

The key idea of our approach is to operate in the domain of the $m - 1$ dimensional simplex \mathcal{S}^m instead of the high-dimensional solution space \mathcal{X} (or its discrete subset that is used in (8) by previous methods). In our PE, the *data* on which the GP is learnt consists of $\mathbf{r}^{-1} \in \mathcal{S}^m$ instead of $\mathbf{x} \in \mathcal{X}$. Using a mapping $\psi_{\mathbf{f}}$ defined below and EPO Search, we find PO solutions and return to \mathcal{X} .

Let $\psi_{\mathbf{f}} : \mathcal{S}^m \rightarrow \bar{\mathbb{R}}^m$, where $\bar{\mathbb{R}} = \mathbb{R} \cup \{\infty\}$ is the extended real line, be a mapping from the simplex \mathcal{S}^m to the objective space \mathcal{O} defined as

$$\psi_{\mathbf{f}}(\mathbf{r}^{-1}) = s^* \mathbf{r}^{-1} \quad \forall \mathbf{r}^{-1} \in \mathcal{S}^m, \quad \text{where } s^* = \min_{s \geq 0} s \quad \text{s.t. } s\mathbf{r}^{-1} \in \mathcal{O}. \quad (28)$$

Algorithm 3 PESA-EPO for Pareto Front approximation

1: **Input:** $MaxDepth$ \triangleright Depth of maximum recursion for PESA-EPO
 2: **procedure** PESA_EPO($R, depth, MaxDepth$)
 3: $PF = \phi$
 4: **if** $depth \leq MaxDepth$ **then**
 5: Compute \mathbf{r}_{new}^{-1} from (27)
 6: **for** \mathbf{x} in R **do**
 7: $Traces =$ Output of EPO Search Algorithm 2 run for \mathbf{r} starting from $p.\mathbf{x}$
 8: $\mathbf{x}_{new} =$ last solution in $Traces$
 9: $R_{new} = \{\mathbf{x}_{new}\} \cup R \setminus \{\mathbf{x}\}$
 10: $PF = PF \cup Traces \cup$ PESA_EPO($R_{new}, depth + 1, MaxDepth$)
 11: **return** PF
 12: $R = \{\mathbf{x}_j^*\}_{j=1}^m$ \triangleright where $\mathbf{x}_j^* = \arg \min_{\mathbf{x} \in \mathcal{X}} f_j(\mathbf{x})$ for all $j \in [m]$
 13: **Output:** $PF =$ PESA_EPO($R, 1, MaxDepth$)

Algorithm 4 GP-EPO for Preference Elicitation

1: **Input:** $\mathbf{x}^0, \mathbf{x}^1$ $\triangleright \mathbf{x}^0, \mathbf{x}^1 \in \mathcal{P}$
 2: **Initialize:** $\mathbf{x}_{inc} = \mathbf{x}^0, \mathbf{x}_{sug} = \mathbf{x}^1, \hat{\mathcal{D}} = \phi, GP$ \triangleright Initialize $GP.\hat{\mu}$ as zero function
 3: **while** maximum queries not reached **do**
 4: $\mathbf{r}_{inc}^{-1} = \frac{\mathbf{f}_{inc}}{\|\mathbf{f}_{inc}\|_1}, \mathbf{r}_{sug}^{-1} = \frac{\mathbf{f}_{sug}}{\|\mathbf{f}_{sug}\|_1}$
 5: response = QueryDM($\mathbf{f}_{inc}, \mathbf{f}_{sug}$)
 6: **if** response = “incumbent preferred to suggestion” **then** $\hat{\mathcal{D}} = \hat{\mathcal{D}} \cup \{(\mathbf{r}_{inc}^{-1}, \mathbf{r}_{sug}^{-1})\}$
 7: **else if** response = “suggestion preferred to incumbent” **then**
 8: $\hat{\mathcal{D}} = \hat{\mathcal{D}} \cup \{(\mathbf{r}_{sug}^{-1}, \mathbf{r}_{inc}^{-1})\}, \mathbf{x}_{inc} = \mathbf{x}_{sug}, \mathbf{r}_{inc}^{-1} = \mathbf{r}_{sug}^{-1}$
 9: **else** $\hat{\mathcal{D}} = \hat{\mathcal{D}} \cup \{(\mathbf{r}_{inc}^{-1}, \mathbf{r}_{sug}^{-1}), (\mathbf{r}_{sug}^{-1}, \mathbf{r}_{inc}^{-1})\}$
 10: Update $GP.\hat{\mu}$ and $GP.\hat{\kappa}$ with $\hat{\mathcal{D}}$ \triangleright Approximates the posterior $P(\hat{u}|\hat{\mathcal{D}})$
 11: Get \mathbf{r}_{sug}^{-1} by maximizing the updated acquisition function $GP.\hat{\mu}$ (29)
 12: Get $\mathbf{x}_{sug}, \mathbf{f}_{sug}$ from EPO Search Algorithm 2 starting from \mathbf{x}_{inc}
 13: **if** $\mu(\mathbf{f}_{sug}, \mathbf{r}_{sug}) > \epsilon$ **then** $\hat{\mathcal{D}} = \hat{\mathcal{D}} \cup \{(\mathbf{r}_{inc}^{-1}, \mathbf{r}_{sug}^{-1})\}$ $\triangleright \psi(\mathbf{r}_{sug}^{-1})$ in (28) is unreachable
 14: **if** $(\|\mathbf{f}_{inc} - \mathbf{f}_{sug}\| < \epsilon)$ or (DM satisfied) **then break**
 15: **Output:** \mathbf{x}_{inc}

$\psi_{\mathbf{f}}$ maps (scales with factor s^*) a point $\mathbf{r}^{-1} \in \mathcal{S}^m$ in the simplex to a point on $\partial\mathcal{O}$, the boundary of the image \mathcal{O} , if the \mathbf{r}^{-1} ray intersects \mathcal{O} . If it does not intersect \mathcal{O} , then it is mapped to a vector at ∞ , since the scaling factor s^* will be ∞ . Clearly, the image of \mathcal{S}^m under $\psi_{\mathbf{f}}$ covers all the PO solutions, $\psi_{\mathbf{f}}(\mathcal{S}^m) \supseteq \mathbf{f}(\mathcal{P})$. Using EPO search Algorithm 2, for a given $\mathbf{r}^{-1} \in \mathcal{S}^m$, we can reach $\psi_{\mathbf{f}}(\mathbf{r}^{-1})$ and the corresponding EPO solution $\mathbf{x}_{\mathbf{r}}^*$ if it exists. Non-existence can be detected through the value of proportionality gauge, i.e. $\omega_{\mathbf{r}}(\mathbf{f}(\hat{\mathbf{x}}_{\mathbf{r}})) > \epsilon$, where $\hat{\mathbf{x}}_{\mathbf{r}}$ is the output of Algorithm 2.

Instead of modeling the GP prior u for the entire \mathcal{O} , we model $\hat{u} : \mathcal{S}^m \rightarrow \mathbb{R}$, where $\hat{u} = u \circ \psi_{\mathbf{f}}$ with $GP(\hat{\mu}, \hat{\kappa})$, where $\hat{\mu} : \mathcal{S}^m \rightarrow \mathbb{R}$ and $\hat{\kappa} : \mathcal{S}^m \times \mathcal{S}^m \rightarrow \mathbb{R}$. We interactively estimate the utility \hat{u} for PE by maintaining a parallel dataset $\hat{\mathcal{D}}_t = \{\hat{c}_1, \dots, \hat{c}_t\}$, where the ordered pair $\hat{c} = (\mathbf{r}^{-1^i}, \mathbf{r}^{-1^j})$ corresponds to the DM’s comparison of two PO solutions $c = (\mathbf{x}^i, \mathbf{x}^j)$ (see §2.2.2) by using the inverse mapping of $\psi_{\mathbf{f}}$: $\mathbf{r}^{-1^i} = \frac{\mathbf{f}(\mathbf{x}^i)}{\|\mathbf{f}(\mathbf{x}^i)\|_1}$, and similarly for \mathbf{r}^{-1^j} . Thus, we convert the PE for $\mathcal{X} \xrightarrow{\mathbf{f}} \mathbb{R}^m \xrightarrow{u} \mathbb{R}$ into a PE for $\mathcal{S}^m \xrightarrow{\psi_{\mathbf{f}}} \mathbb{R}^m \xrightarrow{u} \mathbb{R}$. Analogous to $\mathbb{X}_{\mathcal{D}_t}$ in §2.2.2, we define $\mathcal{S}_{\mathcal{D}_t}^m$ to be the discrete set of \mathbf{r}^{-1} s whose corresponding \mathbf{x} s have been presented to the DM. Similarly, the incumbent \mathbf{r}_{inc}^{-1} corresponds to \mathbf{x}_{inc} . After updating the GP to approximate the posterior $P(\hat{u}|\hat{\mathcal{D}}_t)$, we obtain

$$\mathbf{r}_{sug}^{-1} = \arg \max_{\mathbf{r}^{-1} \in \mathcal{S}^m} \hat{\alpha}_t(\mathbf{r}^{-1}) \quad (29)$$

as the next suggestion, where $\hat{\alpha}_t$ is the acquisition function formulated using the updated $\hat{\mu}_t$ and $\hat{\kappa}_t$. Then we run EPO Search Algorithm 2 starting from \mathbf{x}_{inc} to find \mathbf{x}_{sug} , the EPO solution for \mathbf{r}_{sug}^{-1} .

If $\omega_{\mathbf{r}}(\mathbf{f}(\mathbf{x}_{sug})) > \epsilon$ is detected, i.e. the \mathbf{r}^{-1} ray does not intersect \mathcal{O} and $\psi(\mathbf{r}^{-1})$ maps to a point at infinity, we augment the dataset \hat{D}_t with $(\mathbf{r}_{inc}^{-1}, \mathbf{r}_{sug}^{-1})$, declaring that \mathbf{r}_{sug}^{-1} is inferior to \mathbf{r}_{inc}^{-1} . Thus, we avoid optimization on the high dimensional domain of solutions \mathbb{X} , and instead do it from the domain of $m - 1$ dimensional \mathcal{S}^m . We summarize our method in Algorithm 4.

GP-EPO does not estimate the utility of non-PO solutions. Although u is defined for all possible alternatives, its estimation for the entire range \mathcal{O} of \mathbf{f} is unnecessary due to the monotonicity property of a utility function. Since the DM’s preferred solution is assumed to be PO, it suffices to estimate the utility only for solutions on the PF. Note that for any non-PO solution \mathbf{x} , we can employ Algorithm 1 to obtain the EPO solution $\mathbf{x}_{\mathbf{r}}^*$ for $\mathbf{r}^{-1} = \frac{\mathbf{f}(\mathbf{x})}{\|\mathbf{f}(\mathbf{x})\|_1}$, which is preferred over \mathbf{x} .

Our approach obviates the need to model additional monotonicity constraints on the GP, done in previous GP-based PE methods (Zintgraf et al. 2018, Roijers et al. 2021). Moreover, unlike (8), we do not discretize the domain in (29), since global optimization of non-linear objectives is computationally feasible for low-dimensional problems by running multiple threads initialized at several seeds in \mathcal{S}^m . Therefore, we can explore the PF at its highest possible resolution. This is facilitated by the linear convergence rate of EPO Search Algorithm 2 (see §3.6) to efficiently obtain the next alternative solution \mathbf{x}^{sug} while interacting with the DM. Note that a CS-based GP procedure cannot achieve this, since CS cannot trace the PF requiring a re-initialization for every query. This can have a sub-linear convergence rate at best, akin to a non-convex SOO algorithm.

4.3 Deep Multi-Task Learning

In many MTL applications, model builders may require trade-offs in the form of priorities among the tasks. Consider m tasks for MTL, indexed by $1 \leq i, j \leq m$. We assume priority specification for each task by numeric values, with higher values indicating higher task priority. Let r_i and f_i denote the priority and loss function for the i^{th} task. For any two tasks, if the priority for the i^{th} task is higher than that of the j^{th} task, i.e., if $r_i \geq r_j$, then we want the network to be trained better for the i^{th} task, i.e., we want the corresponding training losses to follow $f_i \leq f_j$. To the best of our knowledge, current MOO-based MTL methods do not model such priorities.

This can be achieved by training the network using scalarized MOO and we propose the use of CS, which overcomes the limitations of LS (see §2) and satisfies the required inverse relationship between priorities and objective values exactly at the EPO solution, i.e., $r_1 f_1 = \dots = r_j f_j = \dots = r_m f_m$, for all m objectives as shown in Figure 2 (right). Both the problems of oscillation and premature stagnation (especially when there are tasks with low priority weights) are effectively addressed by EPO Search. Further, regularization, in the form of constraints on parameters, may be required in deep MTL models to prevent over-fitting. EPO Search can handle both the unconstrained case and cases of equality, inequality and box constraints (see §B).

These advantages in EPO Search are achieved without compromising on its efficiency. In deep MTL, the number of DNN parameters (n) is typically much greater than the number of tasks (m). The most time-consuming step in EPO Search in such cases is the Jacobian matrix multiplication. Thus, the per-iteration complexity of EPO Search is linear in n and quadratic in m . This is comparable to the method of Sener and Koltun (2018) that neither uses input priorities nor handles constraints. In comparison, gradient descent with CS and LS scale linearly with the number of objectives. However, PMTL scales exponentially with m , as the number of reference vectors required for decomposing the objective space increases exponentially with m (see §5.1).

Priority weights are assumed to be provided as inputs during model training. These weights may be determined based on domain knowledge, data-related factors and application-specific requirements. For instance, tasks that are more difficult due to, e.g., lesser training data, may be given higher priority (as done in our case study §5.5). Priorities may be considered as hyperparameters and automated tuning techniques (Yang and Shami 2020) may be used. Many are based on Bayesian optimization and use GP to model the unknown generalization performance of the model.

5 Experimental Results

5.1 Advantages of EPO Search for gradient descent: A synthetic MOO problem

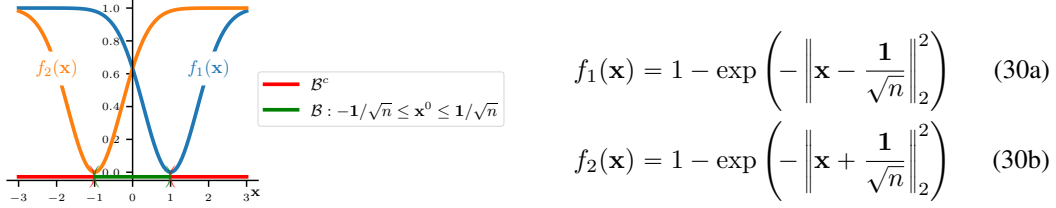


Figure 5: 1d solution space of (30) in hyper-box (31)

We use the problem introduced by Fonseca (1995) to show the advantage of EPO Search (Algorithm 1) over competing approaches: LS, PMTL and CS (where (1) is solved). This problem consists of two non-convex objective functions (30) that are to be minimized over $\mathbf{x} \in \mathbb{R}^n$; Figure 5 shows the functions for $n = 1$. In this problem, the set of PO solutions \mathcal{P} is a subset of the hyper-box defined in (31), where \leq_n denotes the partial ordering induced by the positive cone \mathbb{R}_+^n in the solution space. Note that for $n = 1$, we have $\mathcal{B} = \mathcal{P}$ as shown in Figure 5. We evaluate each MOO algorithm in two scenarios, when the initialization is: (a) inside this hyper-box, i.e., $\mathbf{x}^0 \in \mathcal{B}$, and (b) outside this hyper-box, i.e., $\mathbf{x}^0 \in \mathcal{B}^c$. The latter is more difficult, especially when the EPO is far from the initialization \mathbf{x}^0 . For instance, in Figure 5, if the desired optimal is $x^* = -0.5$ and the initialization is at $x^0 = 2$, the iterate has to escape the minimum of objective f_1 , i.e., $x = 1$, to reach x^* . In other words, without ascending in f_1 , it is not possible to reach x^* from x^0 in a continuous trajectory, i.e., using a gradient-based iterative algorithm. Each algorithm is tested with four weight vectors, spread uniformly over the first quadrant. The number of iterations, step size, and random initializations are the same for all algorithms.

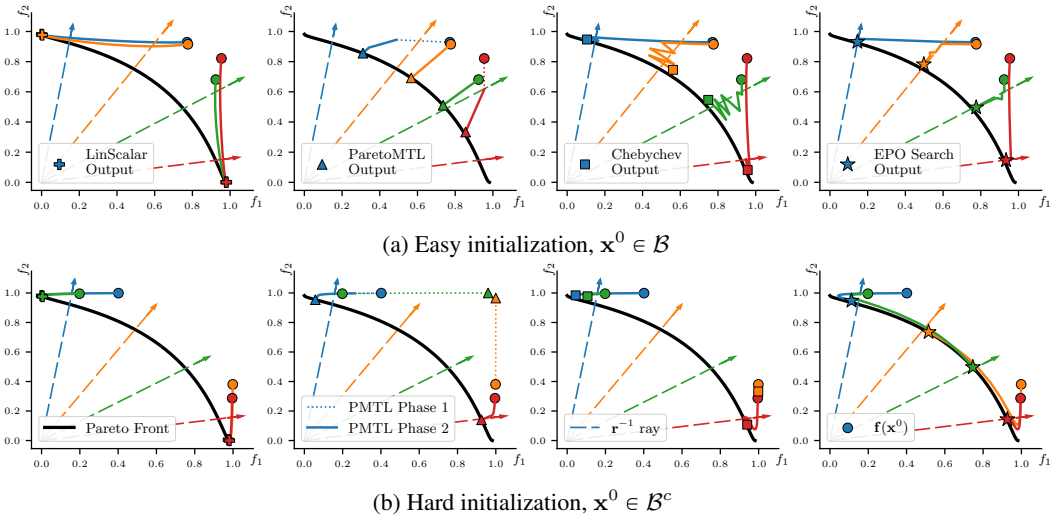


Figure 6: Trajectories of MOO algorithms in \mathbb{R}^2 with $n = 20$ dimensional solution space, when initialized (a) inside and (b) outside the hyper-box (31). In both rows, the results of LS, PMTL, CS, and EPO search are presented from left to right. Each weight vector is shown in a different color, and matched to the color of each algorithm's trajectory towards the corresponding EPO solution. Legend for PF, \mathbf{r}^{-1} , $f(\mathbf{x}^0)$ are for all subfigures.

Figure 6 shows the results. LS does not reach any of the EPO solutions, owing to its theoretical limitations for non-convex MOO problems. In its phase 1, PMTL enters the vicinity of the EPO, and in phase 2 it descends to the PF, although not exactly to the goal. However, PMTL converges

to the PF only when initialized near the EPO, and diverges otherwise, e.g., in the green and yellow trajectories of Figure 6b when $\mathbf{x}^0 \in \mathcal{B}^c$. The CS method theoretically has the EPO as its solution, but in practice, when an iterative procedure is used with a step size, it oscillates around the \mathbf{r}^{-1} ray (Figure 6a), without reaching the goal exactly because only one objective (with the maximum relative value (1)) is considered in each iteration. Although the oscillations could be reduced with a smaller step size, it would demand more number of iterations to reach the EPO. Using only one objective becomes more problematic if its gradient magnitude vanishes. For instance, the green and yellow trajectory in Figure 6b does not make substantial progress. This is similar to the 1d scenario in Figure 5 discussed above, i.e., if $x^* = -0.5$ and $x^0 = 2$, only f_2 will be considered whose gradient is close to zero. On the other hand, EPO search reaches very close to all the EPO solutions. Unlike CS, it uses a linear combination of all the objectives' gradients. As a result, it descends along the \mathbf{r}^{-1} ray without oscillations. Moreover, the ability to ascend enables EPO Search to escape the minima of less preferred objectives in Figure 6b making it robust to initialization.

We extend the above example to create m objective functions and compare PMTL with EPO Search, with respect to their scalability. The objective functions are defined as $f_j(\mathbf{x}) = 1 - \exp(-\|\mathbf{x} - \hat{\mathbf{x}}^j\|_2^2)$, for $j \in [m]$, where the entries of $\hat{\mathbf{x}}^j \in \mathbb{R}^n$ are sampled uniformly in $[-1/n, 1/n]$. For every m , we run both the algorithms for 20 different n (dimension of solution space), randomly sampled within 20 and 100. We randomly select a weight vector in \mathbb{R}_+^m for every (m, n) pair. In addition PMTL requires K reference vectors; for a fair comparison, we provide $K = 2m$ (maximum number of constraints in EPO search in this problem) reference vectors, which are again randomly selected in \mathbb{R}_+^m .

We use ω_r from Lagrange identity (12) as a measure of the quality of the solutions found. For every (m, n) pair, both the algorithms were run for 200 iterations with equal step size. Figure 7a and 7b show the quality and run time, respectively, for different number of objectives (m). Compared to PMTL, EPO search scales better with increasing number of objectives and produces better quality solutions.

5.2 Pareto front tracing by EPO Search: Illustrations on benchmark problems

We show the tracing ability of EPO Search Algorithm 2 on 6 benchmark MOO problems: ZDT1, ZDT2, ZDT3 (Zitzler et al. 2000), DTLZ2 and DTLZ7 (Deb et al. 2005), and TNK (Tanaka et al. 1995). We use PESA (Stanojević and Glover 2020) (see §4.1) to generate \mathbf{r}^{-1} rays.

The ZDT series of problems minimize two objectives: $f_1(\mathbf{x}) = x_1$ and $f_2(\mathbf{x}) = g(\mathbf{x})h(f_1(\mathbf{x}), g(\mathbf{x}))$, where $g(\mathbf{x}) = 1 + \frac{9}{n-1} \sum_{i=2}^n x_i$, $h(f_1, g) = 1 - \sqrt{f_1/g}$ for ZDT1, $h(f_1, g) = 1 - (f_1/g)^2$ for ZDT2 and $h(f_1, g) = 1 - \sqrt{f_1/g} - (f_1/g) \sin(10\pi f_1)$ for ZDT3. The argument \mathbf{x} is bounded as $0 \leq x_i \leq 1$ for $i = 1, \dots, n$. Figures 8a, 8b and 8c show the results. In these results, the depth of PESA procedure is 1 for ZDT1 and ZDT2, and 2 for ZDT3. Note that ZDT3 has a disconnected PF, but its boundary of attainable objective vectors $\partial\mathcal{O}$ is connected. Therefore, while tracing, EPO Search connects the disconnected segments of the PF by tracing the boundary $\partial\mathcal{O}$ through \mathbf{f}_{trace} . This is made possible due to the controlled gradient ascent within EPO Search. In the TNK problem, $m = n = 2$. The two objectives to minimize are $f_1(\mathbf{x}) = x_1$ and $f_2(\mathbf{x}) = x_2$ with bounds $0 \leq x_i \leq \pi$ and the inequality constraints $x_1^2 + x_2^2 - 1 - 0.1 \cos(16 \arctan(x_1/x_2)) \geq 0$, and $(x_1 - 0.5)^2 + (x_2 - 0.5)^2 \leq 0.5$. It has a discontinuous PF. Figure 8d shows the tracing result for this problem.

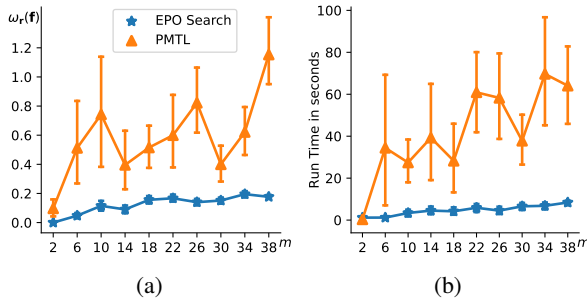


Figure 7: Scalability of PMTL and EPO Search with increasing number of objective functions (m). (a): quality of EPO solution (ω_r), (b): run time for 200 iterations (in seconds).

The DTLZ series of problems have more than two objectives to minimize. Let the last $n - m + 1$ variables of $\mathbf{x} \in [0, 1]^n$ be denoted as \mathbf{x}_m . The m objective functions in DTLZ2 are defined as

$$f_j(\mathbf{x}) = (1 + g(\mathbf{x}_m)) \prod_{i=1}^{m-j} \cos(x_i \pi / 2) \times \begin{cases} 1, & \text{if } j = 1 \\ \sin(x_{m-j+1} \pi / 2), & \text{if } j = 2, \dots, m \end{cases}$$

with $g(\mathbf{x}_m) = \sum_{x_i \in \mathbf{x}_m} (x_i - 0.5)^2$. In DTLZ7, the first $m - 1$ objective vectors are $f_j = x_j$ for $j = 1, \dots, m - 1$. The last objective is defined as $f_m(\mathbf{x}) = (1 + g(\mathbf{x}_m)) h(f_1, f_2, \dots, f_{m-1}, g)$, where $g(\mathbf{x}_m) = 1 + \frac{9}{n-m+1} \sum_{x_i \in \mathbf{x}_m} x_i$, and $h(f_1, f_2, \dots, f_{m-1}, g) = m - \sum_{j=1}^{m-1} \frac{f_j}{1+g} (1 + \sin(3\pi f_j))$. Figures 8e and 8f shows the tracing results for DTLZ problems. Note that DTLZ7 has disconnected PF but has a connected boundary of attainable objective vectors $\partial\mathcal{O}$. Therefore, akin to ZDT3, here also EPO Search connects the PFs while tracing. For clarity of presentation, we show the tracing results for \mathbf{r}^{-1} rays generated up to a recursion depth of 3 in PESA.

5.3 Evaluation of PESA-EPO for Pareto front approximation

We numerically compare the efficacy of PESA-EPO Algorithm 3 in PF approximation with PESA-CS and two state-of-the-art algorithms: CTAEA (Li et al. 2019), and PESA-TDM (Stanojević and Glover 2020). CTAEA (Constrained Two-Archive Evolutionary Algorithm) is an evolutionary algorithm, whereas PESA-TDM (Pattern Efficient Search Algorithm with Targeted Directional Model) is a gradient-based algorithm. Empirically, CTAEA has been found to outperform C-MOEA/D, C-NSGA-III (Jain and Deb 2013), C-MOEA/DD (Li et al. 2014), I-DBEA (Asafuddoula et al. 2014) and CMOEA (Woldesenbet et al. 2009); and the performance of PESA-TDM was found to be similar or better than NSGA-II (Deb et al. 2002), MOEA/DDE (Li and Zhang 2009), MOEA/D-AWA (Qi et al. 2014), MOEA/D-UD1 and MOEA/D-UD2 (Zhang et al. 2015). In PESA-CS, CS (by solving (1)) is used instead of TDM.

To evaluate how closely the obtained solutions approximate the PF, we use *Inverted Generational Distance* (IGD) (Coello Coello and Reyes Sierra 2004), defined in (32), where the ground truth PF $\mathcal{P}_g = \{\mathbf{y}_1^*, \dots, \mathbf{y}_{|\mathcal{P}_g|}^*\}$ is a finely discretized set of solutions from the actual PF \mathcal{P} , and $\mathcal{P}_a = \{\mathbf{f}_1^*, \dots, \mathbf{f}_{|\mathcal{P}_a|}^*\}$ is the set of points found by an algorithm. Ground truth PFs for the problems (§5.2) were obtained from Durillo et al. (2010), Durillo and Nebro (2014). IGD values and time of execution for all the methods are shown in Table 1. The results indicate that PESA-EPO is able to efficiently (lower time of execution) achieve close approximation to the PF (lower IGD). CTAEA uses a decomposition technique similar to PMTL (§2.3 and Appendix D.3). Its computational complexity grows exponentially with the number of objectives, as seen in our experiment as

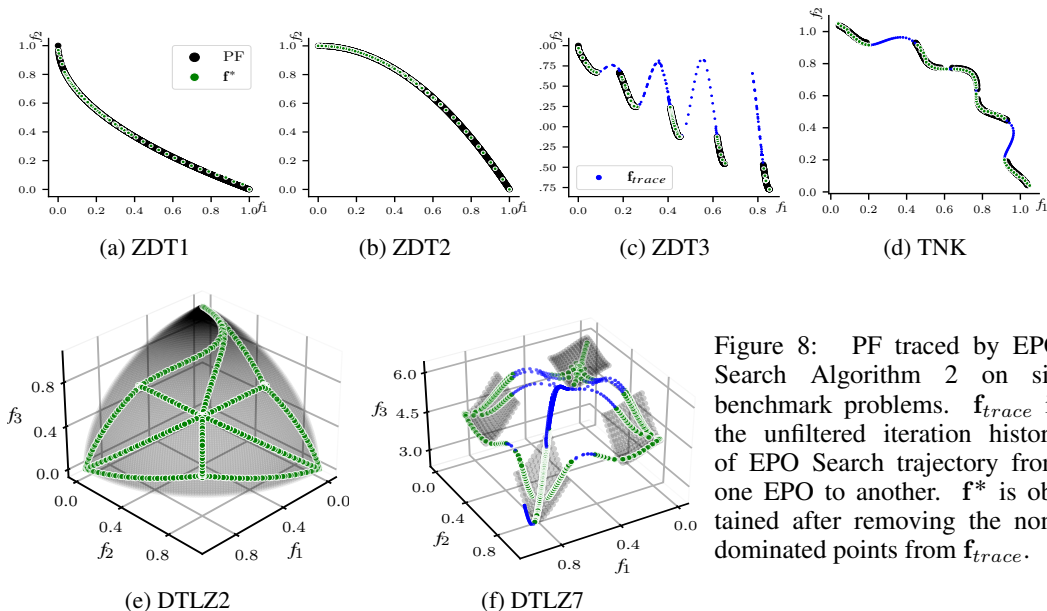


Figure 8: PF traced by EPO Search Algorithm 2 on six benchmark problems. \mathbf{f}_{trace} is the unfiltered iteration history of EPO Search trajectory from one EPO to another. \mathbf{f}^* is obtained after removing the non-dominated points from \mathbf{f}_{trace} .

MOO Problems	Metrics	CTAEA	PESA-TDM	PESA-CS	PESA-EPO
ZDT1 ($m = 2, n = 30$)	IGD	0.0426	0.0088	0.0095	0.0016
	Times (s)	4.01	1.71	2.1	1.38
ZDT2 ($m = 2, n = 30$)	IGD	0.0404	0.0051	0.0059	0.0016
	Times (s)	4.05	9.93	11.75	1.14
ZDT3 ($m = 2, n = 30$)	IGD	0.0572	0.0217	0.062	0.0027
	Times (s)	4.08	20.23	38.75	1.85
TNK ($m = n = p = 2$)	IGD	0.0922	0.0069	0.0117	0.0061
	Times (s)	1.64	0.61	6.48	0.83
DTLZ2 ($m = 3, n = 12$)	IGD	0.0269	0.0681	0.1214	0.0307
	Times (s)	221.77	40.38	68.13	2.9
DTLZ7 ($m = 3, n = 12$)	IGD	0.0369	0.0439	0.1532	0.0384
	Times (s)	60.49	41.74	48.16	2.32

Table 1: PF approximation metric IGD and execution time (lower is better for both) of MOO algorithms CTAEA, PESA-based TDM, CS, and EPO on benchmark MOO problems (m objectives, n variables, p constraints). Row-wise best result is in bold.

$$\text{IGD} = \frac{\sum_{i=1}^{|\mathcal{P}_g|} d(\mathbf{y}_i^*, \mathcal{P}_a)}{|\mathcal{P}_g|} \quad (32)$$

$$d(\mathbf{y}_i^*, \mathcal{P}_a) = \min_{\mathbf{f}_j^* \in \mathcal{P}_a} \|\mathbf{y}_i^* - \mathbf{f}_j^*\|.$$

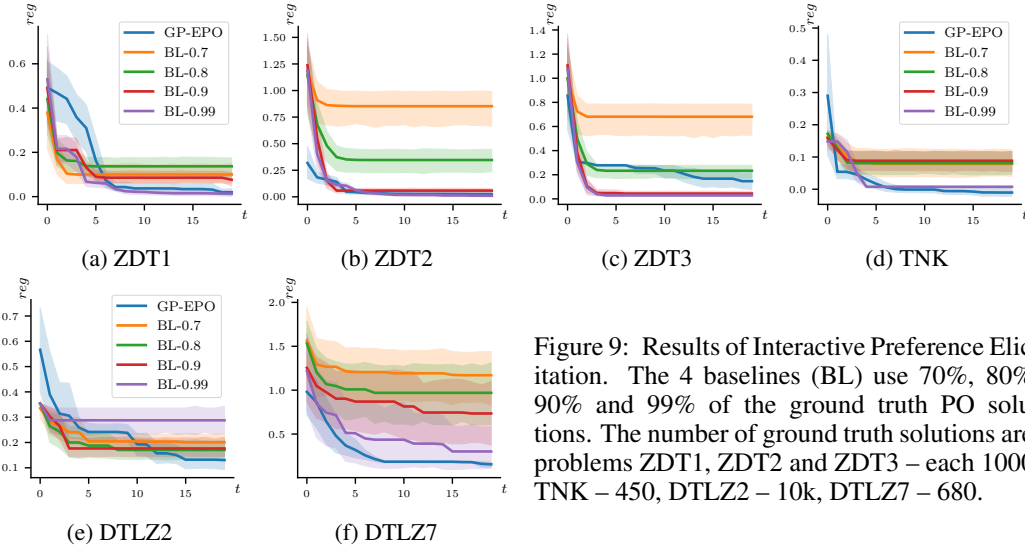


Figure 9: Results of Interactive Preference Elicitation. The 4 baselines (BL) use 70%, 80%, 90% and 99% of the ground truth PO solutions. The number of ground truth solutions are: problems ZDT1, ZDT2 and ZDT3 – each 1000, TNK – 450, DTLZ2 – 10k, DTLZ7 – 680.

well. The time required to reach an IGD value of same scale as that of the competing algorithms is significantly more in DTLZ2 and DTLZ7, where $m = 3$, as compared to the other bi-objective problems. PESA-TDM is efficient and suitable when the dimension of solution space is low: in TNK, it achieves as good an approximation as PESA-EPO with lesser execution time. Although PESA-CS is similar to PESA-TDM, it requires more samples of weight vectors from the PESA recursions (see §4.1) since CS stagnates for some weights and does not reach the PF, thereby requiring more time to achieve similar level of IGD values as that of PESA-TDM. For high-dimensional solution spaces both PESA-TDM and PESA-CS are inefficient because, for every new weight vector in PESA, they have to solve an optimization problem starting from a random initialization. On the other hand, PESA-EPO uses a previously obtained EPO as an initialization to solve the next problem. Moreover, the points in the trajectory of this optimization are PO solutions. As a result, PESA-EPO efficiently achieves very good performance.

5.4 Evaluation of GP-EPO for preference elicitation

To evaluate an interactive PE algorithm, we measure the decrease in regret with the number of queries to the DM. The regret at the t^{th} query is defined as the difference between the oracle utility and the incumbent, i.e., the best solution so far: $reg^t = u(\mathbf{f}(\mathbf{x}_{orc})) - u(\mathbf{f}(\mathbf{x}_{inc}^t))$.

We use the same 6 MOO problems described in §5.2 to evaluate GP-EPO. Following Ozbey and Karwan (2014), we use the Chebyshev utility function (which is unknown to the PE algorithm) to simulate a virtual DM that compares between two alternatives. Previous GP-based PE methods

(Chin et al. 2018, Zintgraf et al. 2018, Roijers et al. 2021), differ from GP-EPO in the use of (8) with a discrete set of points $\check{\mathcal{X}}$ (that could, e.g., be generated by a PF approximator like PESA-EPO). However, we use a stronger baseline by using the ground truth PFs of the 6 MOO problems as the discrete set. We randomly choose (without replacement) $x\%$ of the ground truth PF for the PE, and call it $BL-x$. For all the PE methods, we use Gaussian kernel and expected improvement as the acquisition function. We run each method for 10 trials, and in each trial, the utility of the virtual DM (parameters of Chebyshev utility) are decided randomly, to test the methods for different oracle solutions. We compare the decrement in their regrets for up to 20 queries.

The results are shown in Figure 9. We observe that for every MOO problem, GP-EPO surpasses the baseline methods that use up to 90 % of the ground truth PO solutions. Among the baseline results, the regret consistently decreases with increase in size of the discrete set $\check{\mathcal{X}}$. This decrement in regret is more prominent when the PE problem (7) is non-convex, i.e., when the MOO has a non-convex range \mathcal{O} in the objective space. E.g., in the ZDT family, ZDT1 has a convex MOO problem, and the difference between regret curves for 70%, 80% and 90% are not significant. Whereas, ZDT2 and ZDT3 have non-convex \mathcal{O} , which, we conjecture, makes the difference between regret curves significant. Note that, in the baseline approach, similar to the state-of-the-art for GP-based PE, the discrete set of PO solutions has to be obtained before Bayesian optimization (8) can start for PE. However, in practice, it is unclear as to how many PO solutions would suffice to reach a desired level of regret. From the baseline results it is clear that if the discrete set $\check{\mathcal{X}}$ represents the PF at a coarser resolution, then the regret may not go lower than a certain level, since there may not be enough samples closer to the oracle solution. Whereas, in GP-EPO, only two PO solutions are required a priori for the first query to start PE. We obtain the first PO solution by solving for $\mathbf{r}^{-1} = [1, \dots, 1]^T/m$ and the second one by solving for a random $\mathbf{r}^{-1} \in \mathcal{S}^m$. Since the Bayesian optimization (29) is over a continuous domain, GP-EPO can probe the PF virtually at infinite resolution. Therefore, unlike the baseline approach, its regret keeps decreasing without saturating after few initial queries.

5.5 Evaluation of EPO Search for Multi-Task Learning on Real Data

We demonstrate the efficacy of EPO Search for MTL in three applications from diverse domains. We discuss application 1 in the following and the other two in Appendix F.

5.5.1 Personalized Medicine and Pharmacogenomics.

We consider three drug-related tasks from different stages of drug discovery and development, summarized in Table 2. We use data from multiple publicly available databases summarized in Table 3. More details of these tasks and datasets used are in Appendix E. These tasks model the effects of drugs in hierarchically increasing levels of complexity. Drug-target (DT) prediction models the effect of drugs on specific genes (targets); drug response (DR) prediction models the effect of drugs on cancer cells (or a cancer patient with a given genomic profile); Drug side effect (DS) prediction models the side effects of drugs on patients. Hence, we expect DT to benefit less from auxiliary signal of the other two tasks. Among the three tasks, DR is the most challenging because data for relatively fewer drugs are available and we expect DR to benefit the most from MTL.

MTL Model. A standard deep neural MTL architecture (DNN-MTL) is used, as illustrated in Figure 10, where feature representations of each of the four entities, viz., drug, target gene, cancer cell, and disease, are used. These features are first passed through separate feed-forward neural networks (FNN) to get their corresponding embeddings, then the task-specific embedding pairs are concatenated and passed through task-specific FNN predictors for the final outputs – classifiers for DT and DS, and regressor for DR. The model is trained with binary cross entropy loss for DT and DS, and mean squared error loss for DR. Each embedding FNN has one hidden layer of 256 neurons, and each predictor FNN has two hidden layers, 64 neurons followed by 16, totaling 730, 147 parameters for the entire model. Each sub-network is associated with its parameters denoted by θ_i^j where $j = e, c, r$ represent embedding, classification and regression respectively; $i = 1, 2, 3$ represent each of the tasks and $i = s$ represents the shared drug-related features. In this MTL-DNN model, the network parameters of drug embedding FNN are shared for all the tasks, making it a suitable testbed for MOO training. The dimensions of input feature and embeddings are given in Table 4. Additional details are in Appendix E.

Table 2: Summary of Tasks in our MTL Setup

	Prediction Task	Problem	Inputs	Output(s)
1	Drug Target (DT)	Binary Classification	Drug d , Gene g	1: g is a target of d , 0: otherwise
2a	Drug Response (DR)	Regression	Drug d , Genomic Profile p	Drug efficacy of d on p
2b	Drug Response (DR)	Ranking	Drug list, Genomic Profile p	Top- k most effective drugs for p
3	Drug Side Effect (DS)	Binary Classification	Drug d , Disease s	1: s is a side effect of d , 0: otherwise

Table 3: Details of the datasets used

Task	Dataset	No. of Drugs	No. Sample pairs	
			Training	Test
Drug Target	STITCH	16K	627596	263032
	DrugBank	6K	158708	75820
	Repur	4K	80080	39798
Drug Response	GDSC	235	128004	62849
	CCLC	483	212516	109529
Drug Side-effect	SIDER	1.4K	524395	259471
	OFFSIDE	2.2K	550888	278807

Table 4: Input and embedding dimensions

	Drug	Gene-Target	Cell-line	Disease
Features	300	800	300	300
Embeddings	128	128	128	128

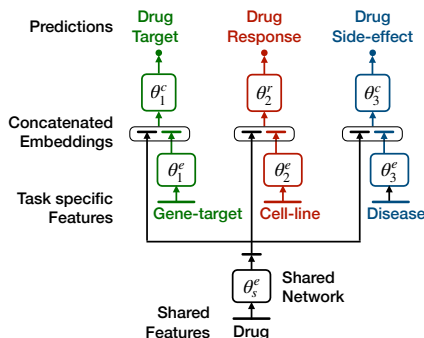


Figure 10: Illustration of MTL-DNN

Experiment Setting. In each dataset, 1/3rd of the drugs are randomly chosen to create a held-out test set; the remaining 2/3rd of the drugs are used for training. The total number of samples used in train and test sets are given in Table 3. For classification tasks, DT and DS, performance is measured using Area Under ROC curve (AUROC) and Area Under PR curve (AUPRC). For DR, we use two metrics: Mean Squared Error (MSE) and the ranking metric Normalized Discounted Cumulative Gain (NDCG@10) to judge how well the top 10 most effective drugs are predicted for a cancer patient and thus evaluate the model from the perspective of clinical use.

We compare EPO Search with LS and CS. In each of these methods, we determine the trade-off between DR and DS by having a higher priority (100) for one and lower priority for the other (1). DT plays a supporting role for both these tasks as it is the most specific task and we expect it to benefit the least from MTL. So, we keep its priority fixed at (10) for all scenarios. We report the results for the model trained with a maximum priority for the corresponding task. In addition, we use Single Task Learning (STL) as a baseline, where each task-specific network of the MTL-DNN model is trained with data for each task independently. For every priority setting, training for each method is repeated over 5 runs to randomize over model initialization and mini-batch formation, and the mean and standard deviations of the metrics are reported. We use paired t -test to determine statistical significance at 0.05 significance level. If a method is pair-wise better than *all* the other 3 methods, then we mark the result with an asterisk. Results are shown in Table 5.

Results. First, we observe that in almost all cases, CS and EPO Search perform better than STL, which demonstrates the advantages of EPO solutions for MTL, and DR, which is a more challenging problem, is most benefited. Although LS uses gradient information from all the tasks, it fails to consistently perform better than STL as the priorities are disproportionate among the tasks. This can be attributed to the non-convexity of loss surface, for which LS gravitates towards an extreme PO solution, as illustrated in §5.1. STL can be considered as a MOO method that finds an extreme solution corresponding to one task only. We observe that in some cases, e.g. CCLC, LS performs even worse than STL. In these cases, the simple weighted sum strategy inhibits LS from reaching the PF as close as STL does. Near an extreme solution the gradient directions are opposing and a fixed weight gradient combination reduces the magnitude of the search direction, especially when the gradient magnitude of a less preferred task is high. A reduced magnitude in the search direction decreases the magnitude of resulting network update. With fixed learning rate and number of iterations, update magnitude finally determines proximity to the PF.

Table 5: Results for Drug Target, Drug Response, and Drug Side-effect Prediction. Percentage values reported for AUROC, AUPRC and NDCG@10 (higher is better). Lower is better for MSE. Row-wise best result is in bold. Statistical significance (from paired t -test) is indicated by asterisk.

Task	Dataset	Metric	Algorithms			
			STL	CS	LS	EPO Search
Drug Target (DT)	STITCH	AUROC	94.90 \pm 0.18	95.17 \pm 0.40	95.08 \pm 0.20	95.55 \pm 0.27*
		AUPRC	79.36 \pm 0.46	79.14 \pm 0.99	79.55 \pm 0.66	79.86 \pm 0.61
	DrugBank	AUROC	91.95 \pm 0.34	92.41 \pm 0.24	91.88 \pm 0.25	92.66 \pm 0.21*
		AUPRC	66.35 \pm 0.60	66.42 \pm 0.99	65.76 \pm 0.67	67.52 \pm 0.59*
	Repur	AUROC	90.80 \pm 0.53	91.35 \pm 0.18	90.45 \pm 0.29	91.16 \pm 0.31
		AUPRC	64.54 \pm 1.59	64.97 \pm 0.15	64.34 \pm 1.09	65.15 \pm 1.13
Drug Response (DR)	GDSC	MSE	1.030 \pm 0.02	1.012 \pm 0.05	1.029 \pm 0.02	0.965 \pm 0.02
		NDCG@10	52.69 \pm 2.15	54.55 \pm 1.55	53.05 \pm 2.11	56.62 \pm 1.84*
	CCLE	MSE	0.854 \pm 0.02	0.857 \pm 0.04	0.862 \pm 0.02	0.827 \pm 0.04
		NDCG@10	48.70 \pm 0.94	50.28 \pm 1.31	47.80 \pm 1.15	53.67 \pm 0.90*
Drug Side-effect (DS)	SIDER	AUROC	77.39 \pm 0.20	77.37 \pm 0.15	77.46 \pm 0.14	78.60 \pm 0.33*
		AUPRC	39.02 \pm 1.25	40.01 \pm 1.33	39.58 \pm 1.07	41.29 \pm 1.25*
	OFFSIDE	AUROC	80.10 \pm 0.19	80.53 \pm 0.20	80.14 \pm 0.14	81.23 \pm 0.33*
		AUPRC	61.43 \pm 0.69	62.00 \pm 0.45	61.23 \pm 0.37	62.93 \pm 0.58*

CS benefits from MTL by amortizing its usage of gradient information from different tasks over many iteration, but only after reaching the r^{-1} ray, as illustrated in §5.1. Before that it behaves like STL, since only the maximum relative objective (1) is minimized. On the other hand, EPO Search adaptively combines the gradient information in every iteration and moves closer to the EPO solution of the training losses as compared to CS. This is reflected, through better performance with respect to the evaluation metrics, on the test data as well.

For DS, EPO Search outperforms other methods in both datasets and both metrics. In DR, EPO search outperforms other methods in the clinically important metric, NDCG@10, in both datasets. In DT, EPO search outperforms other methods in the DrugBank dataset, on both metrics and in the STITCH dataset on AUROC. Overall, in 13 out of 14 cases, EPO Search has the best average performance, and in 10 out of the 13 cases, the improvement is statistically significant.

5.5.2 Summary of Results on Real Data.

In Appendix F we evaluate EPO Search in two other applications. The first, from hydrometeorology, consists of predicting river flow at 8 sites in the Mississippi river network – a problem with 8 regression tasks. The second, from e-commerce, consists of 2 classification problems, predicting the category of multiple fashion product images simultaneously. In all cases, our results demonstrate the advantages of MTL over learning for each task independently, and the superior performance of EPO-Search over competing MTL methods.

6 Conclusion

In this paper we present new first-order iterative algorithms to find EPO solutions, for both unconstrained and constrained non-convex MOO problems. EPO Search is designed for problems with high-dimensional solution spaces where it is computationally more efficient than popular evolutionary algorithms. From a random initialization, EPO Search converges to an EPO solution or, if an EPO solution does not exist, to the closest PO solution. We prove its convergence and empirically demonstrate that our approach addresses the shortcomings of oscillations and premature stagnation in previous methods using the min-max formulation of (1). Similar to existing gradient descent methods, the convergence rate of EPO Search is sub-linear when moving from a random point to a Pareto stationary point. Interestingly, we show that the convergence rate, from any PO point to the EPO is linear under mild conditions. The literature on CS has methods to obtain EPO solutions, but without convergence guarantees; while the literature on gradient-based MOO methods presents convergence guarantees but only to reach arbitrary PO solutions. EPO Search offers both: a robust iteration strategy to reach the desired EPO and with convergence guarantees.

A direct application of the improved MOO through EPO Search is seen in MTL. Most previous MTL models use LS to combine task-specific priorities and losses. While CS is more suitable for

non-convex loss functions, if the the min-max formulation of (1) is used, learning is dominated by the task with highest priority and the influence of other tasks is either low or absent. In contrast, EPO Search uses a combination of gradients of all tasks in every iteration and can escape the minima of low priority objectives through controlled ascent which improves learning and makes it robust to initialization. The per-iteration complexity of EPO Search remains linear in the gradient dimensions (similar to the best previous methods that neither use input priorities nor allow constraints on parameters) enabling its use for deep MTL networks. We demonstrate the superior performance of EPO Search over competing approaches in MTL on synthetic and real datasets. EPO Search allows us to prioritize training for tasks that are more challenging while leveraging the MTL framework which enables shared learning from other datasets and tasks. We observe this in our own experiments where drug response prediction, which has the least number of drugs for training, benefits from collective learning of drug side effects and drug targets.

When initialized on the PF, EPO search can systematically trace the PF to reach an EPO solution, with a theoretically guaranteed linear rate of convergence. This unique ability makes it a computationally efficient alternative in use cases that require traversing the PF from one EPO solution to another. We investigate two such use cases in MCDM and develop new algorithms based on EPO Search. First we develop PESA-EPO for a posteriori MCDM where multiple EPO solutions can be used to approximate a PF. On benchmark datasets, PESA-EPO is faster than competing alternatives, without compromising on the approximation quality, because it does not require multiple optimizer calls and does not stop prematurely at PF discontinuities. Second, we develop GP-EPO for PE in interactive MCDM where we also address two limitations of previous GP-based PE methods by developing a new formulation. We leverage EPO Search to efficiently find PO solutions given a ray in S^m in GP-EPO that samples in a lower-dimensional space S^m , instead of the higher-dimensional solution space which previous methods use; moreover, this obviates the need to explicitly model monotonicity constraints. Numerical experiments on benchmark problems confirm the advantages of GP-EPO in terms of improved regret with very few queries to the DM.

Future Directions.

The key idea of our convergence rate proof is to compose non-convex objective functions with a well behaved function that satisfies the PL inequality (the proportionality gauges in our case) whose minima lie close to the desired PO. This enables reaching the vicinity of the desired solution at a linear rate. This idea may be utilized in other contexts, e.g., to solve non-convex SOO by (a) additional (convex or non-convex) objective functions and (b) a function satisfying PL inequality that, upon composition, models a solution in a convex neighbourhood of the global optimal of the original non-convex objective. A limitation of EPO Search, that may be addressed in future work, is that the tracing procedure can approximate the entire PF starting from the extreme solutions only if the set $\mathcal{O} = \{\mathbf{f}(\mathbf{x}) \mid \mathbf{x} \in \mathbb{X}\}$ is connected, i.e., there are paths connecting the discontinuous segments of the PF. Note that this is the case for disconnected PFs, in problems ZDT3, TNK and DTLZ7 in §5.3. If \mathcal{O} is not connected, e.g. in MOO problems of Wang et al. (2019), then more initial seed points are required in each connected component of \mathcal{O} . For instance, techniques to add relevant non-extreme seed points by detecting discontinuities in the PF during tracing in EPO Search could be investigated. Regularization on the network parameters, through our extension to handle constraints, may be empirically evaluated for MTL in future work. Finally, methods to adaptively find the best priorities for an MTL model may be explored in future work. A possibility is to adapt our method GP-EPO such that the DM’s role is replaced by validation dataset performance to compare solutions.

References

- Adams TE, Pagano T (2016) *Flood forecasting: A global perspective* (Academic Press).
- Angur MG, Lotfi V, Sarkis J (1996) A hybrid conjoint measurement and bi-criteria model for a two group negotiation problem. *Socio-Economic Planning Sciences* 30(3):195–206.
- Armbruster B, Delage E (2015) Decision making under uncertainty when preference information is incomplete. *Management Science* 61(1):111–128.
- Asafuddoula M, Ray T, Sarker R (2014) A decomposition-based evolutionary algorithm for many objective optimization. *IEEE Transactions on Evolutionary Computation* 19(3):445–460.
- Beninger P (2018) Pharmacovigilance: an overview. *Clinical Therapeutics* 40(12):1991–2004.
- Boyd S, Vandenberghe L (2004) Vector optimization. *Convex Optimization*, chapter 4.7, 174–187 (Cambridge University Press).
- Cai X, Wang G, Zhang Z (2013) Complexity analysis and numerical implementation of primal-dual interior-point methods for convex quadratic optimization based on a finite barrier. *Numerical Algorithms* 62(2):289–306.
- Caruana R (1997) Multitask learning. *Machine Learning* 28(1):41–75.
- Chang FJ, Hsu K, Chang LC (2019) *Flood Forecasting using Machine Learning Methods* (MDPI).
- Chen H, Cheng F, Li J (2020) idrug: Integration of drug repositioning and drug-target prediction via cross-network embedding. *PLoS Computational Biology* 16(7):e1008040.
- Cheng WH, Song S, Chen CY, Hidayati SC, Liu J (2021) Fashion meets computer vision: A survey. *ACM Computing Surveys (CSUR)* 54(4):1–41.
- Chin R, Manzie C, Ira A, Nestic D, Shames I (2018) Gaussian processes with monotonicity constraints for preference learning from pairwise comparisons. *2018 IEEE Conference on Decision and Control (CDC)*, 1150–1155.
- Chu W, Ghahramani Z (2005) Preference learning with Gaussian processes. *Proceedings of the 22nd International Conference on Machine Learning*, 137–144, ICML '05.
- Coello Coello CA, Reyes Sierra M (2004) A study of the parallelization of a coevolutionary multi-objective evolutionary algorithm. *MICAI 2004: Advances in Artificial Intelligence*, 688–697 (Berlin, Heidelberg: Springer Berlin Heidelberg).
- Coloma PM, Avillach P, Salvo F, Schuemie MJ, Ferrajolo C, Pariente A, Fourier-Réglat A, Molokhia M, Patadia V, van der Lei J, et al. (2013) A reference standard for evaluation of methods for drug safety signal detection using electronic healthcare record databases. *Drug Safety* 36(1):13–23.
- Corsello SM, Bittker JA, Liu Z, Gould J, McCarren P, Hirschman JE, Johnston SE, Vrcic A, Wong B, Khan M, Asiedu J, Narayan R, Mader CC, Subramanian A, Golub TR (2017) The drug repurposing hub: a next-generation drug library and information resource. *Nature Medicine* 23(4):405–408.
- Das I, Dennis JE (1997) A closer look at drawbacks of minimizing weighted sums of objectives for pareto set generation in multicriteria optimization problems. *Structural Optimization* 14(1):63–69.
- Das I, Dennis JE (1998) Normal-boundary intersection: A new method for generating the Pareto surface in nonlinear multicriteria optimization problems. *SIAM Journal on Optimization* 8(3):631–657.
- Daulton S, Eriksson D, Balandat M, Bakshy E (2022) Multi-objective Bayesian optimization over high-dimensional search spaces. *Uncertainty in Artificial Intelligence*, 507–517 (PMLR).
- Deb K, Jain H (2014) An evolutionary many-objective optimization algorithm using reference-point-based nondominated sorting approach, part i: Solving problems with box constraints. *IEEE Transactions on Evolutionary Computation* 18(4):577–601.
- Deb K, Pratap A, Agarwal S, Meyarivan T (2002) A fast and elitist multiobjective genetic algorithm: NSGA-II. *IEEE Transactions on Evolutionary Computation* 6(2):182–197.
- Deb K, Thiele L, Laumanns M, Zitzler E (2005) Scalable test problems for evolutionary multiobjective optimization. Abraham A, Jain L, Goldberg R, eds., *Evolutionary Multiobjective Optimization: Theoretical Advances and Applications*, 105–145 (Springer London).
- Deisenroth MP, Fox D, Rasmussen CE (2013) Gaussian processes for data-efficient learning in robotics and control. *IEEE Transactions on Pattern Analysis and Machine Intelligence* 37(2):408–423.
- Deldjoo Y, Nazary F, Ramisa A, Mcauley J, Pellegrini G, Bellogin A, Di Noia T (2022) A review of modern fashion recommender systems. *arXiv preprint arXiv:2202.02757*.
- Dell RF, Karwan MH (1990) An interactive MCDM weight space reduction method utilizing a Tchebycheff utility function. *Naval Research Logistics (NRL)* 37(2):263–277.
- Désidéri JA (2012) Multiple-gradient descent algorithm (MGDA) for multiobjective optimization. *Comptes Rendus Mathématique* 350(5-6):313–318.

- DiMasi JA, Grabowski HG, Hansen RW (2016) Innovation in the pharmaceutical industry: new estimates of r&d costs. *Journal of Health Economics* 47:20–33.
- Durillo JJ, Nebro AJ (2014) jMetal: Metaheuristic algorithms in Java. <http://jmetal.sourceforge.net/problems.html>.
- Durillo JJ, Nebro AJ, Alba E (2010) The jMetal framework for multi-objective optimization: Design and architecture. *IEEE Congress on Evolutionary Computation*, 1–8.
- Elahi M, Qi L (2020) Fashion recommender systems in cold start. *Fashion Recommender Systems*, 3–21 (Springer).
- Emmerich MT, Deutz AH (2018) A tutorial on multiobjective optimization: fundamentals and evolutionary methods. *Natural Computing* 17(3):585–609.
- Eric B, Freitas N, Ghosh A (2007) Active preference learning with discrete choice data. *Advances in Neural Information Processing Systems* 20.
- Fishburn PC (1968) Utility theory. *Management Science* 14(5):335–378.
- Fliege J, Svaiter BF (2000) Steepest descent methods for multicriteria optimization. *Mathematical Methods of Operations Research* 51(3):479–494.
- Fliege J, Vaz AIF (2016) A method for constrained multiobjective optimization based on SQP techniques. *SIAM Journal on Optimization* 26(4):2091–2119.
- Fonseca CMMd (1995) *Multiobjective genetic algorithms with application to control engineering problems*. Ph.D. thesis, University of Sheffield.
- Forgas JP (1995) Mood and judgment: The affect infusion model (AIM). *Psychological Bulletin* 117(1):39–66.
- Gandibleux X (2002) *Multiple Criteria Optimization: state of the art annotated bibliographic surveys*, volume 52 of *International Series in Operations Research & Management Science* (Springer US).
- Gembicki F, Haimes Y (1975) Approach to performance and sensitivity multiobjective optimization: The goal attainment method. *IEEE Transactions on Automatic Control* 20:769–771.
- Goodfellow I, Bengio Y, Courville A (2016) *Deep Learning* (MIT Press).
- Greco S, Matarazzo B, Slowiński R (2010) Interactive evolutionary multiobjective optimization using dominance-based rough set approach. *IEEE Congress on Evolutionary Computation*, 1–8 (IEEE).
- Hardt RM (1975) Topological properties of subanalytic sets. *Transactions of the American Mathematical Society* 211:57–70.
- Haskell WB, Huang W, Xu H (2018) Preference elicitation and robust optimization with multi-attribute quasi-concave choice functions. *arXiv preprint arXiv:1805.06632*.
- Hillmermeier C (2001) *Nonlinear Multiobjective Optimization: A Generalized Homotopy Approach*, volume 135 of *International Series of Numerical Mathematics* (Birkhäuser Verlag).
- Huang SM, Lertora JJ, Atkinson Jr AJ (2012) *Principles of Clinical Pharmacology* (Academic Press).
- Hwang CL, Masud ASM, Hwang CL, Masud ASM (1979) Methods for multiple objective decision making. *Multiple Objective Decision Making—Methods and Applications: A State-of-the-Art Survey* 21–283.
- Ismail-Yahaya A, Messac A (2002) Effective generation of the Pareto frontier: The normalized normal constraint method. *43rd AIAA/ASME/ASCE/AHS/ASC Structures, Structural Dynamics, and Materials Conference*.
- Jain H, Deb K (2013) An evolutionary many-objective optimization algorithm using reference-point based nondominated sorting approach, part II: Handling constraints and extending to an adaptive approach. *IEEE Transactions on Evolutionary Computation* 18(4):602–622.
- Jain V (2007) On Cauchy’s bound for zeros of a polynomial. *Bulletin mathématique de la Société des Sciences Mathématiques de Roumanie* 50 (98)(3):273–279.
- Jiang Y, Rensi SE, Wang S, Altman RB (2021) Drugorchestra: Jointly predicting drug response, targets, and side effects via deep multi-task learning. *25th International Conference on Research in Computational Molecular Biology*.
- Jing R, Wang M, Zhang Z, Liu J, Liang H, Meng C, Shah N, Li N, Zhao Y (2019) Comparative study of posteriori decision-making methods when designing building integrated energy systems with multi-objectives. *Energy and Buildings* 194:123–139.
- Jones DR (2001) A taxonomy of global optimization methods based on response surfaces. *Journal of Global Optimization* 21(4):345–383.
- Kaliszewski I (1995) A theorem on nonconvex functions and its application to vector optimization. *European Journal of Operational Research* 80(2):439–445.
- Karimi H, Nutini J, Schmidt M (2016) Linear convergence of gradient and proximal-gradient methods under the Polyak-Lojasiewicz condition. Frascioni P, Landwehr N, Manco G, Vreeken J, eds., *Machine Learning and Knowledge Discovery in Databases*, 795–811 (Cham: Springer International Publishing).

- Keeney RL, Raiffa H, Meyer RF (1993) *Decisions with multiple objectives: preferences and value trade-offs* (Cambridge university press).
- Kiriiri GK, Njogu PM, Mwangi AN (2020) Exploring different approaches to improve the success of drug discovery and development projects: a review. *Future Journal of Pharmaceutical Sciences* 6(1):1–12.
- Köksalan M, Wallenius J (2012) Multiple criteria decision making: foundations and some approaches. *New Directions in Informatics, Optimization, Logistics, and Production*, 171–183 (INFORMS).
- Köksalan MM, Sagala PN (1995) Interactive approaches for discrete alternative multiple criteria decision making with monotone utility functions. *Management Science* 41(7):1158–1171.
- Korhonen P, Wallenius J, Zionts S (1984) Solving the discrete multiple criteria problem using convex cones. *Management Science* 30(11):1336–1345.
- Kuhn M, Letunic I, Jensen LJ, Bork P (2016) The SIDER database of drugs and side effects. *Nucleic Acids Res.* 44(D1):D1075–9.
- LeCun Y, Bottou L, Bengio Y, Haffner P (1998) Gradient-based learning applied to document recognition. *Proceedings of the IEEE* 86(11):2278–2324.
- Li H, Zhang Q (2009) Multiobjective optimization problems with complicated Pareto sets, MOEA/D and NSGA-II. *IEEE Transactions on Evolutionary Computation* 13(2):284–302.
- Li K, Chen R, Fu G, Yao X (2019) Two-archive evolutionary algorithm for constrained multiobjective optimization. *IEEE Transactions on Evolutionary Computation* 23(2):303–315.
- Li K, Deb K, Zhang Q, Kwong S (2014) An evolutionary many-objective optimization algorithm based on dominance and decomposition. *IEEE Transactions on Evolutionary Computation* 19(5):694–716.
- Lin X, Yang Z, Zhang Q, Kwong S (2020) Controllable Pareto multi-task learning. *arXiv preprint arXiv:2010.06313*.
- Lin X, Zhen HL, Li Z, Zhang QF, Kwong S (2019) Pareto multi-task learning. *Advances in Neural Information Processing Systems*, volume 32 (Curran Associates, Inc.).
- Luenberger DG (1997) *Optimization by Vector Space Methods* (USA: John Wiley & Sons, Inc.).
- Luenberger DG, Ye Y (2008) *Primal Methods*, 359–400 (New York, NY: Springer US).
- Luque M, Caballero R, Molina J, Ruiz F (2007) Equivalent information for multiobjective interactive procedures. *Management Science* 53(1):125–134.
- Ma J, Fong SH, Luo Y, Bakkenist CJ, Shen JP, Mourragui S, Wessels LF, Hafner M, Sharan R, Peng J, et al. (2021) Few-shot learning creates predictive models of drug response that translate from high-throughput screens to individual patients. *Nature Cancer* 2(2):233–244.
- Marler RT, Arora JS (2004) Survey of multi-objective optimization methods for engineering. *Structural and Multidisciplinary Optimization* 26(6):369–395.
- Miettinen K (1998) *Nonlinear Multiobjective Optimization*, volume 12 of *International Series in Operations Research & Management Science* (Springer US).
- Močkus J (1975) On Bayesian methods for seeking the extremum. Marchuk GI, ed., *Optimization Techniques IFIP Technical Conference Novosibirsk, July 1–7, 1974*, 400–404 (Berlin, Heidelberg: Springer Berlin Heidelberg).
- Nesterov Y (2004) *Nonlinear Optimization*, 1–50 (Boston, MA: Springer US).
- Ng R (2015) *Drugs: from discovery to approval* (John Wiley & Sons).
- NOAA National Centers for Environmental Information (2022) U.S. Billion-Dollar Weather and Climate Disasters.
- Nocedal J, Wright SJ (2006) Theory of constrained optimization. *Numerical Optimization*, chapter 12.2, 315–320 (New York, NY, USA: Springer), second edition.
- Ozbey O, Karwan MH (2014) An interactive approach for multicriteria decision making using a Tchebycheff utility function approximation. *Journal of Multi-Criteria Decision Analysis* 21(3-4):153–172.
- Oztas GZ, Erdem S (2021) Framework selection for developing optimization algorithms: assessing preferences by conjoint analysis and best–worst method. *Soft Computing* 25(5):3831–3848.
- Pascoletti A, Serafini P (1984) Scalarizing vector optimization problems. *Journal of Optimization Theory and Applications* 42(4):499–524.
- Polyak B (1963) Gradient methods for the minimisation of functionals. *USSR Computational Mathematics and Mathematical Physics* 3(4):864–878.
- Qi Y, Ma X, Liu F, Jiao L, Sun J, Wu J (2014) MOEA/D with Adaptive Weight Adjustment. *Evolutionary Computation* 22(2):231–264.
- Rao VR (2010) *Conjoint Analysis* (John Wiley & Sons, Ltd).
- Rasmussen CE, Williams CK (2004) Gaussian processes in machine learning. *Lecture Notes in Computer Science* 3176:63–71.

- Rees MG, Seashore-Ludlow B, Cheah JH, Adams DJ, Price EV, Gill S, Javaid S, Coletti ME, Jones VL, Bodycombe NE, Soule CK, Alexander B, Li A, Montgomery P, Kotz JD, Hon CSY, Munoz B, Liefeld T, Dančik V, Haber DA, Clish CB, Bittker JA, Palmer M, Wagner BK, Clemons PA, Shamji AF, Schreiber SL (2016) Correlating chemical sensitivity and basal gene expression reveals mechanism of action. *Nat. Chem. Biol.* 12(2):109–116.
- Reeves GR, MacLeod KR (1999) Some experiments in Tchebycheff-based approaches for interactive multiple objective decision making. *Computers & Operations Research* 26(13):1311–1321.
- Rojijers DM, Zintgraf LM, Libin P, Reymond M, Bargiacchi E, Nowé A (2021) Interactive multi-objective reinforcement learning in multi-armed bandits with Gaussian process utility models. Hutter F, Kersting K, Lijffijt J, Valera I, eds., *Machine Learning and Knowledge Discovery in Databases*, 463–478 (Cham: Springer International Publishing).
- Ruder S (2017) An overview of multi-task learning in deep neural networks. *arXiv preprint arXiv:1706.05098*.
- Sabour S, Frosst N, Hinton GE (2017) Dynamic routing between capsules. *Advances in Neural Information Processing Systems*, volume 30 (Curran Associates, Inc.).
- Schenone M, Dančik V, Wagner BK, Clemons PA (2013) Target identification and mechanism of action in chemical biology and drug discovery. *Nature Chemical Biology* 9(4):232–240.
- Sener O, Koltun V (2018) Multi-task learning as multi-objective optimization. *Advances in Neural Information Processing Systems*, volume 31 (Curran Associates, Inc.).
- Senft D, Leiserson MD, Ruppin E, Ze'ev AR (2017) Precision oncology: the road ahead. *Trends in Molecular Medicine* 23(10):874–898.
- Shahriari B, Swersky K, Wang Z, Adams RP, De Freitas N (2016) Taking the human out of the loop: A review of Bayesian optimization. *Proceedings of the IEEE* 104(1):148–175.
- Shukla PK (2007) On the normal boundary intersection method for generation of efficient front. Shi Y, van Albada GD, Dongarra J, Sloot PMA, eds., *Computational Science – ICCS 2007*, 310–317 (Springer Berlin Heidelberg).
- Siddiqui S, Azarm S, Gabriel SA (2012) On improving normal boundary intersection method for generation of Pareto frontier. *Structural and Multidisciplinary Optimization* 46(6):839–852.
- Snoek J, Larochelle H, Adams RP (2012) Practical Bayesian optimization of machine learning algorithms. *Advances in Neural Information Processing Systems*, 2951–2959.
- Spyromitros-Xioufis E, Tsoumakas G, Groves W, Vlahavas I (2016) Multi-target regression via input space expansion: treating targets as inputs. *Machine Learning* 104(1):55–98.
- Stanojević B, Glover F (2020) A new approach to generate pattern-efficient sets of non-dominated vectors for multi-objective optimization. *Information Sciences* 530:22–42.
- Steuer RE (1989) The Tchebycheff procedure of interactive multiple objective programming. Karpak B, Zionts S, eds., *Multiple Criteria Decision Making and Risk Analysis Using Microcomputers* (Springer).
- Steuer RE, Siverman J, Whisman AW (1993) A combined Tchebycheff/aspiration criterion vector interactive multiobjective programming procedure. *Management Science* 39(10):1255–1260.
- Stewart T, Bandt O, Braun H, Chakraborti N, Ehrgott M, Göbel M, Jin Y, Nakayama H, Poles S, Stefano DD (2008) Real-world applications of multiobjective optimization. *Multiobjective Optimization* 285–327.
- Szklarczyk D, Santos A, von Mering C, Jensen LJ, Bork P, Kuhn M (2016) STITCH 5: augmenting protein-chemical interaction networks with tissue and affinity data. *Nucleic Acids Res.* 44(D1):D380–4.
- Tanabe H, Fukuda EH, Yamashita N (2022) Convergence rates analysis of a multiobjective proximal gradient method. *Optimization Letters* .
- Tanaka M, Watanabe H, Furukawa Y, Tanino T (1995) GA-based decision support system for multicriteria optimization. *1995 IEEE International Conference on Systems, Man and Cybernetics. Intelligent Systems for the 21st Century*, volume 2, 1556–1561.
- Tatonetti NP, Ye PP, Daneshjou R, Altman RB (2012) Data-driven prediction of drug effects and interactions. *Sci. Transl. Med.* 4(125):125ra31.
- Tesauro G (1988) Connectionist learning of expert preferences by comparison training. Touretzky D, ed., *Advances in Neural Information Processing Systems*, volume 1 (Morgan-Kaufmann).
- Vamathevan J, Clark D, Czodrowski P, Dunham I, Ferran E, Lee G, Li B, Madabhushi A, Shah P, Spitzer M, et al. (2019) Applications of machine learning in drug discovery and development. *Nature Reviews Drug Discovery* 18(6):463–477.
- Vayanos P, Ye Y, McElfresh D, Dickerson J, Rice E (2020) Robust active preference elicitation. *arXiv preprint arXiv:2003.01899*.
- Ventola CL (2018) Big data and pharmacovigilance: data mining for adverse drug events and interactions. *Pharmacy and Therapeutics* 43(6):340.

- Vieira DAG, Takahashi RHC, Saldanha RR (2012) Multicriteria optimization with a multiobjective golden section line search. *Mathematical Programming* 131(1):131–161.
- Wallenius J, Fishburn PC, Zionts S, Dyer JS, Steuer RE, Deb K (2008) Multiple criteria decision making, multi-attribute utility theory: Recent accomplishments and what lies ahead. *Management Science* 54(7):1336–1349.
- Wang Y, Yu J, Yang S, Jiang S, Zhao S (2019) Evolutionary dynamic constrained optimization: Test suite construction and algorithm comparisons. *Swarm and Evolutionary Computation* 50(6):972–986.
- Watanabe JH, McInnis T, Hirsch JD (2018) Cost of prescription drug–related morbidity and mortality. *Annals of Pharmacotherapy* 52(9):829–837.
- Wiecek MM, Ehrgott M, Engau A (2016) Continuous multiobjective programming. *Multiple Criteria Decision Analysis: State of the Art Surveys* (Springer).
- Wierzbicki AP (1986) On the completeness and constructiveness of parametric characterizations to vector optimization problems. *Operations-Research-Spektrum* 8(2):73–87.
- Wishart DS, Feunang YD, Guo AC, Lo EJ, Marcu A, Grant JR, Sajed T, Johnson D, Li C, Sayeeda Z, Assem-pour N, Iynkkaran I, Liu Y, Maciejewski A, Gale N, Wilson A, Chin L, Cummings R, Le D, Pon A, Knox C, Wilson M (2018) DrugBank 5.0: a major update to the DrugBank database for 2018. *Nucleic Acids Res.* 46(D1):D1074–D1082.
- Woldesenbet YG, Yen GG, Tessema BG (2009) Constraint handling in multiobjective evolutionary optimization. *IEEE Transactions on Evolutionary Computation* 13(3):514–525.
- Xiao H, Rasul K, Vollgraf R (2017) Fashion-MNIST: a novel image dataset for benchmarking machine learning algorithms. *arXiv preprint arXiv:1708.07747*.
- Yang L, Shami A (2020) On hyperparameter optimization of machine learning algorithms: Theory and practice. *Neurocomputing* 415:295–316.
- Yang W, Soares J, Greninger P, Edelman EJ, Lightfoot H, Forbes S, Bindal N, Beare D, Smith JA, Thompson IR, Ramaswamy S, Futreal PA, Haber DA, Stratton MR, Benes C, McDermott U, Garnett MJ (2013) Genomics of drug sensitivity in cancer (GDSC): a resource for therapeutic biomarker discovery in cancer cells. *Nucleic Acids Res.* 41(Database issue):D955–61.
- Zhang C, Tan KC, Lee LH, Gao L (2018) Adjust weight vectors in MOEA/D for bi-objective optimization problems with discontinuous Pareto fronts. *Soft Comput.* 22(12):3997–4012.
- Zhang M, Huang K, Lv Y (2021) A wide neighborhood arc-search interior-point algorithm for convex quadratic programming with box constraints and linear constraints. *Optimization and Engineering* 1–21.
- Zhang Q, Li H (2007) MOEA/D: A multiobjective evolutionary algorithm based on decomposition. *IEEE Transactions on Evolutionary Computation* 11(6):712–731.
- Zhang Q, Zhou A, Jin Y (2008) RM-MEDA: A regularity model-based multiobjective estimation of distribution algorithm. *IEEE Transactions on Evolutionary Computation* 12(1):41–63.
- Zhang Y, Yang Q (2021) A survey on multi-task learning. *IEEE Transactions on Knowledge and Data Engineering* .
- Zhang Y, Yang R, Zuo J, Jing X (2015) Enhancing MOEA/D with uniform population initialization, weight vector design and adjustment using uniform design. *Journal of Systems Engineering and Electronics* 26(5):1010–1022.
- Zintgraf LM, Roijers DM, Linders S, Jonker CM, Nowé A (2018) Ordered preference elicitation strategies for supporting multi-objective decision making. *Proceedings of the 17th International Conference on Autonomous Agents and MultiAgent Systems*, 1477–1485, AAMAS '18 (Richland, SC: International Foundation for Autonomous Agents and Multiagent Systems).
- Zionts S, Wallenius J (1976) An interactive programming method for solving the multiple criteria problem. *Management Science* 22(6):652–663.
- Zitzler E, Deb K, Thiele L (2000) Comparison of multiobjective evolutionary algorithms: Empirical results. *Evolutionary Computation* 8(2):173–195.

Appendix

Table 6: Notations used in sections §3 and §4

Notations	Description
n , and m	number of variables in the solution space, and number of objectives
\mathbf{f}	\mathbb{R}^m -valued objective function, or a vector in \mathbb{R}^m
\mathcal{S}^m	$m - 1$ dimensional simplex
$\mathbf{r} \in \mathcal{S}^m, \mathbf{r}^{-1} \in \mathbb{R}^m$	preference vector, and its point-wise inverse
$\mathbf{x}^*, \mathbf{x}_r^* \in \mathbb{R}^n$	a Pareto Optimal solution, an Exact Pareto Optimal solution w.r.t \mathbf{r}
$\mathbf{x}^t, \mathbf{f}^t$	solution and its objective vector at t^{th} iteration
$\mathbf{b}^l, \mathbf{b}^u \in \mathbb{R}^n$	lower and upper bounds (box constraint) on solution variable: $b_i^l \leq x_i \leq b_i^u$
$\pi : \mathbb{R}^n \rightarrow \mathbb{R}^n$	Projection function that brings \mathbf{x} inside the box constraints element-wise
p, q	number of inequality and equality constraints
\mathbf{g}, \mathbf{h}	\mathbb{R}^p -valued inequality and \mathbb{R}^q valued equality constraints
p_a, q	number of active inequality and equality constraints
$\mathbf{F}, \mathbf{G}, \mathbf{H}$	Jacobians of objectives, active inequality and equality constraints
$\mathcal{X} \subset \mathbb{R}^n, \mathcal{O} \subset \mathbb{R}^m$	Set of feasible solutions, and range of \mathbb{R}^m -valued objective function \mathbf{f}
$\partial\mathcal{X}, \partial\mathcal{O}$	Boundaries of domain and range of \mathbf{f} respectively
$\text{Int}(\mathcal{X}), \text{Int}(\mathcal{O})$	Interior of domain and range of \mathbf{f} respectively
$\mathcal{P}, \mathcal{P}_r$	Set of Pareto optimal solutions, and Exact Pareto Optimal solutions w.r.t \mathbf{r}
$\mathcal{T}_{\mathcal{X}}(\mathbf{x}), \mathcal{F}_{\mathcal{X}}(\mathbf{x}), \mathcal{D}_{\mathcal{X}}^{\mathbf{f}}(\mathbf{x})$	Tangent plane/cone, set of feasible directions, descent directions at \mathbf{x}
$\mathbf{d}, \mathbf{d}_{nd} \in \mathcal{F}_{\mathcal{X}}(\mathbf{x})$	a general search direction, non-dominating search direction
$\beta \in \mathbb{R}^m, \rho \in \mathbb{R}^{p_a}, \gamma \in \mathbb{R}^{q_a}$	coefficients for gradients of objectives, active inequality and equality constraints
$\omega_r(\mathbf{f}) = \omega(\mathbf{f}, \mathbf{r}^{-1})$	A measure of proportionality of \mathbf{f} w.r.t. \mathbf{r}^{-1}
$\mathbf{a}(\mathbf{f}, \mathbf{r})$ or simply \mathbf{a}	Anchor direction at point $\mathbf{f} \in \mathbb{R}^m$ w.r.t. preference \mathbf{r}
λ	maximum relative value of objectives: $\max_j r_j f_j$
\mathbf{J}^*	index set of objectives with maximum relative value
$\mathcal{A}_{\mathbf{f}}^{\mathbf{r}}, \mathcal{V}_{\leq \mathbf{f}}$	set of attainable objective vectors dominated by $\lambda^t \mathbf{r}^{-1}$ and \mathbf{f}
$\mathcal{M}_{\mathbf{f}}^{\mathbf{r}}$	set of attainable objective vectors with measure of proportionality $< \omega_r(\mathbf{f})$
$\mathbb{R}^0, \mathbb{R}^{0ijk}$	discrete sets of m preference vectors at start, and after 3 recursion in PESA
μ, κ, α	mean, kernel and acquisition functions of a Gaussian Process
$\psi_{\mathbf{f}}$	function that maps a point in the Simplex to the PF
\mathcal{D}_t	Pairwise comparison data constructed from the t queries to the DM.
$\check{\mathcal{X}}_{\mathcal{D}_t}$	The discrete set of solutions present in the dataset \mathcal{D}_t

A Proportionality of Vectors and Balancing Direction

A.1 Proportionality Gauge from KL Divergence

One possible approach to measure the proportionality between \mathbf{f} and \mathbf{r}^{-1} is through KL divergence between the normalized vectors of $\mathbf{f} \odot \mathbf{r}$ and $\mathbf{1} = [1, \dots, 1]$, i.e. the uniform distribution:

$$\omega(\mathbf{f}, \mathbf{r}^{-1}) = \sum_{j=1}^m \frac{f_j r_j}{\|\mathbf{f} \odot \mathbf{r}\|_1} \log \left(\frac{m f_j r_j}{\|\mathbf{f} \odot \mathbf{r}\|_1} \right) = \text{KL}(\overline{\mathbf{f} \odot \mathbf{r}} \mid \bar{\mathbf{1}}), \quad (33)$$

where $\bar{\mathbf{v}}$ is the ℓ_1 normalization of a vector \mathbf{v} . This ω satisfies both conditions 1 and 2 of a proportionality gauge. Figure 3c shows the corresponding ω_r in case of 3 objectives and a particular weight vector. Its anchor direction $\mathbf{a} = \nabla_{\mathbf{f}} \omega_r$ is scale invariant to \mathbf{r} :

$$a_j = \frac{r_j}{\|\mathbf{f} \odot \mathbf{r}\|_1} \left(\log \left(\frac{f_j r_j / \|\mathbf{f} \odot \mathbf{r}\|_1}{1/m} \right) - \omega(\mathbf{f}, \mathbf{r}^{-1}) \right), \quad j \in [m]. \quad (34)$$

Notice that, unless all $f_j r_j$ are equal, the anchor elements a_j are non-negative for some objectives and negative for the rest. As a result, if we move against the search direction \mathbf{d} in Theorem 1, we will

be descending for the objectives with $\mathbf{d}^T \nabla_{\mathbf{x}} f_j = s a_j \geq 0$ and ascending for the other objectives, since $s > 0$. This is further clarified by analyzing the relation between \mathbf{f} and \mathbf{a} .

Claim 3. *The anchor direction \mathbf{a} in (34) is always orthogonal to the objective vector \mathbf{f} : $\mathbf{a}^T \mathbf{f} = 0$.*

However, this anchoring direction (34) does not move the objective vectors to the \mathbf{r}^{-1} ray in the shortest possible path. The shortest path between \mathbf{f}^t and the \mathbf{r}^{-1} ray should lie on the hyperplane containing both these vectors. So, in order for $\mathbf{f}^{t+1} \approx \mathbf{f}^t - \eta \mathbf{a}$ to be on the shortest path, a necessary condition is \mathbf{a} should lie in the span of \mathbf{f}^t and \mathbf{r}^{-1} . This does not happen in anchoring direction of (34) as shown in the Figure 3c and 3d. The curved trajectory deviates from the $\text{span}(\{\mathbf{r}^{-1}, \mathbf{f}^0\})$.

A.2 Comparison of Proportionality Gauges

Among the three options discussed above, we use CSZ inequality and Lagrange’s identity based proportionality gauges as their anchoring directions satisfy the PL inequality (see Lemma 5), which we leverage in §3.6 to prove linear convergence in Theorem 4. It is non-trivial to design a scaling factor s for the KL divergence based anchor (34) such that $\mathbf{a} = s \nabla_{\mathbf{f}} \omega_{\mathbf{r}}$ satisfies the PL inequality in Lemma (5). Therefore, we do not use this in our development. We use Lagrange identity based anchoring direction when the initialization is not on the PF, in order to reach the \mathbf{r}^{-1} ray through the shortest path in lesser number of iterations as compared to the CSZ inequality based anchor. However, when the initialization is on the PF, in order to escape the local PO solution, we use the CSZ inequality based anchoring direction. Table 7 summarizes their properties.

Table 7: Comparison among the proportionality gauges

Proportionality Gauge			$\mathbf{a} \perp?$	$\mathbf{a} \in \text{span}(\{\mathbf{f}, \mathbf{r}^{-1}\})?$	Trajectory to \mathbf{r}^{-1} ray	PL inequality in Lemma (5)
based on	ω	a				
CSZ Inequality	(10)	(11)	\mathbf{f}	Yes	Curved	Satisfied
Lagrange Identity	(12)	(13)	\mathbf{r}^{-1}	Yes	Straight	Satisfied
KL Divergence	(33)	(34)	\mathbf{f}	No	Curved	Not Satisfied

B Constrained Multi-Objective Optimization

Our approach for Constrained MOO is similar to that of Fliege and Vaz (2016), where the descent based method (discussed in §2.1.1) is used to handle constraints. But their method cannot obtain EPO solutions specific to an \mathbf{r} like ours, which is facilitated by both ascent and descent. The constrained domain or *Feasible Solution Set* is defined as

$$\mathbb{X} := \left\{ \mathbf{x} \in \mathbb{R}^n \mid \begin{array}{l} b_i^l \leq x_i \leq b_i^u \quad \forall i \in [n], \\ g_k(\mathbf{x}) \leq 0 \quad \forall k \in [p], \\ h_k(\mathbf{x}) = 0 \quad \forall k \in [q] \end{array} \right\}, \quad (35)$$

where b^l & b^u are domain boundaries for each variable, $\mathbf{g} : \mathbb{R}^n \rightarrow \mathbb{R}^p$ are p differentiable inequality constraints, and $\mathbf{h} : \mathbb{R}^n \rightarrow \mathbb{R}^q$ are q differentiable equality constraints.

We check for the infeasibility of boundary, equality and inequality constraints in each iteration. If x^t violates any of the boundary constraints, we project element-wise to $\pi(\mathbf{x}^t)$, to constrain them to remain within the bounds, where

$$\pi(x_i^t) = \begin{cases} b_i^l, & \text{if } x_i^t < b_i^l, \\ x_i^t, & \text{if } x_i^t \in [b_i^l, b_i^u], \\ b_i^u, & \text{if } x_i^t > b_i^u \end{cases} \quad \text{for all } i \in [n]. \quad (36)$$

Let the number of active inequality constraints be p_a , making $p_a + q$ total active constraints, since the equality constraints are always active. Without loss of generality, let the active inequality constraints be g_k for $k = 1, \dots, p_a$. Then the cone of first order feasible directions at \mathbf{x}^t against which we can move to obtain $\mathbf{x}^{t+1} \in \mathbb{X}$ is given by

$$\mathcal{F}_{\mathbb{X}}(\mathbf{x}^t) = \{ \mathbf{d} \in \mathbb{R}^n \mid \mathbf{d}^T \nabla_{\mathbf{x}} g_k^t \geq 0 \quad \forall k \in [p_a], \text{ and } \mathbf{d}^T \nabla_{\mathbf{x}} h_k^t = 0 \quad \forall k \in [q] \}, \quad (37)$$

where $g_k^t = g_k(\mathbf{x}^t)$ and $h_k^t = h_k(\mathbf{x}^t)$. When there is no active constraint it is the same as the tangent plane: $\mathcal{F}_{\mathcal{X}}(\mathbf{x}^t) = \mathcal{T}_{\mathcal{X}}(\mathbf{x}^t) = \mathbb{R}^n$. Note, the tangent plane is the set of directions that keeps the next iterate in the feasible region:

$$\mathcal{T}_{\mathcal{X}}(\mathbf{x}^t) := \{\mathbf{d} \in \mathbb{R}^n \mid \exists \eta > 0 \text{ s.t. } \mathbf{x}^t - \eta \mathbf{d} = \mathbf{x}^{t+1} \in \mathcal{X}\}. \quad (38)$$

When there are active constraints, the tangent plane becomes a tangent cone as certain directions would lead \mathbf{x}^{t+1} out of the feasible region \mathcal{X} . However, the first order feasible directions $\mathcal{F}_{\mathcal{X}}(\mathbf{x}^t)$ may not be equal to $\mathcal{T}_{\mathcal{X}}(\mathbf{x}^t)$ always. The tangent cone $\mathcal{T}_{\mathcal{X}}(\mathbf{x}^t)$ is unique and depends on the geometrical property of \mathcal{X} at \mathbf{x}^t . But, the $\mathcal{F}_{\mathcal{X}}(\mathbf{x}^t)$ cone is not unique and depends on the algebraic specification of the constraints (see (Nocedal and Wright 2006)[Ch 12.2]) through the functions g_k s and h_k s. E.g., although the constraints $g(\mathbf{x}) = x_i \leq 0$ and $g'(\mathbf{x}) = x_i^3 \leq 0$ are algebraically different (at $\mathbf{x} = \mathbf{0}$, $\frac{\partial g}{\partial x_i} = 1$ whereas $\frac{\partial g'}{\partial x_i} = 0$), they are geometrically the same constraints. At a boundary point $\mathbf{x}^t \in \partial\mathcal{X}$, $\mathcal{F}_{\mathcal{X}}(\mathbf{x}^t) = \mathcal{T}_{\mathcal{X}}(\mathbf{x}^t)$ if the $p_a + q$ gradients of the active constraint function are linearly independent (Nocedal and Wright 2006). This is called as *Linear Independence Constraint Qualification* (LICQ). Therefore, to make $\mathcal{F}_{\mathcal{X}}(\mathbf{x}^t)$ same as the tangent cone $\mathcal{T}_{\mathcal{X}}(\mathbf{x}^t)$, and render the conditions in (37) useful, we assume the LICQ to be satisfied at every $\mathbf{x} \in \partial\mathcal{X}$.

B.1 Constrained EPO Search for Random Initialization

We modify the QP (17) into

$$\boldsymbol{\beta}^* = \arg \min_{\boldsymbol{\beta} \in \mathbb{R}^m \mid \|\boldsymbol{\beta}\|_1 \leq 1} \|\mathbf{F}\mathbf{F}^T \boldsymbol{\beta} - \mathbf{a}\|^2 \quad (39a)$$

$$\text{s.t. } \boldsymbol{\beta}^T \mathbf{F} \nabla g_k \geq 0, \quad \text{for all } k \in [p_a], \quad (39b)$$

$$\boldsymbol{\beta}^T \mathbf{F} \nabla h_k = 0, \quad \text{for all } k \in [q], \quad (39c)$$

$$\boldsymbol{\beta}^T \mathbf{F} \nabla f_j \geq 0, \quad \text{for all } j \in \mathbf{J} = \begin{cases} \mathbf{J}^* & \text{in balance mode} \\ [m] & \text{in descent mode} \end{cases}, \quad (39d)$$

where \mathbf{J}^* is as defined in (17c). This is similar to the gradient projection strategy for constrained SOO (Luenberger and Ye 2008). The search direction $\mathbf{d}_{nd} = \mathbf{F}^T \boldsymbol{\beta}$, can be considered as the projection of the search direction obtained from QP (17) onto the set $\mathcal{F}_{\mathcal{X}}(\mathbf{x}^t)$ (37). However in practice, at a boundary point $\mathbf{x}^t \in \partial\mathcal{X}$, the projected gradient may not guarantee to move the iterate to $\text{Int}(\mathcal{X})$, the interior of \mathcal{X} , unless the step size is infinitesimal. Therefore, in our implementation we modify (39b) to $\boldsymbol{\beta}^T \mathbf{F} \nabla g_k \geq \gamma_k$ for a $\gamma_k > 0$ whenever the inequality constraint is violated $g_k(\mathbf{x}^t) > 0$. Similarly, we modify (39c) to $\boldsymbol{\beta}^T \mathbf{F} \nabla h_{k'} \geq \gamma_{k'}$ if $h_{k'}(\mathbf{x}^t) > 0$ and $\boldsymbol{\beta}^T \mathbf{F} \nabla h_{k'} \leq \gamma_{k'}$ if $h_{k'}(\mathbf{x}^t) < 0$ for a $\gamma_{k'} > 0$. We increase the values of γ if $\mathbf{x}^{t+1} \notin \mathcal{X}$, and increase further as $\gamma \leftarrow 2 * \gamma$, until the iterate becomes feasible.

Similar to the unconstrained MOO case, this QP also satisfies the following two Lemmas by construction:

Lemma 6. *If \mathbf{x}^t is a non-PO regular point of the differentiable vector function \mathbf{f} in a balance mode, i.e. $\omega(\mathbf{f}^t, \mathbf{r}^{-1}) > \epsilon_1$, then the non-dominating direction obtained from QP (39) makes*

1. *non-negative angles with the gradients of maximum relative objectives: $\mathbf{d}_{nd}^T \nabla_{\mathbf{x}^t} f_j \geq 0 \forall j \in \mathbf{J}^*$ (17c),*

2. *a positive angle with the balancing anchor direction (13) in the objective space: $\mathbf{a}^T \mathbf{F} \mathbf{d}_{nd} > 0$.*

Lemma 7. *If \mathbf{x}^t is a non-PO regular point of the differentiable vector function \mathbf{f} in a descent mode, i.e. $\omega(\mathbf{f}^t, \mathbf{r}^{-1}) \leq \epsilon_1$, then the non-dominating direction obtained from QP (39) makes a non-negative angle with every gradient, $\mathbf{d}_{nd}^T \nabla_{\mathbf{x}^t} f_j^t \geq 0 \forall j \in [m]$, and a positive angle with at least one gradient.*

B.2 Constrained EPO Search for Tracing the Pareto Front from $\mathbf{x}^0 \in \mathcal{P}$

We modify the QP (22) into

$$\boldsymbol{\beta}^* = \arg \min_{\boldsymbol{\beta} \in [-1,1]^m} \|\mathbf{F}\mathbf{F}^T \boldsymbol{\beta} - \mathbf{a}\|^2 \quad (40a)$$

$$\text{s.t. } \boldsymbol{\beta}^T \mathbf{F} \nabla g_k \geq 0, \quad \text{for all } k \in [p_a], \quad (40b)$$

$$\boldsymbol{\beta}^T \mathbf{F} \nabla h_k = 0, \quad \text{for all } k \in [q], \quad (40c)$$

$$\mathbb{1}_{des} \boldsymbol{\beta}^T \mathbf{F} \mathbf{F}^T \mathbf{a}^{bal} \geq 0, \quad (40d)$$

$$\text{and } \mathbb{1}_{des} \boldsymbol{\beta}^T \mathbf{F} \nabla f_j \geq 0 \quad \forall j \in [m], \quad (40e)$$

where \mathbf{a}^{bal} is the CSZ inequality based anchor direction (11). Note that we have excluded the constraint (39d) associated to objectives of \mathbf{J}^* . Because, if the objective vector \mathbf{f}^t is (approximately) on the Pareto front, then some objectives with highest relative value ($r_j f_j^t$) may require a further increase in their value to move towards an EPO solution.

Pareto Criticality for constrained MOO:

At a point \mathbf{x}^t , the set of descent directions is given by $\mathcal{D}_{\mathcal{X}}^{\mathbf{f}}(\mathbf{x}^t) = \{\mathbf{d} \in \mathcal{T}_{\mathcal{X}}(\mathbf{x}^t) \mid \mathbf{d}^T \nabla_{\mathbf{x}^t} f_j \geq 0, \forall j \in [m]\}$. At a local Pareto optimal point \mathbf{x}^* there does not exist any non-zero feasible descent direction, i.e. $\mathcal{D}_{\mathcal{X}}^{\mathbf{f}}(\mathbf{x}^*) \cap \mathcal{F}_{\mathcal{X}}(\mathbf{x}^*) = \{\mathbf{0}\}$. Note that, if there are no active constraints at \mathbf{x}^* , $\mathcal{D}_{\mathcal{X}}^{\mathbf{f}}(\mathbf{x}^*) = \{\mathbf{0}\}$. A necessary condition to check if a point \mathbf{x}^t is Pareto optimal, i.e., $\mathcal{D}_{\mathcal{X}}^{\mathbf{f}}(\mathbf{x}^t) \cap \mathcal{F}_{\mathcal{X}}(\mathbf{x}^t) = \{\mathbf{0}\}$, is given by Pareto Criticality:

$$\text{there exists a } \boldsymbol{\beta} \in \mathcal{S}^m, \boldsymbol{\rho} \in \mathbb{R}_{+}^{p_a}, \text{ and } \boldsymbol{\gamma} \in \mathbb{R}^q, \text{ s.t. } \mathbf{F}^T \boldsymbol{\beta} + \mathbf{G}^T \boldsymbol{\rho} + \mathbf{H}^T \boldsymbol{\gamma} = \mathbf{0}, \quad (41)$$

where G and H are the Jacobians of inequality and equality constraints. This is formulated by extending the KKT conditions to a multi-objective setup (see (Hillermeier 2001)[Ch 4]). When there are no active constraints at an optimal point $\mathbf{x}^* \in \mathcal{P}$, the Pareto criticality condition in (41) reduces to $\mathbf{F}^T \boldsymbol{\beta} = \mathbf{0}$ for some $\boldsymbol{\beta} \in \mathcal{S}^m$.

Penetration Assumption:

We introduce the penetration assumption to guarantee non-convergence at a non-EPO point when there are active constraints, i.e. $\mathbf{x}^* \in \partial \mathcal{X}$ and $\mathcal{F}_{\mathcal{X}}(\mathbf{x}^*) \subsetneq \mathbb{R}^n$. We assume there exists an $\eta_0 > 0$ such that $\mathbf{f}^* + \eta \vec{\mathbf{f}}^* \in \text{Int}(\mathcal{O})$ for all $\eta \in [0, \eta_0]$, where $\mathbf{f}^* = \mathbf{f}(\mathbf{x}^*)$. In other words, an infinitesimal step along the direction of objective vector $\vec{\mathbf{f}}^*$ starting from $\mathbf{f}^* \in \partial \mathcal{O}$ will take it to the interior of \mathcal{O} . We call this as $\vec{\mathbf{f}}^*$ penetrates \mathcal{O} .

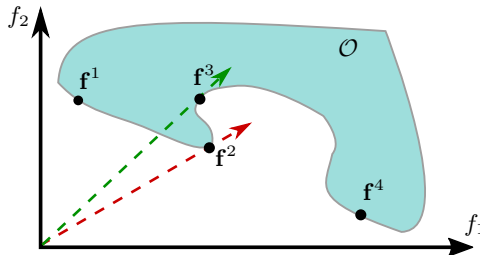


Figure 11: Penetration assumption is violated at \mathbf{f}^2 . Therefore EPO search for tracing in Algorithm 2 will not be able to trace from \mathbf{f}^1 to \mathbf{f}^4 ; the iterations will converge (stop prematurely) at \mathbf{f}^2 . But it can trace from \mathbf{f}^3 to \mathbf{f}^4 . Note that the set of points on boundary $\partial \mathcal{O}$ from \mathbf{f}^2 to \mathbf{f}^3 is not locally Pareto Optimal.

Theorem 5. Let $\mathbf{x}^* \in \mathcal{P}$ such that, if $\mathbf{x}^* \in \text{Int}(\mathcal{X})$ then it is a regular Pareto optimal solution, and if $\mathbf{x}^* \in \partial \mathcal{X}$ then it is a regular point of \mathbf{f} and $\vec{\mathbf{f}}^*$ penetrates \mathcal{O} . Then, at \mathbf{x}^* , the non-dominating direction $\mathbf{d}_{nd} = \mathbf{F}^T \boldsymbol{\beta}^*$ found by the QP (40) with Cauchy-Schwarz anchor (11) is $\mathbf{0} \in \mathbb{R}^n$ if and only if $\mathbf{x}^* \in \mathcal{P}_r$.

We consider the penetration assumption to be mild because, when the range set \mathcal{O} is m dimensional and its boundary $\partial \mathcal{O}$ is $m - 1$ dimensional, almost all points in $\partial \mathcal{O}$ that violate the penetration assumption are not Pareto optimal, not even locally. Figure 11 illustrates a scenario where it is

violated. If a point $\hat{\mathbf{f}} \in \partial\mathcal{O}$ violates penetration along with the points in any of its $m - 1$ dimensional (relative) open neighbourhoods in $\partial\mathcal{O}$, then $-\vec{\hat{\mathbf{f}}}$ penetrates \mathcal{O} , and thus $\hat{\mathbf{f}}$ is dominated by $\hat{\mathbf{f}} - \eta \vec{\hat{\mathbf{f}}}$ for some small η . The assumption of $m - 1$ dimensional boundary is fairly general since it is similar to the assumption of regular Pareto optimal in the unconstrained case.

C Proofs of Lemmas and Theorems

C.1 Proportionality Gauge

Lemma 1. *If all the objective functions are differentiable, then for any direction $\mathbf{d} \in \mathbb{R}^n$ satisfying $\mathbf{a}^T \mathbf{F} \mathbf{d} \geq 0$, where \mathbf{F} is the Jacobian of \mathbf{f} at \mathbf{x} , and $\max_j \{\mathbf{d}^T \nabla_{\mathbf{x}} f_j\} > 0$, there exists a step size $\eta_0 > 0$ such that for all $\eta \in [0, \eta_0]$*

$$\omega(\mathbf{f}(\mathbf{x} - \eta \mathbf{d}), \mathbf{r}^{-1}) \leq \omega(\mathbf{f}(\mathbf{x}), \mathbf{r}^{-1}), \text{ and} \quad (9a)$$

$$\mathbf{f}(\mathbf{x} - \eta \mathbf{d}) \not\prec \mathbf{f}(\mathbf{x}). \quad (9b)$$

Proof. We first prove (9a) by considering $\omega(\mathbf{f}(\mathbf{x}), \mathbf{r}^{-1})$ as a function of \mathbf{x} , $\omega_{\mathbf{r}}^{\mathbf{f}}(\mathbf{x})$. Taylor's expansion of this function can be written with the Peano's form of remainder as

$$\omega_{\mathbf{r}}^{\mathbf{f}}(\mathbf{x} - \eta \mathbf{d}) = \omega_{\mathbf{r}}^{\mathbf{f}}(\mathbf{x}) - \eta \frac{\partial \omega_{\mathbf{r}}^{\mathbf{f}}}{\partial \mathbf{x}} \mathbf{d} + o(\eta), \quad (42)$$

where $\frac{\partial \omega_{\mathbf{r}}^{\mathbf{f}}}{\partial \mathbf{x}}$ is the transpose of gradient $\nabla_{\mathbf{x}} \omega_{\mathbf{r}}^{\mathbf{f}}$, and the asymptotic notation little- $o(\eta)$ represents a function that approaches 0 faster than η . In particular, for every $\epsilon > 0$, there exists an $\eta_0 > 0$ such that

$$\left| \frac{o(\eta)}{\eta} \right| < \epsilon, \text{ for } |\eta| < \eta_0. \quad (43)$$

Applying chain rule of differentiation on ω , we get

$$\frac{\partial \omega_{\mathbf{r}}^{\mathbf{f}}}{\partial \mathbf{x}} = \frac{\partial \omega_{\mathbf{r}}}{\partial \mathbf{f}} \frac{\partial \mathbf{f}}{\partial \mathbf{x}} = \mathbf{a}^T \mathbf{F}.$$

We know that $\mathbf{a}^T \mathbf{F} \mathbf{d}$ is non-negative from the statement of the Lemma 1. Therefore, when positive, we treat $\mathbf{a}^T \mathbf{F} \mathbf{d}$ as ϵ , and use the property of $o(\eta)$ as mentioned in (43) to conclude there exists a step size $\eta_0 > 0$ such that

$$\left| \frac{o(\eta)}{\eta} \right| < \mathbf{a}^T \mathbf{F} \mathbf{d}, \forall \eta \in [0, \eta_0], \quad (44)$$

and hence $\omega_{\mathbf{r}}^{\mathbf{f}}(\mathbf{x} - \eta \mathbf{d}) \leq \omega_{\mathbf{r}}^{\mathbf{f}}(\mathbf{x})$; equality holds when $\mathbf{a}^T \mathbf{F} \mathbf{d} = 0$. That proves (9a).

The above strategy can be applied to prove there exists a step size $\eta_0 > 0$ such that

$$f_{j^*}(\mathbf{x} - \eta \mathbf{d}) \leq f_{j^*}(\mathbf{x}), \quad \forall \eta \in [0, \eta_0], \quad (45)$$

$$\text{where } j^* = \arg \max_{j \in [m]} \mathbf{d}^T \nabla_{\mathbf{x}} f_j. \quad (46)$$

This is true because of the assumption in Lemma 1 that $\mathbf{d}^T \nabla_{\mathbf{x}} f_{j^*} > 0$. And that proves (9b). \square

In the following Lemma 8, we prove a property of scale invariant balancing anchor direction, that will be used in the proves of Theorem 1.

Lemma 8. *If ω is such that the anchoring direction is scale invariant to \mathbf{r} , i.e., $\vec{\mathbf{a}}(\mathbf{f}, s\mathbf{r}) = \vec{\mathbf{a}}(\mathbf{f}, \mathbf{r})$ for all $s > 0$, where $\vec{\mathbf{a}} = \frac{\mathbf{a}}{\|\mathbf{a}\|}$ then*

$$\sum_{j=1}^m f_j a_j = \langle \mathbf{f}, \mathbf{a} \rangle \geq 0 \geq \langle \mathbf{r}^{-1}, \mathbf{a} \rangle = \sum_{j=1}^m \frac{a_j}{r_j}. \quad (47)$$

Proof. We use the second property of ω_r , stated in 2, i.e. $\omega_r(\mathbf{r}^{-1} + \lambda(\mathbf{f} - \mathbf{r}^{-1}))$ increases monotonically with $\lambda \geq 0$. In other words, $\omega_r'(\lambda) = \frac{d\omega_r}{d\lambda} \geq 0$, for $\lambda \geq 0$. At $\lambda = 1$, the chain rule reveals

$$\omega_r'(1) = \langle \mathbf{f} - \mathbf{r}^{-1}, \mathbf{a}(\mathbf{f}, \mathbf{r}^{-1}) \rangle \geq 0 \quad (48)$$

$$\implies \langle \mathbf{f}, \bar{\mathbf{a}}(\mathbf{f}, \mathbf{r}^{-1}) \rangle \geq \langle \mathbf{r}^{-1}, \bar{\mathbf{a}}(\mathbf{f}, \mathbf{r}^{-1}) \rangle. \quad (49)$$

We apply the scale invariance property of the anchor direction to the preference vector in (49):

$$\langle \mathbf{f}, \bar{\mathbf{a}}(\mathbf{f}, s\mathbf{r}^{-1}) \rangle \geq \langle s\mathbf{r}^{-1}, \bar{\mathbf{a}}(\mathbf{f}, s\mathbf{r}^{-1}) \rangle \quad (50)$$

$$\implies \langle \mathbf{f}, \bar{\mathbf{a}}(\mathbf{f}, \mathbf{r}^{-1}) \rangle \geq s \langle \mathbf{r}^{-1}, \bar{\mathbf{a}}(\mathbf{f}, \mathbf{r}^{-1}) \rangle \quad \forall s > 0. \quad (51)$$

Applying $\lim_{s \rightarrow 0}$ to (51), we get $\langle \mathbf{f}, \bar{\mathbf{a}} \rangle \geq 0$. Therefore, applying $\lim_{s \rightarrow \infty}$ to (51), we get $\langle \mathbf{r}^{-1}, \bar{\mathbf{a}} \rangle \leq 0$, i.e. must not be positive. \square

Theorem 1. *If a balancing anchor direction \mathbf{a} is scale invariant to \mathbf{r} and all the objective functions are differentiable at \mathbf{x}^t , then moving against a direction $\mathbf{d} \in \mathbb{R}^n$ with $\mathbf{F}\mathbf{d} = s\mathbf{a}$, for some $s > 0$, yields a non-dominated solution \mathbf{x}^{t+1} such that $\mathbf{f}(\mathbf{x}^{t+1})$ is closer to the \mathbf{r}^{-1} ray than $\mathbf{f}(\mathbf{x}^t)$.*

Proof. From Lemma 8, we know $\langle \mathbf{f}, \mathbf{a} \rangle \geq 0$. Therefore, $a_{j^+} > 0$ for at least one $j^+ \in [m]$, because $f_j \geq 0$ for all $j \in [m]$. As $\mathbf{F}\mathbf{d} = s\mathbf{a}$ for some $s > 0$, we can write

$$1. \ 0 < sa_{j^+} = \mathbf{d}^T \nabla_{\mathbf{x}} f_{j^+} < \max_j \{ \mathbf{d}^T \nabla_{\mathbf{x}} f_j \}, \text{ and}$$

$$2. \ \mathbf{a}^T \mathbf{F}\mathbf{d} = s \|\mathbf{a}\|_2^2 > 0$$

So Lemma 1 is applicable, and that concludes the proof. \square

Claim 1. *The anchor direction \mathbf{a} in (11) is always orthogonal to the objective vector \mathbf{f} : $\mathbf{a}^T \mathbf{f} = 0$.*

Proof. The proof is apparent from the formula of the anchoring direction (11). \square

Claim 2. *The anchor direction \mathbf{a} in (13) is always orthogonal to the \mathbf{r}^{-1} ray: $\mathbf{a}^T \mathbf{r}^{-1} = 0$.*

Proof. The proof is apparent from the formula of the anchoring direction (13). \square

Claim 3. *The anchor direction \mathbf{a} in (34) is always orthogonal to the objective vector \mathbf{f} : $\mathbf{a}^T \mathbf{f} = 0$.*

Proof. We expand $c\mathbf{a}^T \mathbf{f}$, where $c = \|\mathbf{r} \odot \mathbf{f}\|_1$, as

$$\begin{aligned} c\mathbf{a}^T \mathbf{f} &= \sum_{j=1}^m r_j \left(\log(m\hat{f}_j) - \omega_r(\mathbf{f}) \right) \times f_j \\ &= \sum_{j=1}^m r_j f_j \left((1 - \hat{f}_j) \log(\hat{f}_j) - \sum_{j' \neq j} \hat{f}_{j'} \log(\hat{f}_{j'}) \right), \end{aligned}$$

where $\hat{f}_j = f_j r_j / \|\mathbf{r} \odot \mathbf{f}\|_1$. We use the fact that $\sum_{j=1}^m \hat{f}_j = 1$, and further expand as

$$\begin{aligned} c\mathbf{a}^T \mathbf{f} &= \sum_{j=1}^m r_j f_j \left(\sum_{j' \neq j} \hat{f}_{j'} \log(\hat{f}_j) - \sum_{j' \neq j} \hat{f}_{j'} \log(\hat{f}_{j'}) \right) \\ &= \sum_{j=1}^m r_j f_j \left(\sum_{j' \neq j} \hat{f}_{j'} \log\left(\frac{\hat{f}_j}{\hat{f}_{j'}}\right) \right). \end{aligned}$$

In the inner summation we can now add the term for $j = j'$ as $\log\left(\frac{\hat{f}_j}{\hat{f}_{j'}}\right) = \log(1) = 0$ and write the above expression as

$$c\mathbf{a}^T \mathbf{f} = \frac{1}{\sum_{j=1}^m r_j f_j} \sum_{j=1}^m \sum_{j'=1}^m r_j f_j r_{j'} f_{j'} \log\left(\frac{\hat{f}_j}{\hat{f}_{j'}}\right)$$

The double summation in the numerator can be written as the inner product of a symmetric and a skew-symmetric matrix which is equal to 0. \square

C.2 EPO Search for Unconstrained MOO

Lemma 2. *If \mathbf{x}^t is a regular point of the differentiable vector function \mathbf{f} in a balance mode, i.e. $\omega(\mathbf{f}^t, \mathbf{r}^{-1}) > \epsilon_1$, then the non-dominating direction obtained from QP (17) makes*

1. *non-negative angles with the gradients of maximum relative objectives: $\mathbf{d}_{nd}^T \nabla_{\mathbf{x}^t} f_j \geq 0 \forall j \in \mathbf{J}^*$ (17c),*
2. *a positive angle with the balancing anchor direction (13) in the objective space: $\mathbf{a}^T \mathbf{F} \mathbf{d}_{nd} > 0$.*

Proof. We denote the subset of all possible directions in the tangent space $\mathcal{T}_{\mathcal{O}}(\mathbf{f})$ of an objective vector $\mathbf{f} \in \mathcal{O} \subset \mathbb{R}^m$, which is constrained due to ℓ_1 restrictions on the coefficients $\boldsymbol{\beta}$, as

$$\mathcal{CH}_{\mathbf{f}}^{\pm} := \{\mathbf{F}\mathbf{F}^T \boldsymbol{\beta} \mid \|\boldsymbol{\beta}\|_1 \leq 1\} = \{\mathbf{F}\mathbf{d} \mid \mathbf{d} \in \mathcal{CH}_{\mathbf{x}}^{\pm}\}, \quad (52)$$

where $\mathcal{CH}_{\mathbf{x}}^{\pm}$ is defined in (16). We split the proof for two scenarios: 1) $\mathbf{a} \in \mathcal{CH}_{\mathbf{f}}^{\pm}$ and 2) $\mathbf{a} \notin \mathcal{CH}_{\mathbf{f}}^{\pm}$.

In the first scenario, the the minimum value 0 is achieved for the objective (17a) with $\boldsymbol{\beta}^* = (\mathbf{F}\mathbf{F}^T)^{-1} \mathbf{a}$, $\mathbf{d}_{nd} = \mathbf{F}^T \boldsymbol{\beta}^*$, and hence

$$\mathbf{F} \mathbf{d}_{nd} = \mathbf{a}. \quad (53)$$

We can invert $\mathbf{F}\mathbf{F}^T$ due to the regularity assumption. Note that $a_j > 0$ for all $j \in \mathbf{J}^*$ when \mathbf{f}^t and \mathbf{r}^{-1} are not proportional. This can be deduced from its formula in (13) as follows

1. $\text{sign}(a_j) = \text{sign}(r_j a_j) \forall j \in \mathbf{J}^* \quad \because r_j > 0 \text{ for all } j \in [m].$
2. $\max_{j \in [m]} a_j > 0. \quad \because \text{If not true, then Claim 2 is contradicted for any } \mathbf{r} \in \mathbb{R}_{++}^m.$
3. $\max_{j \in [m]} r_j a_j = \max_{j \in [m]} f_j^t r_j - \frac{\langle \mathbf{f}^t, \mathbf{r}^{-1} \rangle}{\|\mathbf{r}^{-1}\|^2} = r_{j^*} a_{j^*}, \text{ for any } j^* \in \mathbf{J}^*. \quad \because \text{definition of } \mathbf{a} \text{ in (13).}$
4. $\therefore 1, 2 \text{ and } 3 \implies \text{sign}(a_j) > 0 \text{ for all } j \in \mathbf{J}^*.$

As a result, the constraint (17b) is inactive when $\mathbf{a} \in \mathcal{CH}_{\mathbf{f}}^{\pm}$, because $\boldsymbol{\beta}^T \mathbf{F} \nabla_{\mathbf{x}^t} f_j = a_j$. Now, with $\mathbf{F} \mathbf{d}_{nd} = \mathbf{a}$ we can invoke Theorem 1, and that proves Lemma 2 for the first scenario.

In the second scenario, i.e., $\mathbf{a} \notin \mathcal{CH}_{\mathbf{f}}^{\pm}$, the \mathbf{d}_{nd} satisfies the first property, i.e., $\mathbf{d}_{nd}^T \nabla_{\mathbf{x}^t} f_j \geq 0$ for all $j \in \mathbf{J}^*$, due to the constraint (17b). We prove the second property, i.e., $\mathbf{a}^T \mathbf{F} \mathbf{d}_{nd} > 0$, by contradiction. Let $\boldsymbol{\beta}^*$ be the optimum of the QP (17), such that $\mathbf{a}^T \mathbf{F} \mathbf{d}_{nd} = \mathbf{a}^T \mathbf{F} \mathbf{F}^T \boldsymbol{\beta}^* \leq 0$. Then the optimal cost value of (17a) can be written as

$$\|\mathbf{F}\mathbf{F}^T \boldsymbol{\beta}^* - \mathbf{a}\|_2 = \|\mathbf{F}\mathbf{F}^T \boldsymbol{\beta}^*\|_2^2 + \|\mathbf{a}\|_2^2 - 2\mathbf{a}^T \mathbf{F}\mathbf{F}^T \boldsymbol{\beta}^* > \|\mathbf{a}\|_2^2. \quad (54)$$

However, this is a contradiction due to the following counterexample that yields a lesser value of the cost than $\boldsymbol{\beta}^*$. The $\hat{\boldsymbol{\beta}} = \frac{(\mathbf{F}\mathbf{F}^T)^{-1} \mathbf{a}}{\|(\mathbf{F}\mathbf{F}^T)^{-1} \mathbf{a}\|_1}$ satisfies the constraints (17b) as proven for the previous scenario, and the cost value of this coefficient is $\left(1 - \frac{1}{\|(\mathbf{F}\mathbf{F}^T)^{-1} \mathbf{a}\|_1}\right)^2 \|\mathbf{a}\|_2^2 < \|\mathbf{a}\|_2^2$. $\therefore \mathbf{a}^T \mathbf{F} \mathbf{d}_{nd} > 0$.

That concludes the proof. \square

Lemma 3. *If \mathbf{x}^t is a regular point of the differentiable vector function \mathbf{f} in a descent mode, i.e. $\omega(\mathbf{f}^t, \mathbf{r}^{-1}) \leq \epsilon_1$, then the non-dominating direction obtained from QP (17) makes a non-negative angle with every gradient, $\mathbf{d}_{nd}^T \nabla_{\mathbf{x}^t} f_j \geq 0 \forall j \in [m]$, and a positive angle with at least one gradient.*

Proof. In the descent mode the anchor direction is $\mathbf{a} = \mathbf{f}^t$. Similar to the proof of Lemma 2, we split this proof into two scenarios: 1) $\mathbf{a} \in \mathcal{CH}_{\mathbf{f}}^{\pm}$ and 2) $\mathbf{a} \notin \mathcal{CH}_{\mathbf{f}}^{\pm}$, where $\mathcal{CH}_{\mathbf{f}}^{\pm}$ is defined in (52).

For the first scenario, the proof is similar to that of Lemma 2, where $\boldsymbol{\beta}^* = (\mathbf{F}\mathbf{F}^T)^{-1} \mathbf{a}$. And the constraint (17b) is redundant, since $\mathbf{d}_{nd}^T \nabla_{\mathbf{x}^t} f_j = f_j^t \geq 0$ for all $j \in [m]$. There exist at least one $j \in [m]$ such that $f_j^t > 0$, and therefore \mathbf{d}_{nd} makes positive angle with the corresponding gradient. The point $\mathbf{0} \in \mathbb{R}^m$ is a utopia point in our formulation and cannot be attained.

For the second scenario the first property is true due to the constraint (17b). The second property of making a positive angle with at least one gradient can be proven by contradiction similar to the proof Lemma 2. \square

Beyond Regularity Assumption: Lemmas 2 and 3 can be true even without the full rank assumption of F . In particular, when \mathbf{x}^t is in the interior of the domain, (53) can be satisfied if the anchor direction $\mathbf{a} \in \text{Col}(FF^T)$, the column space of FF^T .

Lemma 4. *If \mathbf{x}^t is a regular point of \mathbf{f} , there exists a step size $\eta_0 > 0$, such that for every $\eta \in [0, \eta_0]$, the objective vector of $\mathbf{x}^{t+1} = \mathbf{x}^t - \eta \mathbf{d}_{nd}$ lies in the t^{th} admissible set: $\mathbf{f}(\mathbf{x}^{t+1}) \in \mathcal{A}_{\mathbf{f}^t}^r$.*

Proof. We prove for unconstrained MOO using Lemmas 2 and 3 for the QP (17). However, the same proof holds true for constrained MOO by using Lemmas 6 and 7 for the QP (39).

We divide the proof into descent mode and balance mode.

From Lemma 3, in the descent mode, i.e. $\mathbf{a} = \mathbf{f}^t$, The QP in (17), produces a search direction that makes non-negative angle with each gradient, i.e. $\mathbf{d}_{nd}^T \nabla_{\mathbf{x}} f_j \geq 0$ for all $j \in [m]$. As a result, by applying the Taylor's expansion with Peano form of remainder to each f_j along with the property of little-o notation, one can deduce that for every $j \in [m]$ there exists a step size $\eta_{0j} > 0$ such that $f_j(\mathbf{x}^t - \eta \mathbf{d}_{nd}) \leq f_j(\mathbf{x}^t)$ for all $\eta \in [0, \eta_{0j}]$. If we choose $\eta_0 = \min_j \{\eta_{0j}\}$, then for all $\eta \in [0, \eta_0]$, we have

$$\begin{aligned} \mathbf{f}(\mathbf{x}^t - \eta \mathbf{d}_{nd}) &\leq \mathbf{f}(\mathbf{x}^t) \\ \implies \mathbf{f}(\mathbf{x}^{t+1}) &\in \mathcal{V}_{\leq \mathbf{f}^t} \quad (\because \text{definition of } \mathcal{V}_{\leq \mathbf{f}^t} \text{ in (18)}) \quad (55) \\ \implies \mathbf{f}(\mathbf{x}^{t+1}) &\in \mathcal{A}_{\mathbf{f}^t}^r \quad (\because \text{definition of } \mathcal{A}_{\mathbf{f}^t}^r \text{ in (22a)}) \quad (56) \end{aligned}$$

Next, we consider the balance mode. Let $J^+ = \{j \mid \mathbf{d}_{nd}^T \nabla_{\mathbf{x}} f_j \geq 0\}$ be the index set for descending objectives and $J^- = [m] - J^+$ for ascending ones. So, there exists an $\eta_{0j} > 0$ for all $j \in J^+$ such that

$$f_j(\mathbf{x}^t - \eta \mathbf{d}_{nd}) = f_j^{t+1} \leq f_j^t$$

for all $\eta \in [0, \eta_{0j}]$. Let $\eta_0^{J^+} = \min_{j \in J^+} \{\eta_{0j}\}$, and $\tilde{\eta}_0 = \min\{\eta_0^{\omega_r}, \eta_0^{J^+}\}$, where $\eta_0^{\omega_r}$ is the maximum step size one can take so that $\omega_r(\mathbf{f}^{t+1}) \leq \omega_r(\mathbf{f}^t)$. Then for all $\eta \in [0, \tilde{\eta}_0]$, and $\mathbf{f}^{t+1} = \mathbf{f}(\mathbf{x}^t - \eta \mathbf{d}_{nd})$

$$\begin{aligned} \omega_r(\mathbf{f}^{t+1}) &\leq \omega_r(\mathbf{f}^t), \text{ and } \mathbf{f}_j^{t+1} \leq \mathbf{f}_j^t, \quad \forall j \in J^+. \\ \implies r_j f_j^{t+1} &\leq r_j f_j^t \leq \lambda^t \\ \implies f_j^{t+1} &\leq \check{f}_j^t, \quad \forall j \in J^+ \end{aligned}$$

Lemma 2 ensures that $J^* \subset J^+$. If all the other objectives in J^- also satisfy

$$r_j f_j^{t+1} \leq \lambda^t, \forall \eta \in [0, \tilde{\eta}_0]$$

then $\tilde{\eta}_0$ can be used as the step size as it is. If this is not the case, i.e. there exists some $j' \in J^-$ such that

$$r_{j'} f_{j'}(\mathbf{x}^t - \tilde{\eta}_0 \mathbf{d}_{nd}) > \lambda^t,$$

then continuity of the objective functions ensures that there must exist some $\eta_{0j'} < \tilde{\eta}_0$ such that

$$r_{j'} f_{j'}^{t+1} \leq \lambda^t, \forall \eta \in [0, \eta_{0j'}].$$

So choosing $\eta_0 = \min_{j'} \{\eta_{0j'}\}$ we finally get

$$\begin{aligned} \mathbf{r} \odot \mathbf{f}(\mathbf{x}^t - \eta \mathbf{d}_{nd}) &= \mathbf{r} \odot \mathbf{f}^{t+1} \leq \lambda^t \mathbf{r} \\ \implies \mathbf{f}^{t+1} &\leq \check{\mathbf{f}}^t \\ \therefore \mathbf{f}^{t+1} &\in \mathcal{A}_{\mathbf{f}^t}^r \end{aligned}$$

for all $\eta \in [0, \eta_0]$. \square

Theorem 2. *If \mathbf{f} is a differentiable regular vector valued objective, then the sequence of admissible sets $\{\mathcal{A}_{\mathbf{f}^t}^r\}$, which correspond to the solutions $\{\mathbf{x}^t\}$ produced according to Lemma 4 starting from a non-Pareto Optimal point $\mathbf{x}^0 \notin \mathcal{P}$, converges by decreasing monotonically $\mathcal{A}_{\mathbf{f}^{t+1}}^r \subset \mathcal{A}_{\mathbf{f}^t}^r$.*

Proof. We know from Lemmas 2 and 3 that $\mathbf{d}_{nd} \neq \mathbf{0}$ since it has positive angle with at least one gradient. Therefore, $\mathbf{f}^{t+1} \neq \mathbf{f}^t$. Now, using Lemma 4 we can conclude that $\mathcal{A}_{\mathbf{f}^t}^r \subset \mathcal{A}_{\mathbf{f}^t}$, and everywhere regularity assumption ensures that $\{\mathcal{A}_{\mathbf{f}^t}^r\}$ converges. \square

Theorem 3. *If $\mathbf{x}^* \in \mathcal{P}$ is a regular Pareto Optimal solution, and its non-dominating direction $\mathbf{d}_{nd} = \mathbf{F}^T \boldsymbol{\beta}^*$ is obtained by the QP (22) with Cauchy-Schwarz inequality-based balancing anchor (11), then $\mathbf{d}_{nd} = \mathbf{0}$ if and only if $\mathbf{x}^* \in \mathcal{P}_r$.*

Proof. The necessity prove is trivial; because if $\mathbf{x}^* \in \mathcal{P}_r$, then the CSZ inequality based anchor direction \mathbf{a} in (11) is $\mathbf{0}_m \in \mathbb{R}^m$, resulting a $\mathbf{0}_m$ coefficient $\boldsymbol{\beta}$ from the QP (22), and $\mathbf{0}_n$ search direction.

For the sufficiency, we prove the contra-positive: if $\mathbf{x}^* \notin \mathcal{P}_r$, then $\mathbf{d}_{nd} \neq \mathbf{0}_n$. When $\mathbf{x}^* \notin \mathcal{P}_r$, \mathbf{a} is non-zero. For a non-zero \mathbf{a} , the $\boldsymbol{\beta}^*$ in the QP (22) will be zero only when \mathbf{a} lies in the null space of $\mathbf{F}\mathbf{F}^T$. But if $\mathbf{a} \in \text{Null}(\mathbf{F}\mathbf{F}^T)$, then $\mathbf{f}^* = \mathbf{f}(\mathbf{x}^*) \in \text{Col}(\mathbf{F}\mathbf{F}^T)$; because \mathbf{f}^* is orthogonal to the CSZ inequality-based anchor from Claim 1, and $\text{rank}(\mathbf{F}\mathbf{F}^T) = \text{rank}(\mathbf{F}) = m - 1$ from the regularity condition. If \mathbf{f}^* is in the column space of $\mathbf{F}\mathbf{F}^T$ then there exists a $\boldsymbol{\beta} \in \mathbb{R}^m$ such that $\mathbf{F}\mathbf{F}^T \boldsymbol{\beta} = \mathbf{f}^* > \mathbf{0}$, which makes $\mathbf{F}^T \boldsymbol{\beta}$ a descent direction. This is a contradiction, as no descent direction should exist at the Pareto optimal \mathbf{x}^* . In fact, the eigenvector \mathbf{v}_1 of $\mathbf{F}\mathbf{F}^T$ corresponding to its Null space must be an all positive vector like the objective vector \mathbf{f}^* in order to exclude all possible descent direction from the $\text{Col}(\mathbf{F}\mathbf{F}^T)$. Note, the eigenvectors of $\text{Col}(\mathbf{F}\mathbf{F}^T)$ are orthogonal to each other. Therefore $\mathbf{a} \notin \text{Null}(\mathbf{F}\mathbf{F}^T)$ and $\mathbf{F}\mathbf{F}^T \boldsymbol{\beta}^*$ will not be zero from the QP (22), hence $\mathbf{d}_{nd} \neq \mathbf{0}_n$. \square

Beyond Regularity Assumption: In general, this Theorem is true even without the regularity assumptions when the orthogonal projection of the CSZ inequality-based anchor \mathbf{a} (11) onto the hyperplane $\text{Col}(\mathbf{F}\mathbf{F}^T)$ is non-zero.

Issue of Lagrange Identity based Balancing Anchor Direction: The anchor direction in (13) is not orthogonal to the objective vector \mathbf{f}^* . Therefore, in a corner case, the anchor direction \mathbf{a} may be very close to the $\text{Null}(\mathbf{F}\mathbf{F}^T)$ as shown in Figure 12a. Therefore its projection on to $\text{Col}(\mathbf{F}\mathbf{F}^T)$ will vanish. However, CSZ inequality-based anchor (11) mitigates this issue as shown in Figure 12b. Note, the set $\mathcal{M}_{\mathbf{f}^t}^r$ defined in (19) is different for both the proportionality gauges. In practice, although this extreme scenario may not arise, but the projection of \mathbf{a} on to $\text{Col}(\mathbf{F}\mathbf{F}^T)$ will have a lesser magnitude in Lagrange identity based anchor as compared to that of KL divergence based anchor.

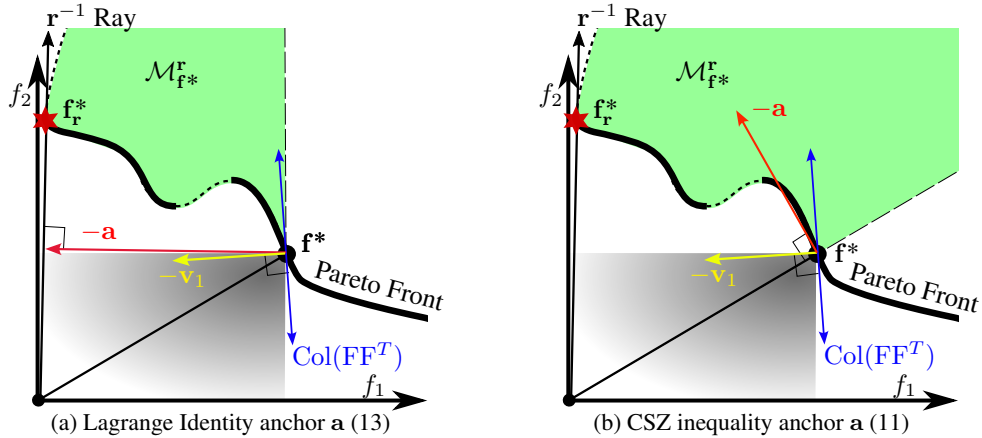


Figure 12: (Color Online) Illustration of a corner case where the Lagrange identity based anchor may not escape a PO solution \mathbf{f}^* , whereas the CSZ inequality based anchor can escape it to reach the EPO solution \mathbf{f}_r^* . The Null space of $\mathbf{F}\mathbf{F}^T$ is \mathbf{v}_1 . The green filled region is the set $\mathcal{M}_{\mathbf{f}^*}^r = \{\mathbf{f} \in \mathcal{O} \mid \omega_r(\mathbf{f}) \leq \omega_r(\mathbf{f}^*)\}$ for CSZ inequality and Lagrange identity based proportionality gauges ω_r defined in (12) and (10) respectively.

Lemma 5. *There exists a $\tau > 0$ such that the proportionality gauges $\omega_{\mathbf{r}}$ (10),(12) and their respective anchor directions \mathbf{a} in (11), (13) satisfy*

$$\frac{1}{2}\|\mathbf{a}(\mathbf{f})\|^2 \geq \tau\omega_{\mathbf{r}}(\mathbf{f}) \quad \forall \tau \leq \begin{cases} \langle \vec{\mathbf{f}}_0, \mathbf{r}^{-1} \rangle^2 \\ 1 \end{cases} \quad \text{and} \quad \forall \mathbf{f} \in \begin{cases} \mathcal{M}_{\mathbf{f}_0}^{\mathbf{r}} & \text{if Cauchy-Schwarz inequality} \\ \mathcal{O} & \text{if Lagrange's identity,} \end{cases} \quad (24)$$

where $\mathbf{f}^0 = \mathbf{f}(\mathbf{x}^0)$ is the initialization, $\vec{\mathbf{v}}$ is the ℓ_2 normalization of vector \mathbf{v} , and $\mathcal{M}_{\mathbf{f}_0}^{\mathbf{r}}$ is as in (19).

Proof. First we prove for the Cauchy-Schwarz inequality based $\omega_{\mathbf{r}}$ and \mathbf{a} .

$$\|\mathbf{a}\|^2 = \|\vec{\mathbf{f}} \langle \vec{\mathbf{f}}, \mathbf{r}^{-1} \rangle^2 - \mathbf{r}^{-1} \langle \vec{\mathbf{f}}, \mathbf{r}^{-1} \rangle\|^2 \quad (57)$$

$$\Rightarrow = \langle \vec{\mathbf{f}}, \mathbf{r}^{-1} \rangle^4 + \langle \vec{\mathbf{f}}, \mathbf{r}^{-1} \rangle^2 - 2 \langle \vec{\mathbf{f}}, \mathbf{r}^{-1} \rangle^4 \quad (58)$$

$$\Rightarrow = \langle \vec{\mathbf{f}}, \mathbf{r}^{-1} \rangle^2 - \langle \vec{\mathbf{f}}, \mathbf{r}^{-1} \rangle^4 \quad (59)$$

$$\Rightarrow = \langle \vec{\mathbf{f}}, \mathbf{r}^{-1} \rangle^2 (1 - \langle \vec{\mathbf{f}}, \mathbf{r}^{-1} \rangle^2) \quad (60)$$

$$\Rightarrow = \langle \vec{\mathbf{f}}, \mathbf{r}^{-1} \rangle^2 2\omega_{\mathbf{r}}(\mathbf{f}) \quad (61)$$

$$\Rightarrow \frac{1}{2}\|\mathbf{a}\|^2 \geq \langle \vec{\mathbf{f}}^0, \mathbf{r}^{-1} \rangle^2 \omega_{\mathbf{r}}(\mathbf{f}) \quad (\because \langle \vec{\mathbf{f}}, \mathbf{r}^{-1} \rangle \geq \langle \vec{\mathbf{f}}^0, \mathbf{r}^{-1} \rangle \quad \forall \mathbf{f} \in \mathcal{M}_{\mathbf{f}_0}^{\mathbf{r}}) \quad (62)$$

$$\therefore \frac{1}{2}\|\mathbf{a}\|^2 \geq \tau\omega_{\mathbf{r}} \quad \text{where } \tau \leq \langle \vec{\mathbf{f}}^0, \mathbf{r}^{-1} \rangle^2 \quad (63)$$

Next we prove for the Lagrange anchor (13).

$$\|\mathbf{a}\|^2 = \|\mathbf{f} - \langle \mathbf{f}, \mathbf{r}^{-1} \rangle \mathbf{r}^{-1}\|^2 \quad \text{where } \mathbf{r}^{-1} = \frac{\mathbf{r}^{-1}}{\|\mathbf{r}^{-1}\|} \quad (64)$$

$$\Rightarrow = \|\mathbf{f}\|^2 + \langle \mathbf{f}, \mathbf{r}^{-1} \rangle^2 - 2 \langle \mathbf{f}, \mathbf{r}^{-1} \rangle^2 \quad (65)$$

$$\Rightarrow = \|\mathbf{f}\|^2 - \langle \mathbf{f}, \mathbf{r}^{-1} \rangle^2 \quad (66)$$

$$\Rightarrow = 2\omega_{\mathbf{r}}(\mathbf{f}) \quad (\because \text{definition of } \omega_{\mathbf{r}} \text{ in (12)}) \quad (67)$$

$$\therefore \frac{1}{2}\|\mathbf{a}\|^2 \geq \tau\omega_{\mathbf{r}}(\mathbf{f}) \quad \text{where } \tau \leq 1. \quad (68)$$

□

Theorem 4 (Convergence Rate, Iteration Complexity). *If the stepsize is any $\eta \in (0, \eta_0)$, where $\eta_0 = \frac{c_0}{c_0 + \max\{2c_1, 3c_2, 4c_3\}}$, $c_0 = \frac{\delta^2}{s_0 \sqrt{m} W^2}$, $c_1 = \frac{1}{2}(L_\omega + \frac{L_{\mathbf{f}} m}{s_1})$, $c_2 = \frac{1}{2}L_\omega L_{\mathbf{f}} m^2$, $c_3 = \frac{1}{8}L_\omega L_{\mathbf{f}}^2 m^2$, $s_0 = s_1 = 1$ when $\omega_{\mathbf{r}} = (10)$, and $s_0 = \|\mathbf{f}^{ndr}\|$ and $s_1 = M$ when $\omega_{\mathbf{r}} = (12)$, then the balance mode iterations, using either (11) or (13) as anchor direction, decrease $\omega_{\mathbf{r}}$ linearly:*

$$\omega_{\mathbf{r}}(\mathbf{f}^{t+1}) \leq (1 - 2\tau \eta p(\eta)) \omega_{\mathbf{r}}(\mathbf{f}^t) \leq \dots \leq (1 - 2\tau \eta p(\eta))^{t+1} \omega_{\mathbf{r}}(\mathbf{f}^0), \quad (26)$$

where the polynomial $p(\eta) = c_0 - c_1 \eta - c_2 \eta^2 - c_3 \eta^3$ is positive for all $\eta \in (0, \eta_0)$. Consequently, the maximum number of iterations (iteration complexity) required to decrease $\omega_{\mathbf{r}}$ down to ϵ is $O(\log(\frac{1}{\epsilon}))$.

Proof. We use a property of Lipschitz smooth functions. If g be a scalar valued function whose gradient is smooth with Lipschitz L_g , then (see Lemma 1.2.3 in Nesterov (2004))

$$|g(\mathbf{y}^{t+1}) - (g(\mathbf{y}^t) + \langle \nabla_{\mathbf{y}^t} g, \mathbf{y}^{t+1} - \mathbf{y}^t \rangle)| \leq \frac{1}{2} L_g \|\mathbf{y}^{t+1} - \mathbf{y}^t\|^2. \quad (69)$$

From Lipschitz smoothness Assumptions 2, we can write the following inequality for ω :

$$\omega_{\mathbf{r}}(\mathbf{f}^{t+1}) - \omega_{\mathbf{r}}(\mathbf{f}^t) \leq \langle \nabla_{\omega_{\mathbf{r}}}, \mathbf{f}^{t+1} - \mathbf{f}^t \rangle + \frac{L_\omega}{2} \|\mathbf{f}^{t+1} - \mathbf{f}^t\|^2, \quad (\because (69)) \quad (70)$$

where $\mathbf{f}^t = \mathbf{f}(\mathbf{x}^t)$. Similarly, with $\mathbf{L} = [L_1, \dots, L_m]^T$, Jacobian at \mathbf{x}^t as $\mathbf{F} \in \mathbb{R}^{m \times n}$, stepsize $\eta > 0$, and

$$\mathbf{x}^{t+1} = \mathbf{x}^t - \eta \mathbf{d}, \quad (71)$$

$$\text{where } \mathbf{d} = \mathbf{F}^T \boldsymbol{\beta}^* \quad (72)$$

is obtained from solving the QP (17) or (22) in the balance mode, we can write the following inequalities for $\Delta \mathbf{f}^t = \mathbf{f}^{t+1} - \mathbf{f}^t$:

$$-\eta \mathbf{F} \mathbf{d} - \frac{\eta^2}{2} \mathbf{L} \|\mathbf{d}\|^2 \leq \Delta \mathbf{f}^t \leq -\eta \mathbf{F} \mathbf{d} + \frac{\eta^2}{2} \mathbf{L} \|\mathbf{d}\|^2 \quad (\because (69) \text{ and } (71)) \quad (73)$$

$$\Rightarrow -\eta \mathbf{F} \mathbf{d} - \frac{\eta^2}{2} \mathbf{L} \langle \boldsymbol{\beta}^*, \mathbf{F} \mathbf{d} \rangle \leq \Delta \mathbf{f}^t \leq -\eta \mathbf{F} \mathbf{d} + \frac{\eta^2}{2} \mathbf{L} \langle \boldsymbol{\beta}^*, \mathbf{F} \mathbf{d} \rangle \quad (\because (72)) \quad (74)$$

$$\Rightarrow -\eta \mathbf{F} \mathbf{d} - \frac{\eta^2}{2} \mathbf{L} \|\boldsymbol{\beta}^*\| \|\mathbf{F} \mathbf{d}\| \leq \Delta \mathbf{f}^t \leq -\eta \mathbf{F} \mathbf{d} + \frac{\eta^2}{2} \mathbf{L} \|\boldsymbol{\beta}^*\| \|\mathbf{F} \mathbf{d}\| \quad (\because \langle \boldsymbol{\beta}^*, \mathbf{F} \mathbf{d} \rangle \leq \|\boldsymbol{\beta}^*\| \|\mathbf{F} \mathbf{d}\|) \quad (75)$$

$$\Rightarrow -\eta \mathbf{F} \mathbf{d} - \frac{\eta^2 \sqrt{m}}{2} \mathbf{L} \|\mathbf{F} \mathbf{d}\| \leq \Delta \mathbf{f}^t \leq -\eta \mathbf{F} \mathbf{d} + \frac{\eta^2 \sqrt{m}}{2} \mathbf{L} \|\mathbf{F} \mathbf{d}\| \quad (\because \|\boldsymbol{\beta}\|_1 \leq 1 \Rightarrow \|\boldsymbol{\beta}\|_2 \leq \sqrt{m}) \quad (76)$$

$$\Rightarrow -\eta \mathbf{F} \mathbf{d} - \frac{\eta^2 \sqrt{m} L_{\mathbf{f}} \|\mathbf{F} \mathbf{d}\|}{2} \mathbf{1} \leq \Delta \mathbf{f}^t \leq -\eta \mathbf{F} \mathbf{d} + \frac{\eta^2 \sqrt{m} L_{\mathbf{f}} \|\mathbf{F} \mathbf{d}\|}{2} \mathbf{1}, \quad (\because L_{\mathbf{f}} = \max_{j \in [m]} L_j) \quad (77)$$

where $\mathbf{1} \in \mathbb{R}^m$ has all ones. If no subscript is mentioned explicitly then $\|\cdot\|$ means ℓ_2 norm. In (75), we have applied Cauchy-Schwarz inequality.

Next, we upper bound the term $\langle \nabla \omega_{\mathbf{r}}, \mathbf{f}^{t+1} - \mathbf{f}^t \rangle$ in (70) as

$$\langle \nabla \omega_{\mathbf{r}}, \Delta \mathbf{f}^t \rangle \leq -\eta \langle \nabla \omega_{\mathbf{r}}, \mathbf{F} \mathbf{d} \rangle + \frac{K}{2} \|\mathbf{F} \mathbf{d}\| \|\nabla \omega_{\mathbf{r}}\|_1, \quad \text{where } K = L_{\mathbf{f}} \eta^2 \sqrt{m} \quad (\because (77)) \quad (78)$$

$$\Rightarrow \leq -\eta \langle \nabla \omega_{\mathbf{r}}, \mathbf{F} \mathbf{d} \rangle + \frac{K'}{2} \|\mathbf{F} \mathbf{d}\| \|\nabla \omega_{\mathbf{r}}\|, \quad K' = K \sqrt{m} \quad (\because \|\nabla \omega_{\mathbf{r}}\|_1 \leq \sqrt{m} \|\nabla \omega_{\mathbf{r}}\|_2) \quad (79)$$

$$\Rightarrow = -\frac{\eta}{s} \langle \mathbf{a}, \mathbf{F} \mathbf{d} \rangle + \frac{K'}{2s} \|\mathbf{F} \mathbf{d}\| \|\mathbf{a}\|, \quad \left(\because \mathbf{a} = s \nabla \omega_{\mathbf{r}}, s = \begin{cases} \|\mathbf{f}^t\| & \text{in } a = (11) \\ 1 & \text{in } a = (13) \end{cases} \right) \quad (80)$$

$$\Rightarrow \leq -\frac{\eta}{s_0} \langle \mathbf{a}, \mathbf{F} \mathbf{d} \rangle + \frac{K'}{2s_1} \|\mathbf{F} \mathbf{d}\| \|\mathbf{a}\|, \quad (\because s_1 \leq s \leq s_0 \text{ from Assumption 1}) \quad (81)$$

$$\Rightarrow \leq -\frac{\eta}{s_0} \langle \mathbf{a}, \mathbf{F} \mathbf{d} \rangle + \frac{K'}{2s_1} \|\mathbf{a}\|^2 \quad (\because \|\mathbf{F} \mathbf{d}\| \leq \|\mathbf{a}\| \text{ by QP (17) or (22)}) \quad (82)$$

$$\Rightarrow \leq -\frac{\eta \delta^2}{s_0 \sqrt{m} W^2} \|\mathbf{a}\|^2 + \frac{L_{\mathbf{f}} \eta^2 m}{2s_1} \|\mathbf{a}\|^2 \quad (\because \text{Lemma 9}) \quad (83)$$

In (78), we use the right (left) inequality in (77) if $\frac{\partial \omega_{\mathbf{r}}}{\partial f_j}$ is positive (negative) for $j \in [m]$. In (81), the factors s_0 and s_1 are as given in the statement of the theorem. The step (78) \Rightarrow (79) is similar to (74) \Rightarrow (76). The step (81) \Rightarrow (82) because, by construction, the solution of QP in (17) or (22) gives $\|\mathbf{F} \mathbf{d}\| \leq \|\mathbf{a}\|$.

Similarly, we upper bound the term $\|\mathbf{f}^{t+1} - \mathbf{f}^t\|^2$ in (70) as

$$\|\mathbf{f}^{t+1} - \mathbf{f}^t\|^2 \leq \eta^2 \|\mathbf{F}\mathbf{d}\|^2 + \frac{1}{4}\eta^4 L_{\mathbf{f}}^2 m^2 \|\mathbf{F}\mathbf{d}\|^2 + \eta^3 L_{\mathbf{f}} \sqrt{m} \|\mathbf{F}\mathbf{d}\|_1 \quad (\because (77))$$

$$(84)$$

$$\Rightarrow \leq \eta^2 \|\mathbf{F}\mathbf{d}\|^2 + \frac{1}{4}\eta^4 L_{\mathbf{f}}^2 m^2 \|\mathbf{F}\mathbf{d}\|^2 + \eta^3 L_{\mathbf{f}} m \|\mathbf{F}\mathbf{d}\|^2 \quad (\because \|\mathbf{F}\mathbf{d}\|_1 \leq \sqrt{m} \|\mathbf{F}\mathbf{d}\|_2)$$

$$(85)$$

$$\Rightarrow \leq \eta^2 \|\mathbf{a}\|^2 + \frac{1}{4}\eta^4 L_{\mathbf{f}}^2 m^2 \|\mathbf{a}\|^2 + \eta^3 L_{\mathbf{f}} m \|\mathbf{a}\|^2. \quad (\because \|\mathbf{F}\mathbf{d}\| \leq \|\mathbf{a}\|)$$

$$(86)$$

Finally, we can rewrite (70) as

$$\omega_{\mathbf{r}}(\mathbf{f}^{t+1}) - \omega_{\mathbf{r}}(\mathbf{f}^t) \leq -\eta p(\eta) \|\mathbf{a}\|^2 \quad (\because (70), (83) \text{ and } (86)) \quad (87)$$

$$\Rightarrow \omega_{\mathbf{r}}(\mathbf{f}^{t+1}) - \omega_{\mathbf{r}}(\mathbf{f}^t) \leq -2\tau\eta p(\eta) \omega_{\mathbf{r}}(\mathbf{f}^t) \quad (\because \text{Lemma (5)}) \quad (88)$$

$$\therefore \omega_{\mathbf{r}}(\mathbf{f}^{t+1}) \leq (1 - 2\tau\eta p(\eta)) \omega_{\mathbf{r}}(\mathbf{f}^t) \quad (89)$$

$$\Rightarrow \omega_{\mathbf{r}}(\mathbf{f}^{t+1}) \leq (1 - 2\tau\eta p(\eta))^{t+1} \omega_{\mathbf{r}}(\mathbf{f}^0) \quad (90)$$

where the polynomial $p(\eta) = c_0 - c_1\eta - c_2\eta^2 - c_3\eta^3$ has the coefficients as given in the statement of the theorem. The ideal stepsize η^* that minimizes $(1 - 2\tau\eta p(\eta))$ is given by the positive root of

$$\frac{d}{d\eta} \eta p(\eta) = c_0 - 2c_1\eta - 3c_2\eta^2 - 4c_3\eta^3 \quad (91)$$

The $\eta_0 > 0$ in the statement of the theorem is such that $\eta_0 \leq \eta^*$. We obtain this lower bound using the following properties of a polynomial.

- (i) Cauchy's upper bound (Jain 2007) U for all the absolute roots $|z|$ of a polynomial $b_3 + b_2x + b_1x^2 + b_0x^3$, i.e., $|z|_i \leq U \forall i \in [3]$, is given by $U = 1 + \max_{i=1}^3 \left| \frac{b_i}{b_0} \right|$
- (ii) $1/U$ is the lower bound for all the absolute roots of polynomial $b_0 + b_1x + b_2x^2 + b_3x^3$.

Finally, applying Properties (i) and (ii) on the polynomial (91), we get the η_0 as given in the statement of the theorem.

The iteration complexity, i.e., the maximum number of iterations until which $\omega_{\mathbf{r}}(\mathbf{f}^t) \geq \epsilon$ is given by

$$\epsilon \leq \omega_{\mathbf{r}}(\mathbf{f}^t) \quad (92)$$

$$\Rightarrow \epsilon \leq (1 - 2\tau\eta_0 p(\eta_0))^t \omega_{\mathbf{r}}(\mathbf{f}^0) \quad (\because (90)) \quad (93)$$

$$\Rightarrow \log(\epsilon) \leq t \log(\rho) + \log(\omega_{\mathbf{r}}(\mathbf{f}^0)), \quad \text{where } \rho = (1 - 2\tau\eta_0 p(\eta_0)) \quad (94)$$

$$\Rightarrow t \log\left(\frac{1}{\rho}\right) \leq \log\left(\frac{\omega_{\mathbf{r}}(\mathbf{f}^0)}{\epsilon}\right) \quad (95)$$

$$\therefore t \leq \log\left(\frac{\omega_{\mathbf{r}}(\mathbf{f}^0)}{\epsilon}\right) / \log\left(\frac{1}{\rho}\right) \leq O(\log(1/\epsilon)) \quad (\because \rho < 1 \Rightarrow \log(1/\rho) > 0) \quad (96)$$

□

Lemma 9. *If Assumption 1 is satisfied for an W and Assumption 3 is satisfied for a δ , then search direction \mathbf{d} obtained in the balance mode of QP (17) or (22) at a point \mathbf{x} with Jacobian \mathbf{F} satisfies*

$$\langle \nabla \omega_{\mathbf{r}}, \mathbf{F}\mathbf{d} \rangle \geq \frac{\delta^2}{\sqrt{m}W^2} \|\nabla \omega_{\mathbf{r}}\|^2 \quad (97)$$

Proof. We can write

$$\langle \nabla \omega_{\mathbf{r}}, \mathbf{F}\mathbf{d} \rangle = \|\nabla \omega_{\mathbf{r}}\| \|\mathbf{F}\mathbf{d}\| \cos(\theta), \quad (98)$$

where θ is the angle between the anchor direction $\mathbf{a} = \nabla \omega_{\mathbf{r}}$ and the direction $\mathbf{F}\mathbf{d} = \mathbf{F}\mathbf{F}^T \beta^*$. In this prove we find lower bound for $\|\mathbf{F}\mathbf{d}\| \cos(\theta)$. Note, if $\mathbf{a} \in \mathcal{CH}_{\mathbf{f}}^{\pm}$ (defined in (52)), then

$\|\mathbf{F}\mathbf{d}\| \cos(\theta) = \|\nabla\omega_{\mathbf{r}}\|$ (e.g., see proof of Lemma 2), which is an upper bound for $\|\mathbf{F}\mathbf{d}\| \cos(\theta)$. Therefore, we only consider for $\mathbf{a} \notin \mathcal{CH}_{\mathbf{f}}^{\pm}$.

First, we lower bound $\cos(\theta)$. The maximum possible value of $\cos(\theta) = 1$; it occurs when $\boldsymbol{\beta}^* = \frac{(\mathbf{F}\mathbf{F}^T)^{-1}\mathbf{a}}{\|(\mathbf{F}\mathbf{F}^T)^{-1}\mathbf{a}\|}$, which results in $\mathbf{F}\mathbf{d} = s\mathbf{a}$, where $s = \frac{1}{\|(\mathbf{F}\mathbf{F}^T)^{-1}\mathbf{a}\|_1}$. This is a feasible solution even for the constrained balance mode in the QP (17) as proven in Lemma 2. Here, the residue $\mathbf{a} - \mathbf{F}\mathbf{F}^T\boldsymbol{\beta}^*$ is aligned with $\mathbf{F}\mathbf{d}$. The minimum possible value of $\cos(\theta)$ (or the maximum angle between $\mathbf{F}\mathbf{d}$ and \mathbf{a}) will occur when the residue $\mathbf{a} - \mathbf{F}\mathbf{F}^T\boldsymbol{\beta}^*$ is orthogonal to $\mathbf{F}\mathbf{F}^T\boldsymbol{\beta}^*$. In other words, $\mathbf{F}\mathbf{d}$ and \mathbf{a} are the base and hypotenuse of a right triangle. Therefore,

$$\cos \theta \geq \frac{\|\mathbf{F}\mathbf{d}\|}{\|\mathbf{a}\|} \quad (99)$$

$$\Rightarrow \geq \frac{\|\mathbf{F}\mathbf{d}\|}{W} \quad (\because \|\mathbf{a}\| \leq W \text{ from Assumption (1)}). \quad (100)$$

Next, we lower bound $\|\mathbf{F}\mathbf{d}\|$. To minimize the quadratic cost $\|\mathbf{F}\mathbf{F}^T\boldsymbol{\beta} - \mathbf{a}\|^2$, the vector $\mathbf{F}\mathbf{d}$ must lie on the boundary of $\mathcal{CH}_{\mathbf{f}}^{\pm}$, resulting in

$$\|\boldsymbol{\beta}^*\|_1 = 1 \quad (101)$$

We first lower bound $\|\mathbf{F}\mathbf{d}\|$ when $\mathbf{x} \in \mathcal{X} \setminus \mathcal{P}^{\delta}$:

$$\|\mathbf{F}\mathbf{d}\| = \|\mathbf{F}\mathbf{F}^T\boldsymbol{\beta}^*\| \quad (102)$$

$$\Rightarrow \geq \|\mathbf{F}\mathbf{F}^T\|_{\circ} \|\boldsymbol{\beta}^*\|_2 \quad \text{where } \|A\|_{\circ} = \min_{\boldsymbol{\beta}} \frac{\|A\boldsymbol{\beta}\|_2}{\|\boldsymbol{\beta}\|_2}. \quad (103)$$

$$\Rightarrow = \sigma_1^2 \|\boldsymbol{\beta}^*\|_2 \quad \text{where } \sigma_1 \text{ is the smallest singular value of } \mathbf{F} \quad (104)$$

$$\Rightarrow \geq \delta^2 \|\boldsymbol{\beta}^*\|_2 \quad (\because \text{Assumption 3}) \quad (105)$$

$$\Rightarrow \geq \delta^2 \frac{\|\boldsymbol{\beta}^*\|_1}{\sqrt{m}} \quad (\because \|\boldsymbol{\beta}^*\|_2 \geq \frac{\|\boldsymbol{\beta}^*\|_1}{\sqrt{m}}) \quad (106)$$

$$\Rightarrow = \frac{\delta^2}{\sqrt{m}} \quad (\because (101)) \quad (107)$$

Now, we consider the case $\mathbf{x} \in \mathcal{P}^{\delta}$. From the definition of \mathcal{P}^{δ} (25), we know that the lowest singular value σ_1 vanishes as \mathbf{x} approaches the PF. As a result, the corresponding singular vector (eigenvector of $\mathbf{F}\mathbf{F}^T$) $\mathbf{v}_1 : \mathcal{X} \rightarrow \mathbb{R}^m$ turns into the null space of $\mathbf{F}\mathbf{F}^T$ as \mathbf{x} approaches² the PF, because according to Assumption 3, the second singular value σ_2 does not vanish in \mathcal{P}^{δ} . In other words, the column space of $\mathbf{F}\mathbf{F}^T$ becomes equal to the columns space of $\{\mathbf{v}_2, \dots, \mathbf{v}_m\}$. The QP (22) is used in such cases. Its balancing anchor direction $\mathbf{a} \notin \text{Null}(\mathbf{F}\mathbf{F}^T)$ as proven in Theorem 3, where we deduced that \mathbf{v}_1 must be an all positive vector like the descending anchor direction \mathbf{f} . Moreover, since \mathbf{a} and \mathbf{f} are orthogonal (see Claim 1), to minimize $\|\mathbf{F}\mathbf{F}^T\mathbf{d} - \mathbf{a}\|$, \mathbf{a} gets projected onto the span($\{\mathbf{v}_2, \dots, \mathbf{v}_m\}$) in $\mathcal{CH}_{\mathbf{f}}^{\pm}$. Therefore, instead of σ_1 in (103) and (104), the second singular value σ_2 is applicable, which results in

$$\|\mathbf{F}\mathbf{d}\| \geq \sigma_2^2 \|\boldsymbol{\beta}^*\|_2 \quad (108)$$

$$\Rightarrow \geq \delta^2 \|\boldsymbol{\beta}^*\|_2 \quad (\because \text{Assumption 3}) \quad (109)$$

$$\Rightarrow \geq \delta^2 \frac{\|\boldsymbol{\beta}^*\|_1}{\sqrt{m}} \quad (\because \|\boldsymbol{\beta}^*\|_2 \geq \frac{\|\boldsymbol{\beta}^*\|_1}{\sqrt{m}}) \quad (110)$$

$$\Rightarrow = \frac{\delta^2}{\sqrt{m}} \quad (\because (101)) \quad (111)$$

Therefore, for any $\mathbf{x} \in \mathcal{X}$ we can write

$$\|\mathbf{F}\mathbf{d}\| \geq \frac{\delta^2}{\sqrt{m}} \quad (112)$$

²Note, similar to the singular values, the singular vectors are also smooth w.r.t. variations in $\mathbf{x} \in \mathcal{X}$ due to the smoothness of Jacobian $\mathbf{F} : \mathcal{X} \rightarrow \mathbb{R}^{m \times n}$.

Finally, we can lower bound the inner product as

$$\langle \nabla \omega_{\mathbf{r}}, \mathbf{F}\mathbf{d} \rangle = \|\nabla \omega_{\mathbf{r}}\| \|\mathbf{F}\mathbf{d}\| \cos(\theta) \quad (113)$$

$$\Rightarrow \geq \|\nabla \omega_{\mathbf{r}}\| \frac{\delta^2}{\sqrt{mW}} \quad (\because (112) \text{ and } (100)) \quad (114)$$

$$\Rightarrow = \|\nabla \omega_{\mathbf{r}}\|^2 \frac{\delta^2}{\|\nabla \omega_{\mathbf{r}}\| \sqrt{mW}} \quad (115)$$

$$\therefore \geq \|\nabla \omega_{\mathbf{r}}\|^2 \frac{\delta^2}{\sqrt{mW^2}} \quad (\because \text{Assumption 1}) \quad (116)$$

□

C.3 EPO Search for Constrained MOO

Lemma 6. *If \mathbf{x}^t is a non-PO regular point of the differentiable vector function \mathbf{f} in a balance mode, i.e. $\omega(\mathbf{f}^t, \mathbf{r}^{-1}) > \epsilon_1$, then the non-dominating direction obtained from QP (39) makes*

1. *non-negative angles with the gradients of maximum relative objectives: $\mathbf{d}_{nd}^T \nabla_{\mathbf{x}^t} f_j \geq 0 \forall j \in \mathbf{J}^*$ (17c),*

2. *a positive angle with the balancing anchor direction (13) in the objective space: $\mathbf{a}^T \mathbf{F}\mathbf{d}_{nd} > 0$.*

Proof. The statement is true by construction of the QP (39). □

Lemma 7. *If \mathbf{x}^t is a non-PO regular point of the differentiable vector function \mathbf{f} in a descent mode, i.e. $\omega(\mathbf{f}^t, \mathbf{r}^{-1}) \leq \epsilon_1$, then the non-dominating direction obtained from QP (39) makes a non-negative angle with every gradient, $\mathbf{d}_{nd}^T \nabla_{\mathbf{x}^t} f_j \geq 0 \forall j \in [m]$, and a positive angle with at least one gradient.*

Proof. The statement is true by construction of the QP (39). □

Theorem 5. *Let $\mathbf{x}^* \in \mathcal{P}$ such that, if $\mathbf{x}^* \in \text{Int}(\mathcal{X})$ then it is a regular Pareto optimal solution, and if $\mathbf{x}^* \in \partial\mathcal{X}$ then it is a regular point of \mathbf{f} and $\vec{\mathbf{f}}^*$ penetrates \mathcal{O} . Then, at \mathbf{x}^* , the non-dominating direction $\mathbf{d}_{nd} = \mathbf{F}^T \beta^*$ found by the QP (40) with Cauchy-Schwarz anchor (11) is $\mathbf{0} \in \mathbb{R}^n$ if and only if $\mathbf{x}^* \in \mathcal{P}_r$.*

Proof. The proof for $\mathbf{x}^* \in \text{Int}(\mathcal{X})$ is same as the unconstrained case in Theorem (3).

When $\mathbf{x}^* \in \partial\mathcal{X}$, the penetration assumption ensures that the orthogonal projection of the CSZ inequality-based balancing anchor direction \mathbf{a} (11) into the cone $\{\mathbf{F}\mathbf{d} \mid \mathbf{d} \in \mathcal{F}_{\mathcal{X}}(\mathbf{x}^*)\} \subset \mathbb{R}^m$ is non-zero, because \mathbf{a} and $\vec{\mathbf{f}}^*$ are orthogonal according to Claim (1).

□

D Useful variations in EPO Search

In practice, for high-dimensional solution spaces $\mathcal{X} \subset \mathbb{R}^n$, e.g. DNN parameters, we use a fixed step size instead of adaptively deciding by line search. So, for proper movement in the objective space, we introduce few variations in the EPO search algorithm.

D.1 Momentum in Anchor While Tracing

While tracing the Pareto front, i.e. starting from a Pareto optimal $\mathbf{x}^0 \in \mathcal{P}$, we use the Cauchy-Schwarz anchor direction (11), which is always perpendicular to the objective vector (see Claim 1). The first order change in the objective space created by the search direction found from QP (40) is $\delta\mathbf{f} = \mathbf{F}\mathbf{d}_{nd} = \mathbf{F}\mathbf{F}^T \beta^*$. This change $\delta\mathbf{f}$ is same as the orthogonal projection of \mathbf{a} onto the cone $\text{Col}(\mathbf{F}\mathbf{F}^T) \cap \mathbf{F}\mathcal{F}$. When the Pareto front is connected, at any point on the Pareto front, $\mathbf{a} \in \text{Col}(\mathbf{F}\mathbf{F}^T) \cap \mathbf{F}\mathcal{F}$, so the magnitude of $\delta\mathbf{f}$ is significant enough to move the iterate with a small

step size. But when, the Pareto front is disconnected, e.g. ZDT3 in Figure 8c, and the iterate is at a boundary point outside the Pareto front, $\mathbf{f}^t \in \partial\mathcal{O} - \mathbf{f}(\mathcal{P})$, then $\mathbf{a} \notin \text{Col}(\mathbf{F}\mathbf{F}^T) \cap \mathbf{F}\mathcal{F}$, and the magnitude of its projection $\delta\mathbf{f}$ may not be enough to propel the iterate ahead with a small step size. The movements in objective slows down. To mitigate this we use a momentum term in the anchor,

$$\mathbf{a}_m = \mathbf{a} + (\mathbf{f}^t - \mathbf{f}^{t-1}), \quad (117)$$

and use \mathbf{a}_m in the QP. Using this anchor if the next iterate $\mathbf{f}^{t+1} \sim \mathbf{f}^t + \eta\Delta\mathbf{f}$ is dominated by the current one, i.e. $\mathbf{f}^{t+1} \succ \mathbf{f}^t$, then we conclude that $\mathbf{f}^t \in \partial\mathcal{O} - \mathbf{f}(\mathcal{P})$, and don't enter the descent mode in the subsequent iterations and only operate in the balance mode. As soon as a non-dominated iterate is found, i.e. $\mathbf{f}^{t+1} \not\succeq \mathbf{f}^t$, we resume alternating the modes of operation.

D.1.1 Importance of Alternating Mode of Operation While Tracing.

It is important to use the descent mode of operation in every other iteration to keep the iterate close to the Pareto front, especially in case of convex objectives. Otherwise the trajectory will drift away from the Pareto front. This is shown in Figure 13 for ZDT1 problem.

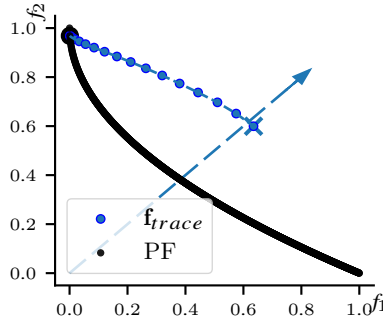


Figure 13: Tracing the Pareto front of ZDT1 without the descent mode: the trajectory drifts away from PF.

D.2 Restricting Trajectory in Descent Mode When not Tracing

When reaching the EPO solution starting from an arbitrary initialization, ideally the algorithm should enter the descent mode only when the iterate \mathbf{f}^t reaches exactly onto the \mathbf{r}^{-1} ray. Because, when $\omega_{\mathbf{r}}(\mathbf{f}^t) = 0$, the anchor direction of descent becomes $\vec{\mathbf{a}} = \vec{\mathbf{f}}^t = \vec{\mathbf{r}}^{-1}$, and the iterates descend along the \mathbf{r}^{-1} to reach the EPO solution. But achieving $\omega_{\mathbf{r}}(\mathbf{f}^t) = 0$ while using a fixed step size is less likely. Therefore we perform a descent mode operation whenever the objective vector \mathbf{f}^t lies in the cone

$$\mathcal{M}_\epsilon^{\mathbf{r}} = \{\mathbf{f} \in \mathbb{R}_+^m \mid \omega_{\mathbf{r}}(\mathbf{f}) \leq \epsilon\}, \quad (118)$$

for a small $\epsilon > 0$. As a result, the descending anchor direction, and hence the first order change in objective space $\delta\mathbf{f} = \mathbf{F}\mathbf{F}^T\boldsymbol{\beta}^*$, will no longer be aligned with the \mathbf{r}^{-1} ray. This causes oscillations around the \mathbf{r}^{-1} ray while descending, as shown in Figure 14a. To mitigate this, we add the following equality constraint to the QP (15) for unconstrained MOO and (39) for constrained MOO:

$$\begin{aligned} \delta\mathbf{f} &= \vec{\mathbf{r}}^{-1} \langle \vec{\mathbf{r}}^{-1}, \delta\mathbf{f} \rangle \\ \implies \mathbf{F}\mathbf{F}^T\boldsymbol{\beta} &= \vec{\mathbf{r}}^{-1} \vec{\mathbf{r}}^{-1^T} \mathbf{F}\mathbf{F}^T\boldsymbol{\beta} \\ \implies (\mathbf{I}_m - \vec{\mathbf{r}}^{-1} \vec{\mathbf{r}}^{-1^T})\mathbf{F}\mathbf{F}^T\boldsymbol{\beta} &= 0, \end{aligned} \quad (119)$$

where $\vec{\mathbf{r}}^{-1}$ is the ℓ_2 normalized vector, and \mathbf{I}_m is the $m \times m$ identity matrix. This constraint ensures that the movement in the objective space will be aligned with \mathbf{r}^{-1} ray. We apply this equality constraint only when there are no active constraints, i.e. $\mathbf{x}^t \in \text{Int}(\mathbb{X})$. The restriction in (119) makes the trajectory of descent mode non-oscillatory as shown in Figure 14b. The objective functions used in Figure 14 is described in section 5.1.

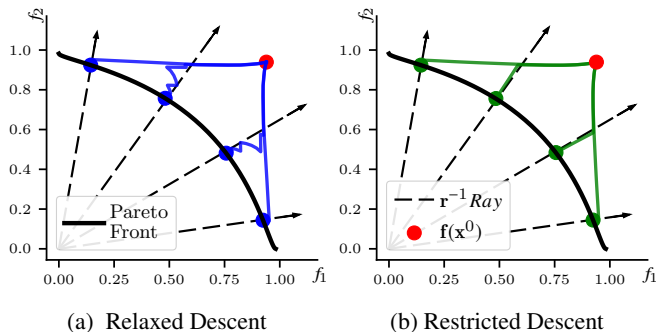


Figure 14: Restricting the QP with the constraint (119) eliminates fluctuations in descent mode.

D.3 Further Comparison with Pareto MTL

Our EPO Search algorithm switches from balance mode to descent mode after entering a narrow conical region around the \mathbf{r}^{-1} ray. This may appear similar to Pareto MTL (Lin et al. 2019) (described in section 2.3), where in the first phase one finds a solution $\mathbf{x}_r^0 \in \Omega_k$, where

$$\Omega_k := \left\{ \mathbf{x} \in \mathbb{R}^n \mid \langle \mathbf{u}^k, \mathbf{f}(\mathbf{x}) \rangle \geq \langle \mathbf{u}^{k'}, \mathbf{f}(\mathbf{x}) \rangle, \forall k' \neq k \right\}, \quad (120)$$

such that the EPO solution is in Ω_k , and in the second phase one does pure descent. The construction of Ω_k is such that $\mathbf{f}(\Omega_k)$ is also a cone.

However, their method does not guarantee that the outcome of second phase \mathbf{x}^* also lies in Ω_k . Because while descending, the objective vector may go outside the cone $\mathbf{f}(\Omega_k)$. On the other hand, our method guarantees that the objective vector of the final solution will be inside the cone \mathcal{M}_ϵ^r in (118). Because, if in some iteration the $\mathbf{f}^t \notin \mathcal{M}_\epsilon^r$, then a balancing anchor direction is used in the QP to bring it back inside the cone \mathcal{M}_ϵ^r in the subsequent iterations.

Moreover, the angular fineness of their cone $\mathbf{f}(\Omega_k)$, which dictates the accuracy of the final solution, is dependent on how many reference vectors \mathbf{u}^k , $k = 1, \dots, K$ are used, which increases exponentially with the number of objectives m . On other hand, the angular fineness of our cone \mathcal{M}_ϵ^r can be set by merely choosing a small value of ϵ .

E Case Study: Personalized Medicine

Drug development is an elaborate, long and expensive process – estimates show the average duration between discovery and market launch to be around 15 years (Ng 2015) and the cost per approved new drug to be roughly \$2.6 billion in 2013 dollars (DiMasi et al. 2016) and is continuing to increase (Kiriiri et al. 2020). The entire process consists of multiple stages that can be broadly categorized into: (i) Drug Discovery (ii) Pre-clinical Development (iii) Clinical Trials and (iv) Post-marketing surveillance (Huang et al. 2012, Beninger 2018). The first stage involves finding and validating a biological entity (called “target”, e.g., a gene) and a chemical (which may or may not be a previously used drug) such that their interaction has a therapeutic effect on the considered disease. After such a pair is found, pre-clinical studies are performed to understand the mechanism of drug action, e.g., through experimental studies on response of administering the drug on animals or cells in laboratory conditions. If a drug is found to be safe and efficacious, multiple clinical trials are conducted on increasing number of human subjects. Post-marketing surveillance or pharmacovigilance continues even after the drug is approved and in clinical use, to identify adverse side effects not found in previous stages. Each stage in turn has multiple steps, with several regulatory constraints and complex technical challenges; predictive models are utilized for many tasks at each stage (Vamathevan et al. 2019).

E.1 Task Details

- *Drug Target Prediction.* Drugs that act on specific disease-causing genes are instrumental for personalized medicine, and are actively studied (Schenone et al. 2013), particularly in

early stages of drug discovery. Lab-based genomic techniques to find such drug targets are expensive, time-consuming and have high failure rates; hence, computational methods to predict new targets of drugs are used to prioritize drug-target pairs before subsequent testing (Chen et al. 2020). Large collections of experimental data of known drug targets have been made publicly available that can be used for supervised learning. Using such data, the binary classification task is to predict, for a given drug-gene pair, whether or not the gene can be targeted by the drug.

- *Drug Response Prediction.* Here we consider a single disease, cancer, that is caused by genetic aberrations leading to uncontrolled cell reproduction. Cells with differing genomic profiles may differ in their response to treatment (Senft et al. 2017). To enable personalized cancer treatment based on individual genomic profiles, the effect of anti-cancer drugs on many cancer cells under laboratory conditions are being actively studied and documented (Yang et al. 2013, Rees et al. 2016). Broadly, in these experiments, cancer cells are subjected to varying concentrations of drugs, whose capacity to inhibit the reproduction of cancer cells is measured. A widely adopted measure of drug efficacy is half maximal inhibitory concentration (IC50) which is the concentration required to inhibit 50% of the cells (Huang et al. 2012). Genomic profiles of cells can be constructed through various measurements and used as feature vectors, containing information relevant to cancer, such as mutations and indicators of gene activity. Experimental data on drug efficacy can be used to build a regression model that predicts, for a given drug and genomic profile, the efficacy of the drug on cells with such a profile. Such models can provide deeper insights into the mechanism of action of the drugs by uncovering the genomic factors that enable therapeutic action of drugs. They can also potentially be used to personalize drug recommendation for cancer patients, whose genomic profiles can be measured in hospitals (Ma et al. 2021). For the genomic profile of a patient, and a given list of drugs (approved for use in the hospital), clinicians typically seek the top ranking drugs that are predicted to be most effective, which in turn can support subsequent decision-making for treatment planning. Thus, in addition to predicting the drug efficacy, it is also important to obtain accurate ranking of drugs based on efficacy for a given genomic profile.
- *Drug Side Effect Prediction.* Adverse drug events (ADEs) are unintended side effects of drugs that often lead to emergency visits, prolonged hospital stays, and worse patient outcomes (Ventola 2018). Worldwide, they remain a leading cause of morbidity and mortality, posing substantial clinical and economic burden (Watanabe et al. 2018). Clinical trials are limited by the number and characteristics of patients tested as well as the duration of the observation period, and they may not detect all ADEs, especially those with long latency or those that affect only certain patient groups (Coloma et al. 2013). So, pharmacovigilance is routinely conducted to document reports of ADEs of approved drugs. Large databases have been created (Kuhn et al. 2016, Tatonetti et al. 2012) that correct for biases and omissions in the reports due to concomitant medication, patient demographics and medical histories. This enables development of supervised learning models that can be used to predict potential ADEs of a drug, which can be further investigated by pharmacovigilance teams. The problem is that of binary classification, where given a disease-drug pair, the model predicts whether the disease may be a side-effect of a drug.

E.2 Data

Data from multiple publicly available drug-related databases have been collected and preprocessed by Jiang et al. (2021) for integrative analysis. For Drug Target (DT) prediction we use data from STITCH (Szklarczyk et al. 2016), DrugBank (Wishart et al. 2018) and Repurposing Hub (Corsello et al. 2017); for Drug Response (DR) prediction, we use GDSC (Yang et al. 2013) and CCLE (Rees et al. 2016) databases; for Drug Side-effect (DS) prediction, we use SIDER (Kuhn et al. 2016) and OFFSIDES (Tatonetti et al. 2012). A summary of the datasets is given in Table 3; more details can be found in Jiang et al. (2021).

E.3 Additional Details of Model and Training

We used ReLU activation function for all the layers, except the final layers of the predictors; sigmoid activation is used for DT and DS classifiers, and an identity map for DR regressor. The training hyper

parameters used are identical for all methods: Adam optimizer with learning rate 0.001, mini-batch size of 256 for each training dataset, and 10K iterations. We did not compare with PMTL, because, as noted in Lin et al. (2019) and observed in our experiment in §5.1, it fails to scale for more than two objectives when the solution space is high-dimensional (in this case, more than 0.73 million).

F Additional Experimental Results

F.1 Multi-Task Learning in Hydrometeorology

Flooding and other hydrological threats pose critical risks to lives and property, and can impact multiple industries such as agriculture, fishing, forestry, transportation and construction (Adams and Pagano 2016). Billions of dollars are lost in major disasters, including floods, in the US alone (NOAA National Centers for Environmental Information 2022). Timely river flow forecasts play a crucial role in mitigating the adverse effects of such events (Chang et al. 2019). River flow forecasts are also used for water supply management, reservoir operations, and navigation planning. Forecasts are required at strategic sites along rivers where flow levels along with other meteorological variables (e.g., rainfall and temperature) are regularly recorded. A predictive model for all the considered sites can be developed jointly using MTL, where a task is a site-specific prediction.

We use the River Flow dataset (Spyromitros-Xioufis et al. 2016) that has $m = 8$ tasks: predicting the flow at 8 sites in the Mississippi River network. Each sample contains, for each site, the most recent and time-lagged flow measurements from 6, 12, 18, 24, 36, 48, 60 hours in the past. Thus, there are 64 features and 8 target variables. We remove samples with missing values and use 6,300 samples

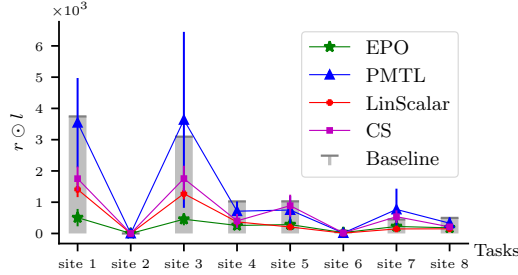


Figure 15: (Color Online) Comparison of mean RLP (with standard deviation; lower is better) of MTL methods after training the same neural network model to predict flow at 8 sites in the Mississippi River.

for training and 2,700 for testing. We use a fully connected feed-forward neural network (FNN) with 4 layers (layerwise sizes: $64 \rightarrow 32 \rightarrow 16 \rightarrow 8 \rightarrow 8$) with $n = 6,896$ parameters to fit the data. We randomly choose 20 input priority vectors $\mathbf{r} \in \mathbb{R}_+^8$ (with $\sum_j r_j = 1$) and train the FNN using EPO search, PMTL, Linear Scalarization (LinScalar) and Chebychev Scalarization (CS). We use each of the 8 objectives trained separately as baselines. We used Mean Squared Error (MSE) as the loss for each task. For all the methods stochastic gradient descent is used for training with the same hyperparameters: number of epochs, number of mini-batches and learning rate. Since visualization is difficult for 8 dimensions, we compare the methods using the relative loss profile (RLP) $\mathbf{r} \odot \mathbf{f}$ on the test data as shown in Figure 15.

We observe that EPO Search outperforms the other methods, indicating that it complies better with the input user priorities; the RLP of EPO search is more uniform (in the sense of definition (33)). The improvement over PMTL is higher in this experiment compared to the e-commerce experiment in F.2 with two tasks. This is expected since the number of reference vectors required by PMTL, to reach a desired \mathbf{r}^{-1} ray, grows exponentially with m . The problem with the min-max strategy of CS gets highlighted in this experiment showing how combining information from all the task gradients in each iteration is important in an MTL setup. LS does that, therefore performs better than CS in this experiment. However, it does not comply with the priority specification, resulting in a non-uniform RLP in Figure 15. Interestingly, except PMTL, all other MOO based MTL methods improve over the baseline which shows the advantage of MTL for correlated tasks over learning each task independently: predicting river flow at one site helps improving the prediction at other sites as all the sites are from the same river.

F.2 Multi-Task Learning in E-Commerce

Fashion and lifestyle items, such as bags, footwear and apparel, constitute a large portion of e-commerce sales (Elahi and Qi 2020, Deldjoo et al. 2022). Visual appearance of these items plays an influential role in purchase decisions. Search and recommendation engines in e-commerce websites, that are traditionally based on text-based keywords and descriptions, are increasingly using systems that can utilize images directly (Cheng et al. 2021). An important element in such systems is a classifier that can classify the input image into various categories, in order to restrict subsequent search and recommendation within the category. In many cases the image may have multiple items, for instance in bundled sales, from the same or different categories. When multiple items are present in the input image MTL can be effectively used, by considering each task as a classification problem for an item in the image (Lin et al. 2020).

We use three benchmark classification datasets: (1) MultiMNIST, (2) MultiFashion, and (3) Multi-Fashion+MNIST. In the MultiMNIST dataset (Sabour et al. 2017), two images of different digits are randomly picked from the original MNIST dataset (LeCun et al. 1998), and combined to form a new image, where one is in the top-left and the other is in the bottom-right. There is zero padding in the top-right and bottom-left. The MultiFashion dataset is generated in a similar manner from the FashionMNIST dataset (Xiao et al. 2017). In Multi-Fashion+MNIST dataset, one image is from MNIST (top-left) and the other image is from FashionMNIST (bottom-right). In each dataset, there are 120,000 samples in the training set and 20,000 samples in the test set.

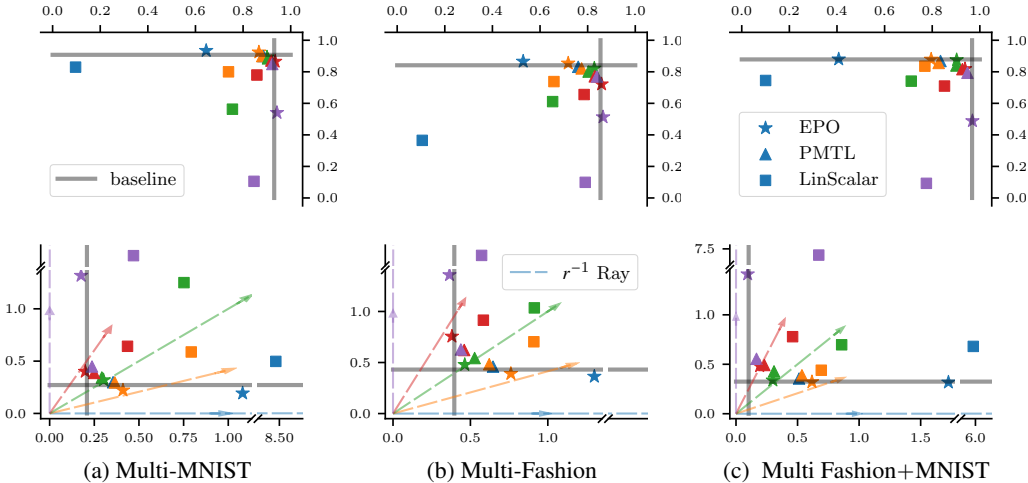


Figure 16: (Color Online) The top row show the accuracies, and the bottom row losses for 3 datasets. In each Figure, x axis corresponds to task-1 while y axis corresponds to task-2. Different colors indicate different \mathbf{r}^{-1} vectors, which are shown with corresponding r^{-1} rays. EPO solutions have the highest per-task accuracy and are closest to the \mathbf{r}^{-1} vectors.

For each dataset, there are two tasks: 1) classifying the top-left image, and 2) classifying the bottom-right image. Cross entropy losses are used for training. We use the same network (LeNet (LeCun et al. 1998) with 31,910 trainable free parameters) used in Lin et al. (2019) as the MTL neural network. The baseline for comparison is training the network for individual tasks. In addition we compare with the results from linear scalarization (LinScalar) and Chebyshev Scalarization.

For all the methods stochastic gradient descent is used for training with the same hyperparameters: number of epochs, number of mini-batches and learning rate. We test the performance of all methods for the *same* 5 \mathbf{r}^{-1} vectors, shown as rays in the bottom row of Figure 16. Ideal solutions should lie on these rays. Thus, each method has exactly 5 points corresponding to the test set losses in the bottom row and the top row shows the test set accuracies of the corresponding 5 DNN solutions.

The results in Figure 16. show that the per-task accuracy of EPO search is higher than that of PMTL in every single run (top). The test set losses (bottom) show that the solutions from EPO search are closer to the corresponding \mathbf{r}^{-1} vectors, compared to the solutions from PMTL. For the reasons discussed in previous experiments, our method outperforms CS. To avoid clutter in the Figures 16,

the results of CS are not shown. We observe that the performance of LinScalar is worse than all the other methods.

Apart from the domains, the 3 applications we consider also differ in terms of predictive models developed for the tasks, data usage, and subsequent use of the model. In application 1 (personalized medicine), the tasks considered are different and the corresponding predictive models are typically developed independently with data sources that are partly shared and partly task-specific. In contrast, in application 3 (e-commerce), the tasks are identical, use the same data sources for model building and, most often, are used together in subsequent applications. Application 2 (hydrometeorology) is similar to the third one in terms of the prediction task and data used for model building. However, models for each task may or may not be used together subsequently.

G Preference Elicitation

PE methods may be classified based on how the utility function is modeled.

Deterministic PE. Here the utility function is modelled deterministically, i.e., as a parametric function of the objective values. E.g., Zionts and Wallenius (1976) used linear scalarization of the objectives as the utility function, which cannot model all Pareto optimal solutions as DM’s preferred solution for non-convex MOO problems. Since LS cannot model all PO solutions for non-convex MOO problems, many interactive methods, such as Steuer (1989), Steuer et al. (1993), Dell and Karwan (1990), Ozbey and Karwan (2014), Reeves and MacLeod (1999), were developed that use Chebyshev scalarization as utility function due to its ability to model all the Pareto optimal solutions, even for non-convex objectives. Chebyshev scalarization can be considered as a proxy utility function to reach the best preferred alternative for the DM. These *Weight Space Reduction Methods* reduce the parameter space of the utility, after every interaction, to be consistent with the DM’s responses. However, interactive MCDM with Chebyshev utility is inefficient, because the reduced weight space consists of several disconnected components, which grows exponentially with the number of interactions with the DM. Therefore, selecting a weight from the fragmented weight space to probe for the next alternative becomes computationally expensive for large and complex problems (Miettinen 1998).

Another deterministic PE approach is Preference Robust Optimization (PRO), where the set of all possible utility functions are restricted to only those that are consistent with the previous pair-wise comparisons, and the worst utility in this restricted set is optimized to find the next alternative. E.g., Vayanos et al. (2020) model the utility as a linear function and Haskell et al. (2018) model it as a quasi-concave function, using several support (“hockey stick”) functions, where the number of parameters of the utility function grows linearly with the number of interactions. PRO methods assume the MOO to be convex and the utility to be quasi-convex in the most general case. They cannot model non-convex PE problems, where either the MOO problem or the utility function could be non-convex.

Probabilistic PE. Here, the utility function is modelled using probabilistic methods. There are parametric models of utility for probabilistic PE, e.g., Armbruster and Delage (2015) which does not model non-convex utility functions. In contrast, non-parametric methods, such as Gaussian processes can model any class of functions – see §H and 2.2.2.

H Bayesian optimization with Gaussian Process

Bayesian optimization (BO) is a sequential model-based approach for solving black-box function optimization problems (see, e.g. Shahriari et al. (2016)). The key idea is to learn a *surrogate probabilistic model* $P(u)$ that captures our beliefs about the unknown function $u(\mathbf{x})$. The functional form of u is unknown but it is assumed that the function can be evaluated at any given point \mathbf{x} . The model is learnt from *data*, $\mathcal{D}_t = \{(\mathbf{x}^1, u(\mathbf{x}^1)), \dots, (\mathbf{x}^t, u(\mathbf{x}^t))\}$, that consists of sequential evaluations of $u(\mathbf{x})$ for different values of \mathbf{x} .³

Generating this data sequence requires making the decision of which \mathbf{x} to evaluate next, at each step. This decision is made through an *acquisition function* α . These functions are designed to have

³Note, in our setup of PE, we do not have direct evaluation of the utility at a point \mathbf{x}^t . Instead the data is in the form of pairwise comparisons $\mathcal{D}_t = \{(\mathbf{x}^i, \mathbf{x}^j)\}$ such that $u(\mathbf{x}^i) > u(\mathbf{x}^j)$.

optima at points with high uncertainty in the surrogate model (thus facilitating exploration) and/or at points with high predictive values in the surrogate model (thus facilitating exploitation). Acquisition functions have known functional forms and are usually easier to optimize than the original objective function. The surrogate model is updated sequentially with each observed data point. Over multiple steps, the landscape of the black-box function $u(\mathbf{x})$ is learnt by the surrogate model and can be exploited by the acquisition function to yield values of \mathbf{x} that are, on average, closer to the optimal \mathbf{x}^* .

Many different choices of surrogate models and acquisition functions have been explored. A Gaussian process (GP) may be used to model priors over functions. GPs can be viewed as an infinite-dimensional extension to a multivariate Gaussian distribution (Rasmussen and Williams 2004), and can approximate general non-linear functions. A GP (μ, κ) is specified by a mean function $\mu : \mathbb{R}^m \rightarrow \mathbb{R}$ and a covariance function $\kappa : \mathbb{R}^m \times \mathbb{R}^m \rightarrow \mathbb{R}_+$, e.g., Gaussian or Matérn kernel. This models the uncertainty in the unknown objective function value at a particular solution \mathbf{x}^i as a Gaussian distribution, $u(\mathbf{f}^i) \sim \mathcal{N}(\mu(\mathbf{f}^i), \kappa(\mathbf{f}^i, \mathbf{f}^i))$. The joint probability of the function values at more than one solution, e.g., $[\mathbf{x}^i, \mathbf{x}^j]^T$, is modelled as multivariate Gaussian, $[u(\mathbf{f}^i), u(\mathbf{f}^j)]^T \sim \mathcal{N}([\mu(\mathbf{f}^i), \mu(\mathbf{f}^j)]^T, K(\mathbf{f}^i, \mathbf{f}^j))$, where K is the gram matrix of kernel κ evaluated at $\mathbf{f}^i, \mathbf{f}^j$.

A common choice for the acquisition function is *Expected Improvement (EI)* (Jones 2001), that has a closed form for GP, does not require its own tuning parameter and has been shown to perform well (Snoek et al. 2012). EI is the expectation that \mathbf{x}^{t+1} will improve u over \mathbf{x}^{t*} which is the best observation from t steps of BO so far, i.e. $\mathbf{x}^{t*} = \arg \max_{\mathbf{x}^{i \leq t}} u(\mathbf{x}^i)$, and $EI^t(\mathbf{x}^{t+1}) = \mathbb{E}_t \left[\max\{u(\mathbf{x}^{t*}) - u(\mathbf{x}^{t+1}), 0\} \right]$, where the expectation \mathbb{E}_t is under the posterior distribution given evaluations of u at $\mathbf{x}^1, \dots, \mathbf{x}^t$. The next value is chosen by $\mathbf{x}^{t+1} = \arg \max EI^t(\mathbf{p}_{n+1})$. For a GP with predictive variance $\kappa^t(\mathbf{x}) = \kappa(\mathbf{x}; \mathcal{D}_t)$ and predictive mean $\mu^t(\mathbf{x}) = \mu(\mathbf{x}; \mathcal{D}_t)$:

$$EI^t(\mathbf{x}^{t+1}) = \kappa[\gamma(\mathbf{x}^{t+1})\Phi(\gamma(\mathbf{x}^{t+1})) + \phi(\gamma(\mathbf{x}^{t+1}))] \quad (121)$$

where, $\gamma(\mathbf{x}^{t+1}) = (u(\mathbf{x}^{t*}) - \mu^t(\mathbf{x}^{t+1}))/\sigma^t(\mathbf{x}^{t+1})$, and Φ and ϕ denote the CDF and PDF of the standard normal distribution respectively.

I Optimization in Neural Networks

A neural network is a parametric function $L : \mathbb{R}^{d_I} \rightarrow \mathbb{R}^{d_T}$, where d_I is the input dimension and d_T is the target dimension, created by composition of multiple constituent functions L_k represented by layers in the network. For example a three layered network can be written as

$$L(\mathbf{x}; \theta_1, \theta_2, \theta_3) = L_3(L_2(L_1(\mathbf{x}; \theta_1); \theta_2); \theta_3), \quad (122)$$

where θ_k is the set of parameters for the k^{th} layer $L_k : \mathbb{R}^{d_{k-1}} \rightarrow \mathbb{R}^{d_k}$, d_{k-1} and d_k are the input and output dimensions of the k^{th} layer (here $d_0 = d_I$, and $d_3 = d_T$). A layer L_k performs an affine transformation followed by an elementwise nonlinear transformation, e.g., sigmoid or ReLU. The function parameters $\Theta = \{\theta_k\}$ (aka network weights) are learnt by optimizing the training objective which is determined by the learning task and targets given by a training dataset $\mathcal{D} = \{(\mathbf{x}^i, \mathbf{y}^i)\}_{i=1}^N$:

$$\min_{\Theta} f(\Theta; \mathcal{D}) = \sum_{i=1}^N l(L(\mathbf{x}^i; \Theta), \mathbf{y}^i), \quad (123)$$

where l is a differentiable loss function measuring the deviation of the output $L(\mathbf{x}; \Theta)$ from the expected value \mathbf{y} . Common loss functions include the mean-squared error loss for regression tasks and cross-entropy loss for classification tasks. Note, here \mathbf{x}_i 's are not the variables of optimization, they are input data features and \mathbf{y}_i 's are the targets. It is customary in the neural network literature to denote the model parameters, which are the optimization variables, as θ . A neural network with three or more layers is generally considered deep. Training such a model requires learning large number of parameters, which makes it prohibitively expensive to use second-order methods. First order optimization techniques, based on gradient descent, are most widely used. More details can be found in books on deep learning, e.g., by Goodfellow et al. (2016).

I.1 Deep Neural Networks for Multi-task Learning

In MTL, there are more than one training objectives each stemming from a task. The MTL datasets may have multiple targets, for different tasks, e.g., $\mathcal{D} = \{(\mathbf{x}^i, \mathbf{y}_1^i, \mathbf{y}_2^i, \dots, \mathbf{y}_m^i)\}_{i=1}^N$ has targets for m different tasks and a common input for all of them, like in our experiments in §F. Another example of a MTL dataset is $\mathcal{D} = \{(\mathbf{x}_s^i, \mathbf{x}_1^i, \dots, \mathbf{x}_m^i, \mathbf{y}_1^i, \mathbf{y}_2^i, \dots, \mathbf{y}_m^i)\}_{i=1}^N$, where there is a common input \mathbf{x}_s for all the tasks, task specific inputs \mathbf{x}_j , $j \in [m]$ for each task, and the corresponding targets \mathbf{y}_j , $j \in [m]$, like in our experiment in §5.5.

MTL models are designed according to the format of data. For example, the model in Figure 2 can be considered as two parametric functions designed for the first type of MTL dataset:

$$\mathbf{L}(\mathbf{x}; \Theta) = \begin{bmatrix} L_1(L_s(\mathbf{x}; \theta_s); \theta_1) \\ L_2(L_s(\mathbf{x}; \theta_s); \theta_2) \end{bmatrix}, \quad (124)$$

where θ_s is the network parameter for embedding the common input, and θ_j 's are for the task specific layers. The m simultaneous optimization problems for training this model is given by

$$\min_{\Theta} f_j(\Theta; \mathcal{D}) = \sum_{i=1}^N l_j(L(\mathbf{x}^i; \Theta), \mathbf{y}_j^i), \quad \forall j \in [m], \quad (125)$$

where l_j 's are task-specific loss functions.